Novel strategies for decoding the functions of Polo-like kinase 1

By

Robert F Lera

A dissertation submitted in partial fulfillment of

the requirements for the degree of

Doctor of Philosophy

(Cellular and Molecular Biology)

at the

University of Wisconsin-Madison

2015

Date of final oral examination: 11/19/2015

This dissertation is approved by the following members of the Final Oral Committee:

Mark E Burkard, Associate Professor, Medicine
Patricia J Keely, Professor, Cell & Regenerative Biology
Pamela K Kreeger, Assistant Professor, Biomedical Engineering
Randal S Tibbetts, Professor, Human Oncology
Beth A Weaver, Associate Professor, Cell & Regenerative Biology

Abstract

Novel strategies for decoding the functions of Polo-like kinase 1

Robert F Lera

Under the supervision of Professor Mark E Burkard

At the University of Wisconsin-Madison

Mitosis is the critical phase during the eukaryotic cell cycle in which replicated DNA is equally partitioned into the two halves of a dividing cell. Errors in this process often result in an improper distribution of chromosomes to the daughter cells, which is a hallmark of cancer. Polo-like kinase 1 (Plk1) regulates many critical activities during mitosis, including spindle assembly, chromosome alignment, chromosome segregation, and cytokinesis. Coincident with this, hundreds of substrates have been identified as potential effectors of its activities. However, a detailed understanding of Plk1 has been obscured by this multi-functionality and expansive substrate list. Moreover, Plk1 operates primarily within a 60-minute mitotic window, which impedes isolation of its individual functions for study. To overcome these obstacles, I have developed several strategies to isolate and decode the functions of Plk1. By titrating chemical inhibition, I have uncoupled Plk1's role in chromosome alignment and segregation from its role in bipolar spindle formation. This has revealed that Plk1 regulates anaphase both by promoting spindle elongation and chromosome segregation. Failure to perform these functions results in tetraploidy, senescence and impaired proliferation. Furthermore,

impaired chromosome segregation is characterized by a striking loss of kinetochore integrity. Combining inhibitor titration with protein tethering and quantitative phosphoproteomics, I have further elucidated Plk1's function at the kinetochore. I have discovered that Plk1 localizes to the inner kinetochore and its role in chromosome alignment and segregation is partially mediated from this region, which is distinct from its more established role at the outer kinetochore. Additionally, this strategy has revealed two proteins, Kif4a and Usp16, that potentially mediate chromosome segregation. To conclude, the strategies presented in this dissertation reveal new mechanistic insight into Plk1 activity and suggest potential mediators of these functions. Moreover, these findings may benefit the development and rational use of Plk1 inhibitors in cancer chemotherapy.

Table of Contents

Abstract.....i

Table of Contents.....iii

List of Figures and Tables.....vi

Acknowledgements.....x

List of Abbreviations.....xii

Chapter I—Introduction.....1

Mitosis: an introduction.....2

Mitotic regulation by protein kinases.....3

Polo-like kinase 1: an essential regulator of mitosis.....5

The Polo kinase family.....5

Regulation of Plk1 expression and localization.....6

Current challenges to studying Plk1.....8

Scope of project.....9

Chapter II—Strategies for decoding Plk1 functions.....16

Introduction.....17

Encoding specificity and temporal control with analog-sensitive (AS) alleles.....17

Partitioning Plk1 activity by inhibitor titration.....19

Partitioning Plk1 activity by subcellular locale to identify functionally relevant substrates.....20

Conclusions.....23

Chapter III—High Mitotic Activity of Polo-like kinase 1 is required for chromosome segregation and genomic integrity in human epithelial cells.....28

Abstract.....29

Introduction.....30

Results.....32

Discussion.....41

Materials and Methods.....47

Acknowledgements.....51

Chapter IV—Decoding Polo-like kinase 1 signaling along the kinetochore-centromere axis.....72

Abstract.....73

Introduction.....73

Results.....76

Discussion.....86

Materials and Methods.....90

Acknowledgements.....101

Chapter V—Perspectives.....134

Partitioning Plk1 function by chemical titration elucidates its role in maintaining genomic fidelity.....135

Partitioning Plk1 function by kinetochore locale reveals that Plk1 operates at the inner centromere and chromatin.....136

A novel role for Plk1 in maintaining kinetochore architecture.....137

Conclusion.....139

References.....143

List of Figures and Tables

Chapter I

1.1. Stages of mitosis……...11

1.2. Plk1 structure and activation……..……12

1.3. Cell cycle localization of Plk1……..……13

1.4. Mapping the Plk1 phosphoproteome……..……...15

Chapter II

2.1. Chemical-genetic strategy for specific kinase inhibition……..……....24

2.2. Allele-specific control of Plk1 in RPE1 cells……..……..25

2.3. Chemical genetic complementation strategy to probe for functional Plk1 locales…….26

2.4. Assay for fusion construct complementation.....27

Chapter III

3.1. Individual Plk1 phenotypes have distinct thresholds of inactivation……..52

Table 3.1. IC_{50} values for various phenotypes associated with loss of Plk1 activity……..55

3.2. $Plk1^{as}$ activity is inhibited by 3-MB-PP1...……..56

3.3. Live-cell imaging reveals partial loss of Plk1 activity results in impaired chromosome alignment and segregation……..57

3.4. Anaphase chromosome segregation is most sensitive to Plk1 inhibition

and impairment is associated with shortened spindles and lagging chromosomes…….59

3.5. Spindle elongation and chromosome segregation are impaired with partial loss of Plk1 activity……..……..…61

3.6. The Polo-box domain (PBD) is required for chromosome segregation, but dispensable for bipolar spindle formation……..…...63

3.7. Impaired chromosome segregation is not caused by a mitotic checkpoint failure or persistent topologic linkages, but includes merotelic attachments……..……..…65

3.8. Impaired chromosome segregation produces progeny that exhibit abnormal nuclear morphologies, are tetraploid, and fail to proliferate…..…….68

3.9. Separation of Plk1 function by activity threshold reveals its most sensitive functions and may help link these to substrates…….…….70

Supplementary Movie Links

Movie 3.S1. H2B-mCherry expressing Plk1^{as} cell undergoing a normal division……..…71

Movie 3.S2. H2B-mCherry expressing Plk1^{as} cell dividing with a lagging chromosome..…….71

Movie 3.S3. H2B-mCherry expressing Plk1^{as} cell exhibiting severely impaired chromosome segregation during anaphase…….....71

Movie 3.S4. H2B-mCherry expressing Plk1^{as} cell exhibiting initial chromosome congression with subsequent loss of chromosome alignment.....71

Chapter IV

4.1. Plk1 signaling at the kinetochore requires binding via its PBD……....102

4.2. High-resolution microscopy identifies discrete localization of endogenous Plk1 and kinetochore-tethered Plk1 constructs along the kinetochore-centromere axis…….....104

4.3. 10-plex TMT phosphoproteomic analysis of Plk1 partitioned by locale within the kinetochore-centromere axis…….....106

4.4. Restricting Plk1 activity along the kinetochore-centromere axis produces distinct phosphoproteomic and functional signatures..... 108

4.5. Outer kinetochore tethering of Plk1 fails to restore chromosome alignment or segregation……..…….....…..110

4.6. Functional/proteomic signatures and a model for Plk1 activity in the kinetochore.....……...113

Supplementary Figures

4.S1. Plk1 substrates and interactors are found along the entire kinetochore-centromere axis.....115

4.S2. Plk1 signaling at the kinetochore requires binding via its PBD (companion to Figure 4.1).....117

4.S3. Analysis of kinetochore-tethered Plk1 constructs (companion to Figure 4.2).....119

4.S4. Validation of high-resolution Plk1 localization in cells (companion to Figure 4.2).....121

4.S5. Sample preparation and results for mass spectrometry (MS) of Plk1 cell lines (companion to Figures 4.3 and 4.4).....122

4.S6. Plk1 activity tethered to chromatin or the inner centromere promotes chromosome alignment and segregation (companion to Figure 4.4).....125

4.S7. Plk1 activity tethered to the inner centromere pool of Kif2c rescues chromosome alignment and segregation (companion to Figure 4.4).....127

4.S8. Analysis of outer kinetochore-tethered Plk1 constructs (companion to Figure 4.5).....129

Supplementary Tables

Table 4.S1. Table of primers used for USER cloning and mutagenesis.....132

Table 4.S2. Table of antibodies used for immunofluorescence and immunoblotting.....133

Chapter V

5.1. Schematic demonstrating differential clinical effects of Plk1 inhibitors.....140

5.2. Plk1 inhibition induces lagging chromosomes characterized by loss of kinetochore proteins.....141

Acknowledgements

As I come to the conclusion of these 5 chapters of my life, I would like to say a few words to give credit where it is due.

To the faculty at JMU. Mark, you started me on this path and you reminded me that a PhD isn't so much about intelligence as it is perseverance. Tim, you prepared me for the long and cold Madison winters. Terrie, you pushed me to communicate my work in a simple, but effective manner.

To the CMB program. I am grateful for the opportunity that you have provided to learn and develop at UW-Madison.

To my rotation labs (Bill, Rup, Bruce, Nicole). You were patient as I experienced a steep learning curve. Bill, thank you for your words: *It is always easier to be critical than collaborative*.

To my collaborators, Aussie, Greg, Ted and Josh. Thank you for accompanying me for part of this journey and lending your considerable talents. *To James*, you stepped in during crunch time and delivered.

To my committee. I did not accomplish all that I set out to do, but I grew considerably thanks to your high standards. We only met once a year, but your words stay seared into my head: Randy (*Do you really think you're gonna find this one substrate out of hundreds, thousands maybe?*), Pam (*What is your 'Go/No-Go' experiment?*), Patti (*Sometimes we can only see with what we are given to look through*), and Beth (*Just show me the data and I'll shut up!*)

To my advisor, Mark. You gave me the chance to work in your lab. Your persistent optimism helped when things looked bleak. You challenged me to lead and you always had *another crazy idea*.

To the members of the Burkard and Weaver labs, past and present. It's been real and it's been fun and it's been not real fun.

Finally, to my friends, family, and my wife, Kay. I cannot write anything here that will make up for the time I have missed with you, nor will it cover the gratitude I feel for your support. I look forward to coming back into your lives.

List of Abbreviations

3-MB-PP1	3-methylbenzyl-pyrazolopyrimidine 1
AA	denotes mutated PBD (H538A/K540M
ACA	Anti-centromere antibody
ANOVA	Analysis of variance
AS	Analog sensitive
ATCC	American Type Culture Collection
ATP	Adenosine triphosphate
Bub	Budding uninhibited by benzimidazoles
CCD	Charge-coupled device
Cdc	Cell division control
Cdk	Cyclin-dependent kinase
CENP	Centromere Protein
CREST	Calcinosis, Raynaud's phenomenon, Esophageal dysmotility, Sclerodactyly, and Telangiectasia
DAPI	4',6-diamidino-2-phenylindole
ΔC	Lacks C-terminal domain
DMSO	Dimethyl sulfoxide
DNA	Deoxyribonucleic acid
EDTA	Ethylene diamine tetraacetic acid
EGTA	Ethylene glycol tetraacetic acid
GFP	Green fluorescent protein
H2B	Histone protein 2B

Hec	Highly expressed in cancer
HEPES	4-(2-hydroxyethyl)-1-piperazineethanesulfonic acid
hTert	Human telomerase reverse transcriptase
IC_{50}	Half-maximal inhibitory concentration
INCENP	Inner centromere protein
MCAK	Mitotic centromere-associated kinesin
Mps	Monopolar spindle
PBD	Polo box domain
PBIP	Polo-box interacting protein
PBS	Phosphate buffered saline
PICH	Plk1 interacting checkpoint helicase
PIPES	Piperazine-N,N′-bis(2-ethanesulfonic acid)
PLK1	Polo-like kinase 1
PMSF	Phenylmethylsufonyl flouride
RacGAP1	Rac GTPase-activating protein 1
RNA	Ribonucleic acid
RNAi	RNA interference
RPE	Retinal pigment epithelium
RT	Room temperature
SDS-PAGE	Sodium dodecyl sulfate - polyacrylamide gel electrophoresis
SEM	Standard error of measurement
TBS	Tris buffered saline
TMT	Tandem mass tags

WT	Wildtype

Chapter I—Introduction

Mitosis: an introduction

Mitosis is the critical phase during the eukaryotic cell cycle in which replicated DNA is equally partitioned into the two halves of a dividing cell. To do this, the cell dynamically reorganizes to spatially isolate the sister chromatids before membrane abscission, ensuring faithful inheritance of the genome by each daughter cell. As a component of the cell cycle, the mitotic program occurs regularly throughout human development and maintains adult tissues such as blood, bone, skin, and lining of the digestive tract. In an adult over the age of 70, the cell cycle will have occurred approximately 10 million billion times[1].

Mitosis is divided into five phases: prophase, prometaphase, metaphase, anaphase and telophase (Figure 1.1). During prophase, the DNA condenses into observable chromosomes and microtubules begin to nucleate from the separated centrosomes. The breakdown of the nuclear envelope signifies the onset of prometaphase, where centrosome-originating microtubules capture individual chromatids of a sister pair, also called mono-orientation. Mono-oriented pairs are then moved toward the spindle equator to allow for capture of the unattached sister by microtubules from the opposite pole. Metaphase is characterized by the alignment of all chromosome pairs at the spindle equator with each sister chromatid attached to microtubules emanating from opposite spindle poles, also called bi-orientation. During anaphase, the microtubules pull the sister chromatids to opposite spindle poles, while the machinery designated to divide the cell membrane assemble at the spindle midzone and equator. At the poles, chromosome decondensation and nuclear envelope

reformation signifies the onset of telophase, which coincides with cell membrane abscission, also called cytokinesis.

In general, errors in any of the mitotic phases negatively impact the cell. For example, if some chromosomes fail to attach correctly to spindle microtubules, the cell may still divide, but partition the chromosomes unequally to each daughter cell, a state termed aneuploidy. Alternatively, if a spindle fails to form or many chromosomes fail to attach to microtubules, the cell may exit mitosis without segregating its chromosomes or attempting cytokinesis, resulting in one cell with twice the number of chromosomes, a state termed tetraploidy. A tetraploid state may also occur when a cell segregates its chromosomes but fails to complete cytokinesis[2]. Although aneuploidy and tetraploidy occur naturally in some human tissues and a few whole-human aneuploid states are non-lethal, these conditions are usually associated with inviability during development and disease states in adults[3–6]. Notably, the majority of cancers are aneuploid, with a small fraction exhibiting near-tetraploid karyotypes[3], suggesting that failures in the mitotic program can initiate or contribute to disease progression. Furthermore, emerging evidence linking oncogenic signaling with impaired mitotic fidelity[7] illustrates the complexity of cellular signaling networks that must be considered when contemplating therapeutic targets.

Mitotic regulation by protein kinases

(adapted from Lera & Burkard[8])

The mitotic program is typically executed within an hour, at a time when DNA is condensed and largely inaccessible to transcription factors[9]. Therefore, it is not

surprising that mitotic progression is predominantly regulated by posttranslational modifications such as phosphorylation. Protein kinases comprise 1.7% of the proteins encoded in the human genome[10] and ~200 are thought to be active during mitosis[11,12]. Fortunately, several kinase families have emerged as key regulators of mitosis and cytokinesis: the cyclin-dependent kinases (Cdks), Polo-like kinases (Plks), Aurora kinases, 'never in mitosis A' (NIMA) kinases, mitotic checkpoint kinases (Bub1, BubR1, Mps1), and cytokinesis kinases (myosin light chain kinase (MCLK), Rho-associated kinase (ROCK), and citron kinase)[13,14].

Protein kinases perform critical cellular signaling functions by catalyzing the transfer of the γ-phosphate from ATP onto the hydroxyl group of a serine, threonine, or tyrosine of a target protein. Removal of the phosphate is catalyzed by protein phosphatases. The addition and removal of phosphates on a target protein can drastically alter local charge, which regulate protein conformation, enzymatic activity, or protein-protein interactions. Thus, protein phosphorylation and dephosphorylation, performed by a handful of kinases and phosphatases, provides the diverse molecular signaling events required for much of the dramatic intracellular remodeling required to faithfully partition identical sets of chromosomes into the two daughter cells[13,14].

Because kinases perform essential functions during mitosis and mitosis is a critical event for cancer development, it is not surprising that mitotic kinases have been identified as chemotherapy targets. Numerous inhibitors targeting the Aurora kinases, Cdk1, Plk1, Haspin kinase and Mps1 are in various stages of pre-clinical and clinical development[15], however none have yet received approval. There are many reasons why promising chemicals fail to reach their potential (e.g. chemical efflux pumps, poor

pharmacokinetics/pharmacodynamics, acquired resistance), however one important (and likely overlooked) reason is a failure to identify the clinically relevant mechanism of action.

This dissertation addresses strategies and techniques to decode the functions of one of the essential mitotic kinases, Plk1. In doing so, I will highlight how these innovations elucidate specific activities of Plk1 during mitosis and address how these findings improve our understanding of mitotic regulation in general and inform the rational development and use of Plk1 inhibitors in cancer chemotherapy.

Polo-like kinase 1: an essential regulator of mitosis

Polo-like kinase 1 (Plk1) is essential for maintaining genomic fidelity during mitosis. The *PLK1* gene maps to p12 on chromosome 16[16], encoding a serine/threonine protein kinase of 603 amino acids with a mass of approximately 67 kilodaltons[16,17]. Homozygous deletion of the PLK1 gene in mice is embryonic lethal and notably, heterozygous deletion produces viable animals that exhibit aneuploid splenocytes (12% vs 1.5% in wildtype littermates) and an increase in tumor incidence (27.5% vs 9% wildtype controls)[18]. Structurally, the Plk1 protein contains two primary domains: an N-terminal catalytic domain (aa 53-305) and a C-terminal Polo-Box domain (PBD; aa 372-592) (Figure 1.2A).

The Polo kinase family

Polo was originally identified from a mutational analysis of genes critical for development in *Drosophila*[19]. Cells from *polo* mutants exhibited mitotic spindles that were “highly branched” with “defective poles”. The *polo* gene encodes a

serine/threonine-directed protein kinase expressed primarily in dividing tissues[20] and homologues, named Polo-like kinases (Plks), were identified in mice[17,21,22], humans[16,17,23], and frogs[24]. Importantly, the Polo-like kinase 1 homologues share high sequence similarity with budding yeast Cdc5[16], an essential regulator of cell division[25], suggesting an evolutionarily conserved role of Polo kinases in cell division.

There are 5 members of the mammalian Polo-like kinase family, numbered 1 to 5, with Plk1 the best studied of the family[26]. Plk4 is also expressed in a number of eukaryotes and is required for centriole duplication[27,28]. Less is known about the remaining three. Plk2 appears to regulate centriole duplication[29] and neuronal activity[30]. Plk3 is important for S-phase entry[31] and cellular stress responses[32]. Plk5, which lacks a kinase domain, functions in neuronal activity as well[33].

Regulation of Plk1 expression and localization

Plk1 is primarily expressed in tissues with a high proliferative index[16,17,20–23] and its expression is cell cycle regulated at both the mRNA and protein level, with peak expression occurring during G2/M[16,22], although basal protein levels have been observed during G0, G1 and S-phases[34]. Transcript expression is stimulated by the forkhead transcription factors, although repression during G1 is mediated by p53-p21 and Rb-E2F pathways[35]. During late mitosis, Plk1 is degraded in the proteasome[36] after ubiquitylation at the D-box-like motif (RxxL) located at aa 337-40 (Figure 1.2A). However this proteasome-mediated degradation appears important only for timely cytokinesis[37].

Consistent with its expression, Plk1 activity peaks during G2 and mitosis[34]. Structural and biochemical analysis indicate that Plk1 is auto-inhibited by interactions between the Polo-Box domain (PBD) and kinase domain[38–40] (Figure 1.2B). During G2, Plk1 is bound by the protein Bora, which interacts with both the kinase domain and PBD, partially relieving the auto-inhibition[41]. This binding allows for phosphorylation at T210 by Aurora A kinase, dramatically increasing Plk1 catalytic activity[41,42]. During mitosis, Bora is degraded, which allows substrate targeting and further Plk1 activation by phosphopeptide binding[40,41] (Figure 1.2B). It remains unclear if this sequence of events is precisely followed *in vivo* and there is some debate regarding the exclusivity of Aurora A as the upstream activator of Plk1[43,44]. Plk1 commonly targets serine and threonine residues contained within an D/E/N/Q-X-pS/pT motif[45–47], where 'X' indicates any amino acid and 'p' indicates a phosphorylated residue.

A specialized feature of Plk1 is its C-terminal phosphopeptide-binding domain, termed the Polo-Box domain (PBD). This domain is composed of an N-terminal extension (aa 372-410), Polo-Box 1 (aa 411-492), linker region (aa 493-507) and Polo-Box 2 (aa 511-592)[48]. Mike Yaffe's group[49] originally identified the PBD as a phosphopeptide-binding domain, recognizing an optimal motif of S-pS/pT-P/X, where 'X' indicates any amino acid and 'p' indicates a phosphorylated residue. Crystal structures of the PBD bound to a phosphopeptide indicate that both Polo-Boxes contact the peptide with two residues in Polo-Box 2, H538 and K540, directly contacting the phosphate group[39,48]. Notably, both Polo Boxes and the N-terminal extension are necessary for phosphopeptide binding[49], suggesting the overall conformation of the

PBD is important, however phosphopeptide binding may be abolished simply by introducing H538A/K540A mutations[39].

Plk1 diversely localizes in cells. During mitosis, it localizes to centrosomes, centromeres/kinetochores, chromosome arms, the central spindle and midbody (Figure 1.3A-B). An intact PBD is required for Plk1 localization to these structures[39,50–53], suggesting that signaling events regulates its subcellular localization. How Plk1 is specifically targeted to each of these locales is not fully understood, however localization is thought to occur via two general mechanisms: self-priming and non-self-priming[54,55]. With self-priming, Plk1 initially phosphorylates the target proteins, which then recruits additional Plk1 molecules via PBD-dependent binding, creating a self-amplifying signal. With non-self-priming, other kinases, such as Cdk1, generate the phosphoepitope on the target protein that recruits Plk1. Both of these mechanisms have been reported: self-primed binding to MgcRacGAP[53] and CENP-U/CENP50/PBIP[56],and Cdk1-primed binding to Bub1[57] and BubR1[58]. Moreover, it remains unclear whether Plk1 must bind each of its substrates to exert its activities (termed processive), or if it also phosphorylates nearby proteins that it does not directly bind (termed distributive).

Current challenges to studying Plk1

Consistent with its localization pattern, Plk1 exhibits an array of mitotic functions. It is important for mitotic entry[59], particularly after repair of DNA damage[60]. It is also required for centrosome maturation and bipolar spindle formation[59–70], chromosome arm resolution[71,72], metaphase chromosome alignment[51,52,56,58,73–80], anaphase chromosome segregation[81–83] and spindle elongation[84], and cytokinesis[84–89]. To date, hundreds of

substrates have been identified as potential mediators of these activities. Our group and others[46,47,90,91] have performed mass spectrometry analyses to identify the Plk1-dependent phosphoproteome. Combined, these studies have identified 584 unique proteins containing phosphopeptides with the Plk1 consensus motif (D/E/N/Q-X-pS/pT) that are down-regulated in response to Plk1 inhibition or depletion (Figure 1.4). Linking these substrates with specific functions to detail the molecular mechanisms of Plk1 activity has proved challenging. A major reason for this is an inability to isolate specific Plk1 functions for detailed mechanistic analysis. Current strategies using protein depletion or chemical inhibition abrogate all Plk1 activity, resulting in a prometaphase-arrested cell with a monopolar spindle. This obscures mid-late mitotic activities of Plk1 without some form of timed inhibition. These timed inhibition strategies may fail to identify relationships if the phosphorylation event and biologic function are sufficiently separated in time. For example, preventing Plk1 substrate phosphorylation is believed to generate segregation errors during anaphase[81–83], yet Plk1 inhibition at the onset of anaphase fails to replicate this defect[53,84,86]. A second challenge is the diverse localization of Plk1 and its substrates within the cell (Figures 1.3,1.4). Identification of specific functional phosphorylations may require uncoupling Plk1 activity from one region in the cell from its other locales. Finally, the expansive list of substrates limits the utility of traditional mutation techniques for screening purposes.

Scope of project

To overcome the barriers outlined above, I will introduce the strategies developed by myself and others in the Burkard lab to a) specifically interrogate Plk1

activity with a high degree of temporal control, b) isolate Plk1 activities through titration of chemical inhibition, and c) partition Plk1 activity to discrete subcellular locales to match specific functions with cognate substrates (Chapter 2). Additionally, I will present findings from our efforts using inhibitor titration (Chapter 3) and partitioning Plk1 activity to discrete regions of the kinetochore (Chapter 4). Finally, I will address how these efforts have enhanced our understanding of mitotic regulation by Plk1 and discuss areas for additional investigation as well as comment on development of Plk1 inhibitors for cancer chemotherapy (Chapter 5).

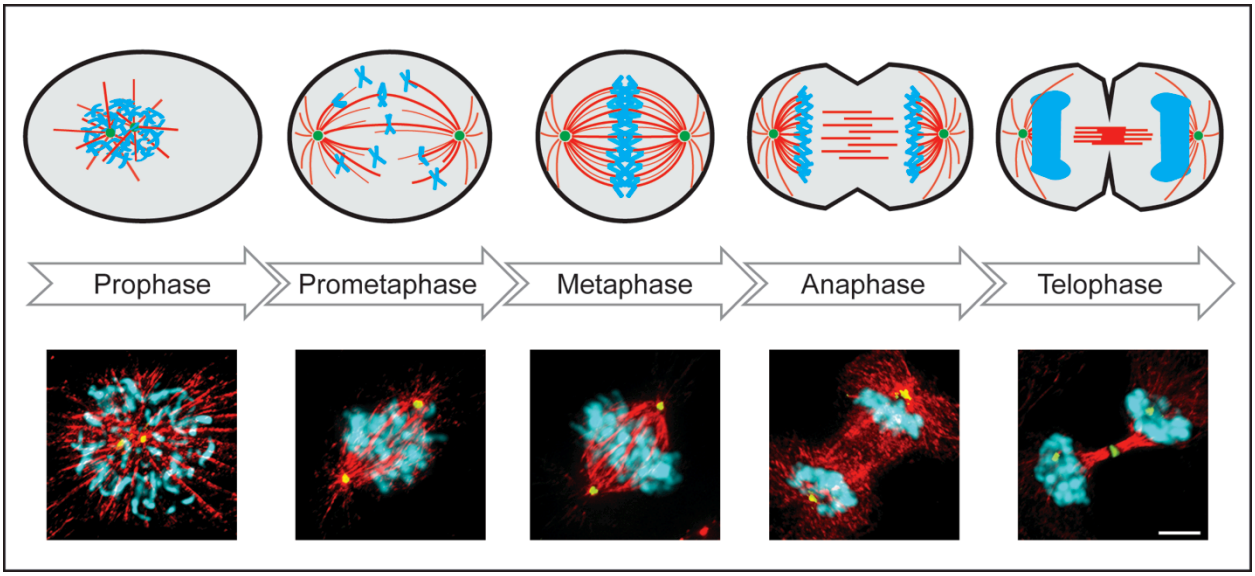

Figure 1.1. Stages of mitosis

(Top) Schematic illustration of a cell progressing through the five stages of mitosis. (Bottom) Representative micrographs of RPE1 cells during each stage. DNA (cyan), microtubules (red) and spindle poles (green) are highlighted. Scale bar, 5 μm.

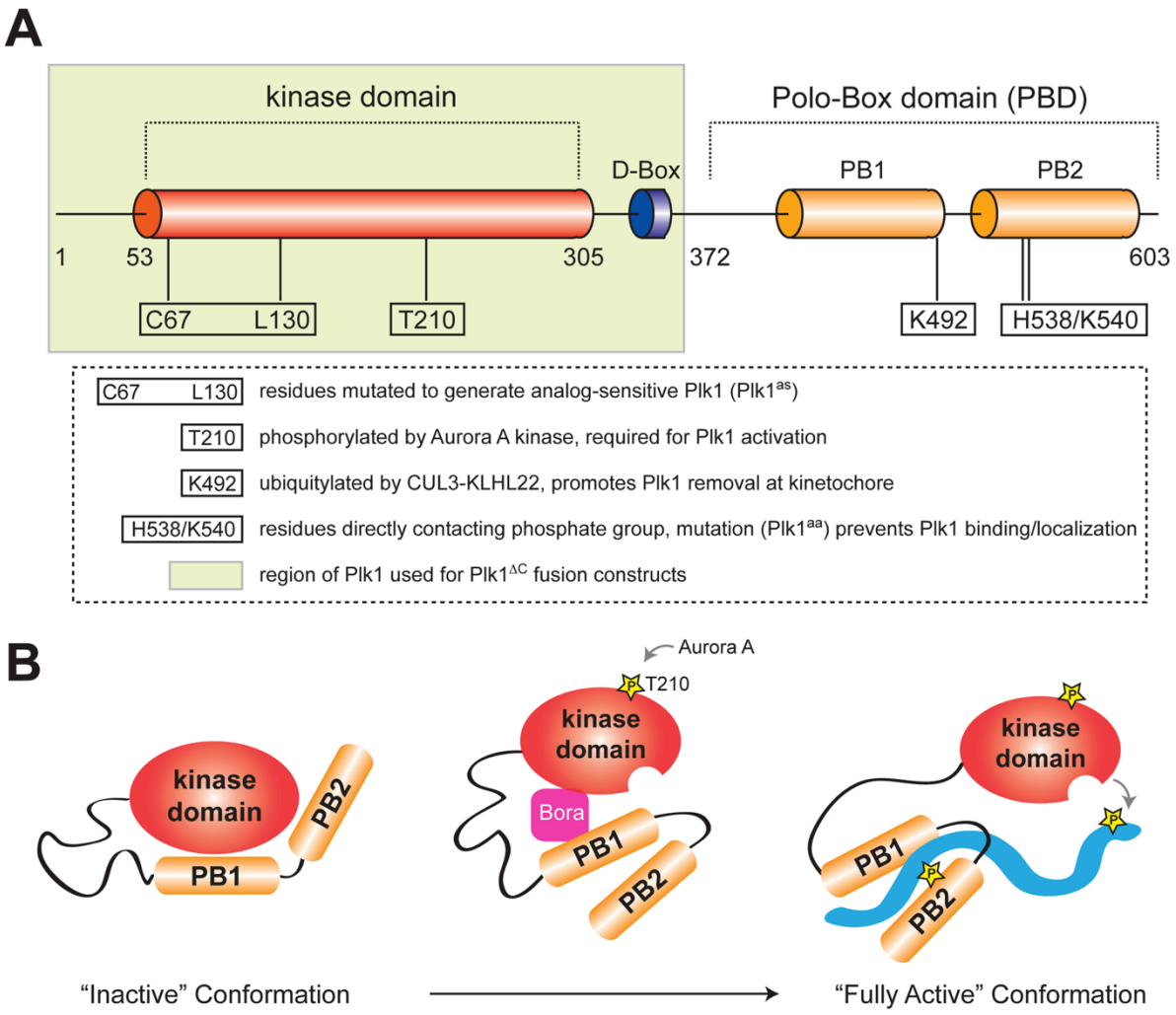

Figure 1.2. Plk1 structure and activation

A, Linear schematic of the Plk1 protein with important amino acid residues highlighted. *B*, Model of Plk1 transitioning from its inactive to fully active conformation. Plk1 is initially autoinhibited by contacts between its Polo Boxes (PB1 & PB2) and the kinase domain. Binding by Bora facilitates Aurora A phosphorylation at T210. Degradation of Bora permits Polo Box interaction with a target substrate (blue), allowing phosphorylation by the kinase domain. Yellow stars labeled 'P' indicate phosphorylations.

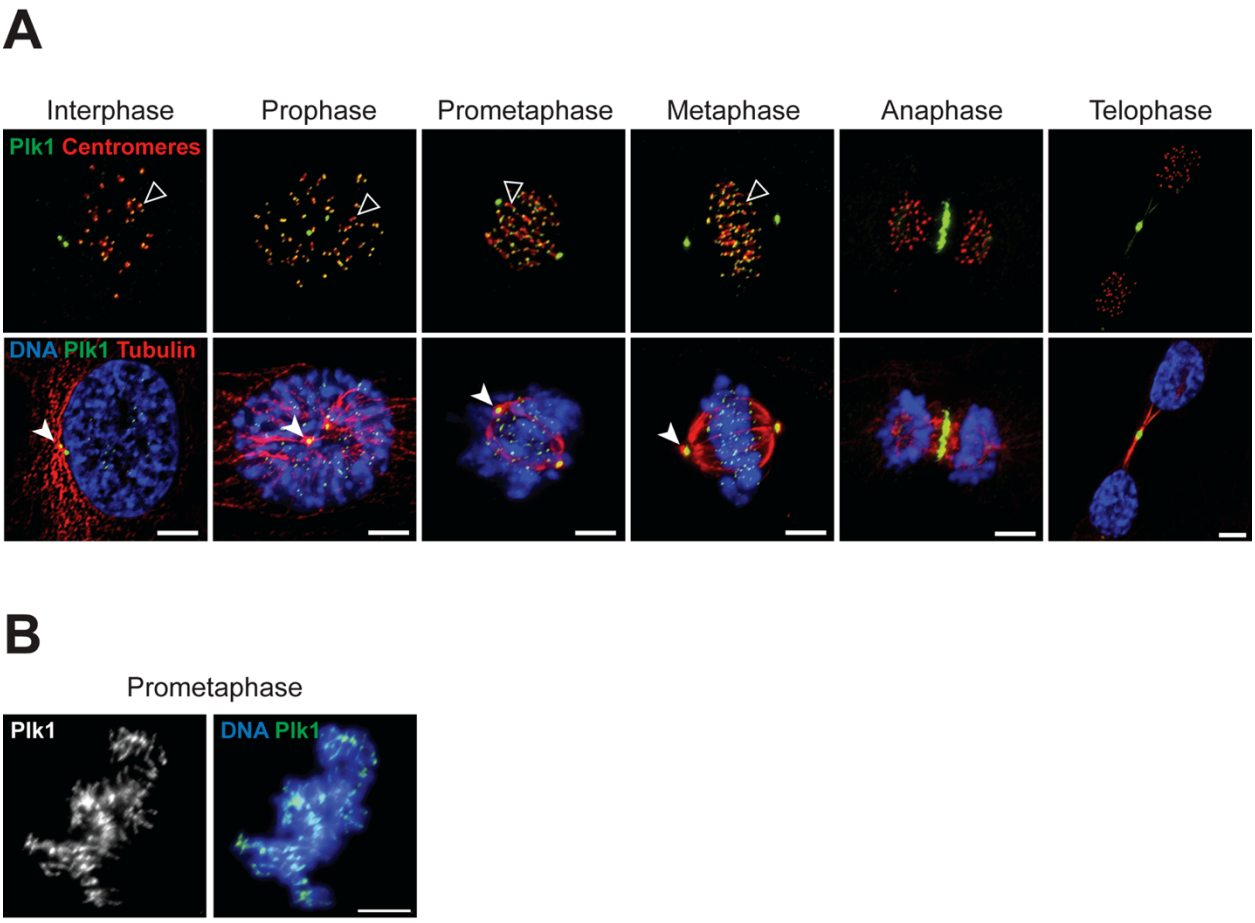

Figure 1.3. Cell cycle localization of Plk1

Representative micrographs of Plk1 localization (green) to the centrosomes, chromosome arms, centromeres/kinetochores, central spindle and midbody. *A*, Centrosomal localization, indicated by association with tubulin (closed arrowheads, bottom row), is prominent from interphase through metaphase. Centromere/kinetochore localization, indicated by overlap with a centromere marker (open arrowheads, top row), is observed during interphase, becomes more prominent from prophase to metaphase, and declines markedly during anaphase and telophase. During anaphase, Plk1 localizes to the microtubule-rich (red) central spindle region between the two DNA

masses (blue, bottom row). Central localization persists into telophase, becoming part of the midbody structure. *Top row*, Plk1 (green), centromeres (red). *Bottom row*, DNA (blue), Plk1 (green), microtubules (red). *B*, Plk1 chromosome arm localization, which is better visualized with pre-extraction prior to fixation, highlighted in a prometaphase cell. Scale bars, 5 μm.

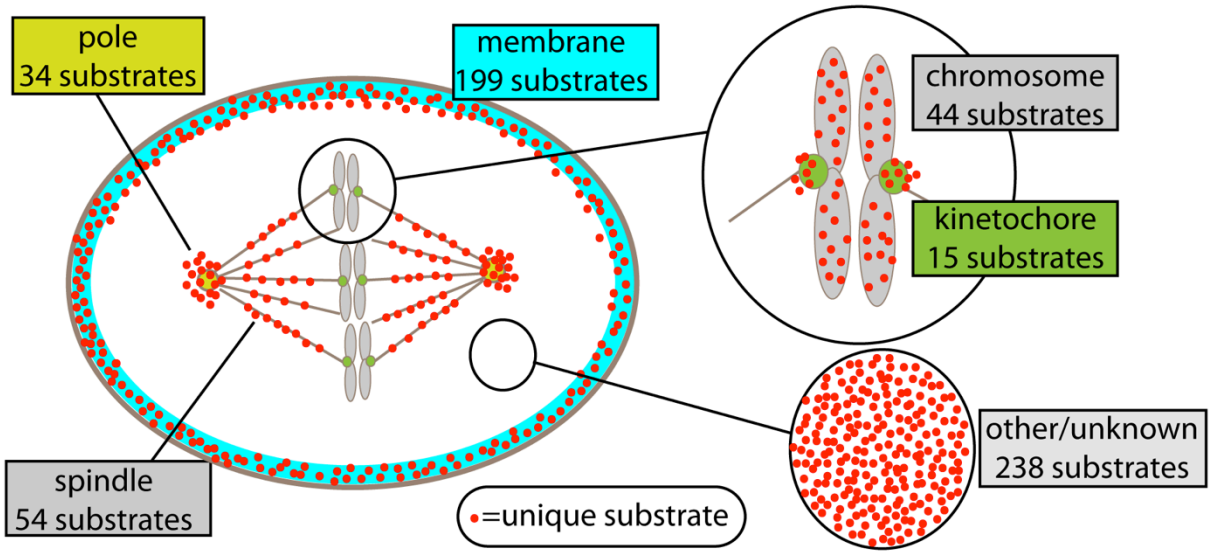

Figure 1.4. Mapping the Plk1 phosphoproteome

Mass Spectrometry analyses by our group and others[46,47,90,91] have identified 584 proteins containing phosphopeptides with the Plk1 consensus motif (D/E/N/Q-X-pS/pT) that are downregulated in response to Plk1 inhibition or depletion. Localization of these proteins was determined using the COMPARTMENTS database[92].

Chapter II—Strategies for decoding Plk1 functions

Adapted from: Lera RF and Burkard ME (2012) *Molecules*, 17 (12), 12172-12186.

Introduction

Polo-like kinase 1 (Plk1) is a pleomorphic mitotic kinase that exerts its activities in a diverse set of locales within the cell. Furthermore, a large number of substrates have been described as effectors of its function. Importantly, a majority of these relationships have been established by generating non-phosphorylatable mutants of the protein of interest. This strategy, while informative, presents a fragmented picture of Plk1 function. Additionally, the findings are limited when considering which activities or phosphorylation events are disrupted in the setting of pharmacologic inhibition. Conversely, pharmacologic inhibition of a multifunctional kinase will reveal defects only in the first function encountered. Moreover, the diverse localization pattern of Plk1, including multiple locales during each phase of mitosis, necessitates the isolation of activity by locale to ascribe functional significance and identify relevant substrates. In this chapter, I will illustrate our approach to studying Plk1, highlighting the novel strategies used to decode its functions.

Encoding specificity and temporal control with analog-sensitive (AS) alleles

Genetic manipulations, such as gene deletion or knockdown, offer powerful and specific strategies to elucidate functions of mitotic genes. However, the slow onset of action and irreversibility limit the utility of these techniques in probing the dynamic and distinct activities of protein kinases that occur during the brief mitotic window. Moreover, when contemplating functions of a protein kinase, it is important to distinguish its catalytic and structural roles. Although both roles are of interest, only its catalytic functions can be attributed to molecular phosphorylations. Conversely, the functional

consequence of genetic deletion can be masked by homologs, which can supply essential kinase functions. For example, chemical inhibition, but not gene knockdown, of Cdk2 significantly inhibits cell cycle progression[93,94]. Thus chemical inhibition of a kinase (more relevant to pharmacologic therapy) can yield remarkably different outcomes than genetic removal.

In contrast to genetics, chemical inhibitors of kinases allow rapid interrogation of catalytic function without altering kinase expression. These chemicals typically act by competitive inhibition of the ATP-binding domain to disrupt catalytic function. However, this strategy often has limited specificity because of high conservation of the ATP-binding domain across members of the human kinome. For this reason, off-target activity is encountered among pharmacologic kinase inhibitors, most often among kinases within the same family[95,96]. Nevertheless, inadvertent attribution of non-specific inhibitor effects to an incorrect target can be minimized. First, structurally unrelated compounds specific to one kinase, but with non-overlapping off-targets can be used in parallel[96]. Second, enzyme kinetic modeling may reveal conditions to allow for selective inhibition even when kinases with similar inhibitory profiles[97]. Finally, the kinase may be mutated to accept non-natural ligands to inhibit activity[98,99]. This chemical-genetic approach is accomplished by mutating the kinase 'gatekeeper' residue to a smaller one such as glycine, to enlarge the ATP-binding pocket, which can then accommodate a bulky ATP analog as a competitive inhibitor. These analogs are typically pyrazolo-pyrimidine (PP) derivatives (Figure 2.1A) originally discovered as inhibitors of Sarcoma kinase (Src). By adding bulky napthylmethyl or methylbenzyl sidechains, these compounds lose their ability to disrupt Src activity. Because most wildtype protein

kinases lack a glycine in the gatekeeper position of the binding pocket, they are insensitive to these ATP analogs (Figure 2.1B). Thus, the catalytic functions of the 'analog-sensitive' kinase may be interrogated in a rapid, reversible manner, with a specificity that is ensured by encoding the mutation genetically.

Remarkably, this chemical-genetic approach has been used successfully for many protein kinases. Since its introduction, analog-sensitive alleles have been generated to interrogate the functions of mitotic kinases in diverse model systems: Cdk1/Cdc2[100–102], Cdk7/Crk1[100,103], Aurora B/Ark1[104,105], Mps1[106–108], and Plk1/Cdc5/Plo1[86,100,109].

In this dissertation, I use immortalized human retinal pigment epithelial (RPE1) cells that are depleted of both copies of PLK1 and restored with an analog-sensitive allele (Plk1^{as}) stably expressed by retroviral transduction[86]. The Plk1^{as} allele is generated by introducing two point mutations (L130G/C67V) into the kinase domain (Figure 1.2). Lysine-130 is the gatekeeper residue and the cysteine-67 mutation restores catalytic activity lost with the gatekeeper mutation. Notably, this cysteine mutation also confers resistance of the Plk1^{as} allele against pharmacologic inhibitors of wildtype Plk1[110] (Figure 2.2).

Partitioning Plk1 activity by inhibitor titration

Plk1's multiplicity of function genuinely represents a double-edged sword. On one edge, Plk1's array of activities makes it an excellent tool for probing mechanisms of mitotic progression. On the other edge, the same activity array obscures our ability to appreciate most functions in an unbiased manner. Complete Plk1 inhibition or depletion

prevents cells from establishing a bipolar spindle, activating the mitotic checkpoint, and halting mitotic progression beyond prometaphase. This arrest prohibits interrogation of later Plk1 functions, unless inhibition is introduced after satisfaction of the mitotic checkpoint. Indeed, this strategy has been used to probe Plk1's role during cytokinesis[53,84,86]. Unfortunately, this strategy precludes analysis of phosphorylations that occur between spindle assembly and anaphase onset, specifically those related to proper attachment of chromosomes to the mitotic spindle.

In this dissertation, I use inhibitor titration to elucidate Plk1 functions, reasoning that some activities may be more sensitive to inhibition due to different concentrations of Plk1, its target substrate, or counteracting phosphatases among the various pools of Plk1 within the cell. This approach is not without precedent as different mitotic phenotypes have been observed among polo mutants in *Drosophila*[111]. Moreover, impaired cell proliferation without concomitant elevation of mitotic index has been reported for Plk1^{as} cells using inhibitor titration[86], suggesting that Plk1 inhibition disrupts cell division in the absence of a spindle-associated mitotic arrest.

Partitioning Plk1 activity by subcellular locale to identify functionally relevant substrates

An effective strategy to define a functional relationship between a kinase and substrate is to replace the endogenous wildtype substrate with a mutant non-phosphorylatable form. The first step involves mutating each identified phosphorylated serine/threonine on the substrate to a non-hydroxyl-containing residue (alanine or valine), preventing phosphorylation by the kinase. To confirm that no other residues are

phosphorylated on the substrate, an *in vitro* kinase assay is performed with wildtype and mutant substrates. Finally a “knockdown/add-back” experiment is performed in which the candidate substrate is removed from cells (e.g., by RNAi) and the non-phosphorylatable mutant is added back. If a functional relationship exists between substrate and kinase, the non-phosphorylatable mutant should phenocopy kinase inhibition. Unfortunately, obtaining sufficient homogenous substrate knockdown and mutant expression in human cells can be challenging; therefore it is difficult to interpret the experiment if no phenotypic effects are observed. More importantly, it is an inefficient strategy to use to screen large sets of candidate substrates, requiring a candidate to be selected prior to initiating this set of experiments. Furthermore, it requires prior identification of phosphorylation sites. This can impair interpretation because of both false negatives and false positives. False negatives will occur when a candidate substrate is selected but one of a series of redundant phosphorylations has not been identified so that no phenotype is seen. Conversely, false positives occur when mutations inadvertently disrupt protein folding or function through removal of a critical hydroxyl group (the difference between serine and alanine side chains); the risk of this is significant when mutations are simultaneously introduced at multiple phosphorylation sites.

Genetic replacement is a powerful tool for understanding the functional significance of phosphorylation events but it is low throughput and results need to be interpreted cautiously. Moreover, kinases frequently perform multiple functions, so it may be difficult to reconcile effects of kinase function (observed by inhibition) with a large number of phosphorylations (observed with replacement strategies for individual

substrates). Because of these considerations, I have sought intermediate tools to dissect specific kinase functions and to recover them with targeted re-introduction of activity.

In this dissertation, I utilize a chemical genetic complementation strategy that exploits the unique feature of the as-kinase system, namely the insensitivity of wildtype kinases to the bulky analog that inhibits the as-kinase (Figure 2.1B). For my kinase of interest, Plk1, I have created fusion constructs containing the catalytic domain of the wildtype allele tethered to proteins that localize to discrete regions within the cell (Figure 2.3A) and then individually introduced them into cells that express the as-allele (Figure 2.3B). Removal of the PBD prevents off-target binding of the fusion construct, ensuring localization to a discrete subcellular region.

The as-allele can be inhibited with the ATP analog, whereas the wildtype allele will remain active. Importantly, this activity will be restricted to the proximity of the substrate. In cells where an abnormal phenotype (*i.e.*, functional defect) is observed, the fusion construct is deemed to have failed complementation and Plk1 activity within that specific locale is considered unlikely to mediate that function (Figure 2.4, constructs A and C). Conversely, in cells where a normal phenotype is observed, the fusion construct is deemed to have complemented the as-allele, suggesting a functional role for Plk1 activity within that locale (Figure 2.4, construct B). This is termed phenotypic rescue. To increase the power of this activity partitioning approach, I have performed mass spectrometry analyses to identify the substrates targeted by each Plk1 localization construct. By combining the phosphoproteomic data with the functional data, I can

identify the phosphorylations (and substrates) that are most likely to mediate each function.

Conclusions

To summarize, the decision to use an analog-sensitive (AS) system to inhibit Plk1 activity enables the specificity and temporal control necessary to probe the functions of a mitotic kinase. Utilizing inhibitor titration allows for uncoupling of Plk1 activities that are conducted close in time. Additionally, my approach enables separable control of Plk1 alleles, providing the flexibility necessary to isolate specific activities and substrates localized at discrete regions within the cell.

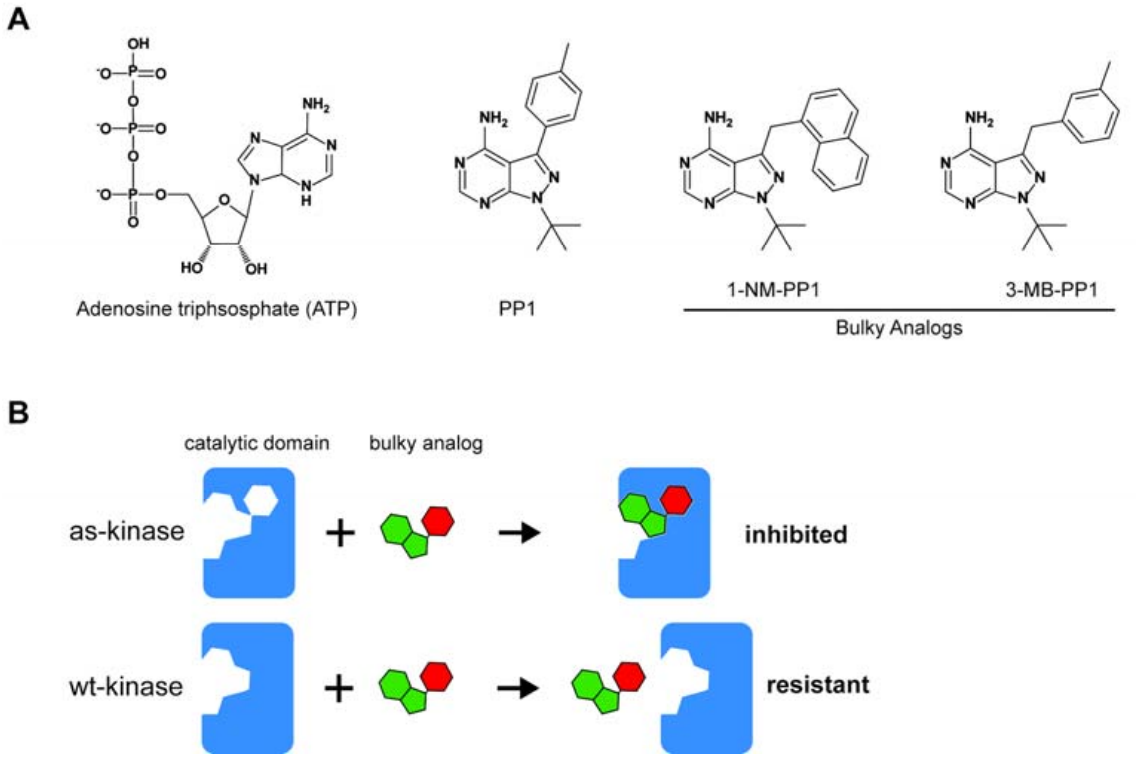

Figure 2.1. Chemical-genetic strategy for specific kinase inhibition

A, Chemical structures of Adenosine triphosphate (ATP), the Src inhibitor PP1, and its bulky analogs, 1-NM-PP1 and 3-MB-PP1. *B,* An enlarged ATP-binding pocket in the catalytic domain of the analog sensitive kinase (as-kinase) accommodates the analog, inhibiting activity, whereas the non-enlarged pocket of the wildtype kinase (wt-kinase) is resistant.

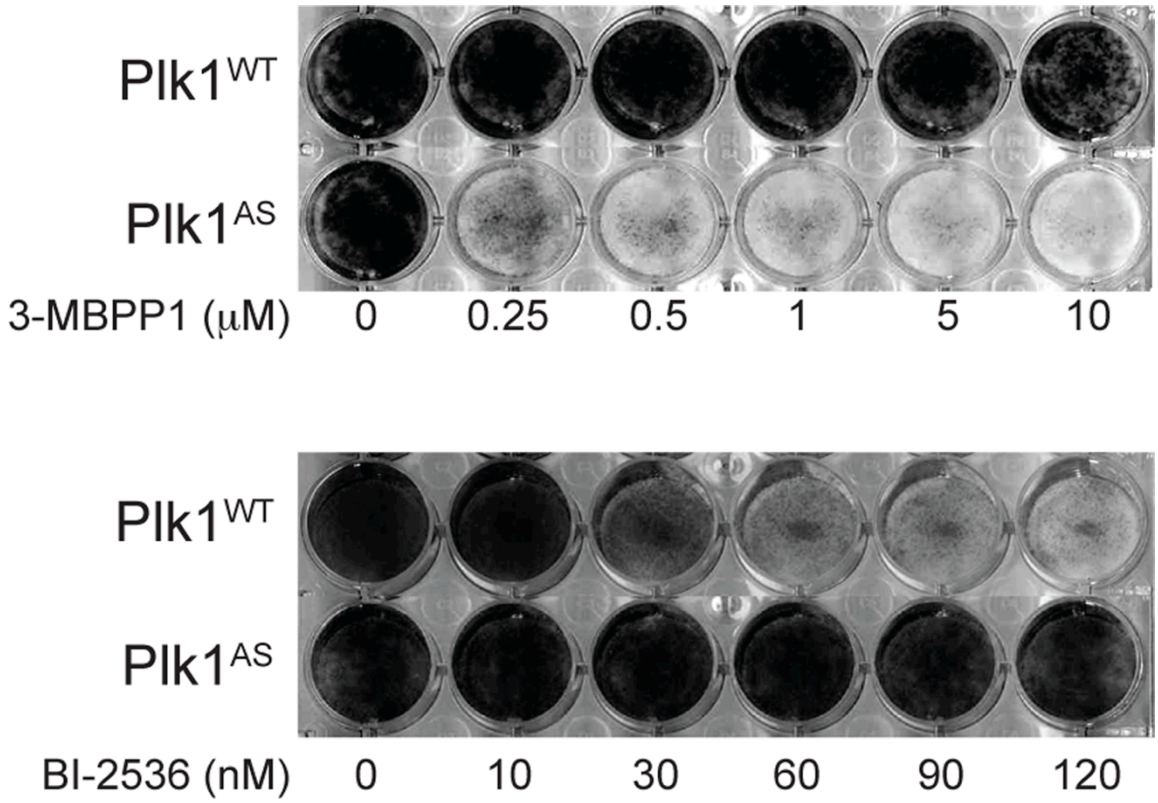

Figure 2.2. Allele-specific control of Plk1 in RPE1 cells

RPE1 cell lines expressing either the wildtype ($Plk1^{WT}$) or analog-sensitive ($Plk1^{AS}$) allele were seeded at low density in 24-well plates and grown for 6 days in increasing concentrations of the bulky ATP analog, 3-MB-PP1 (top) or the pharmacologic inhibitor of wildtype Plk1, BI-2536 (bottom). A crystal violet assay was then performed to detect viable cells.

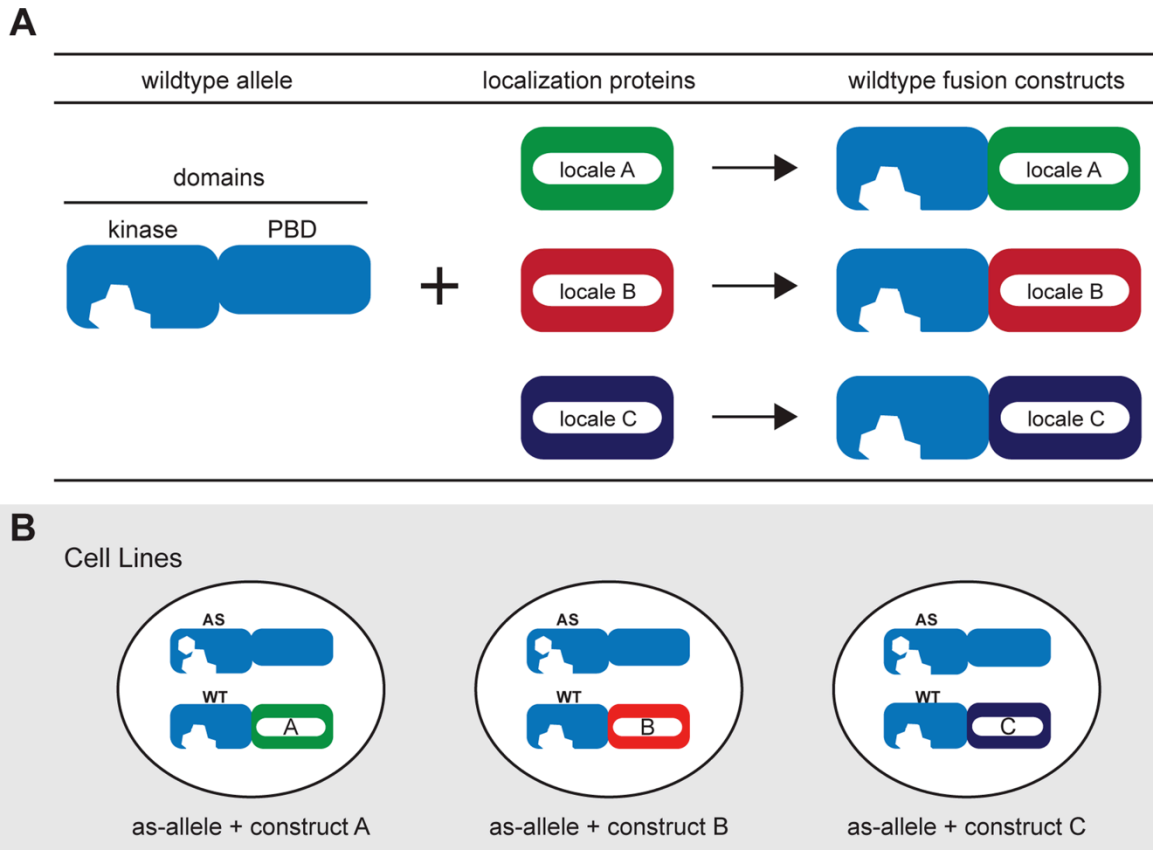

Figure 2.3. Chemical genetic complementation strategy to probe for functional Plk1 locales

A, Fusion constructs are generated by replacing the Polo-Box domain (PBD) of wildtype Plk1 (WT) with proteins that localize to discrete subcellular locales. *B*, Fusion constructs are introduced into cells expressing the analog-sensitive (AS) allele.

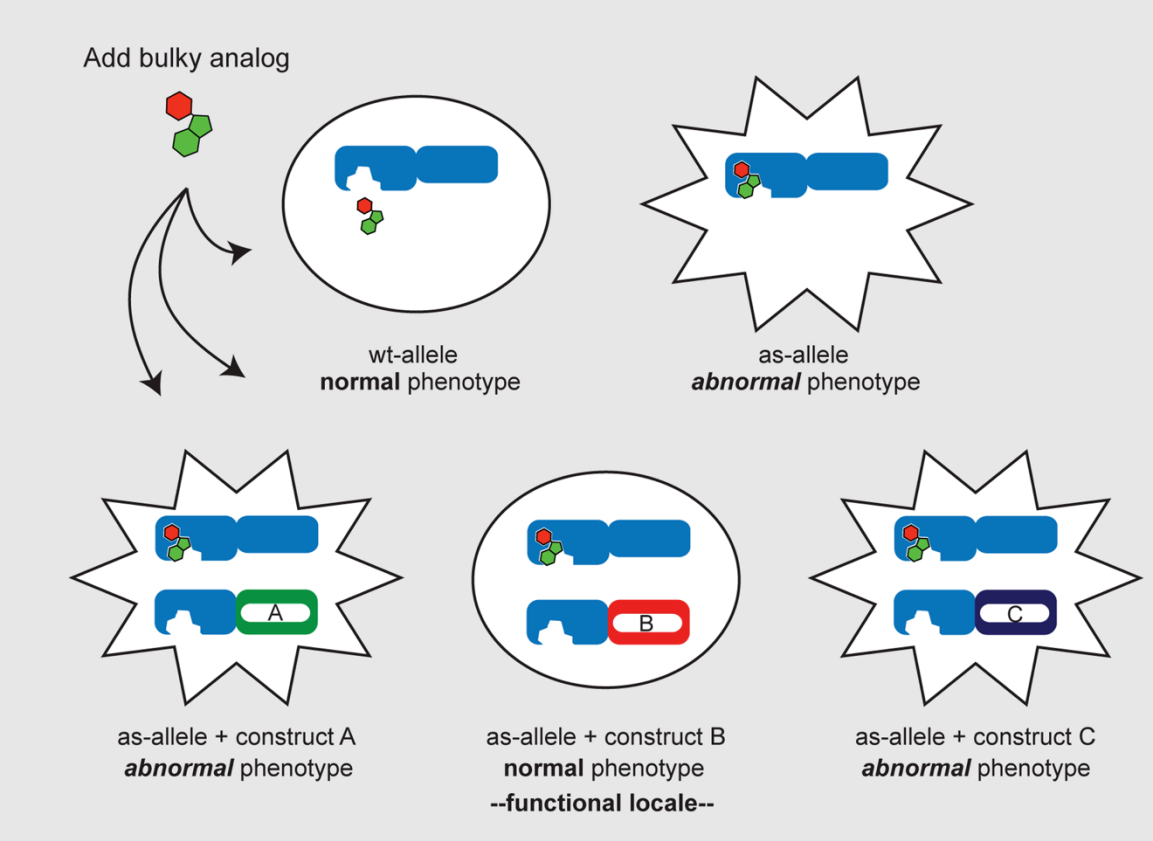

Figure 2.4. Assay for fusion construct complementation

Challenging cells with the ATP analog inhibits the Plk1^{as}-allele (AS), producing an abnormal phenotype (illustrated here as starburst cell shape). Note the wildtype (WT) allele is resistant to the analog, maintaining a normal phenotype. In cells expressing the fusion constructs, rescue of a normal phenotype suggests a subcellular locale important for Plk1 function and a starting point for identification of cognate substrates.

Chapter III—High Mitotic Activity of Polo-like kinase 1 is required for chromosome segregation and genomic integrity in human epithelial cells

---

Adapted from: Lera RF, and Burkard ME (2012) *J Biol Chem*, 287 (51), 42812-25.

Abstract

Protein kinases play key roles in regulating human cell biology, but manifold substrates and functions make it difficult to understand mechanism. We tested whether we could dissect functions of a pleiotropic mitotic kinase, Polo-like kinase 1 (Plk1) via distinct thresholds of kinase activity. We accomplished this by titrating Plk1 activity in RPE1 human epithelial cells using chemical genetics and verifying results in additional lines. We find that distinct activity thresholds are required for known functions of Plk1 including (from low to high activity): bipolar spindle formation, timely mitotic entry, and formation of a cytokinesis cleavage furrow. Subtle losses in Plk1 activity impair chromosome congression and produce severe anaphase dysfunction characterized by poor separation of chromosome masses. These two phenotypes are separable, suggesting that they stem from distinct phosphorylation events. Impaired chromosome segregation in anaphase is the most sensitive to modest loss in Plk1 activity. Mechanistically, it is associated with unpaired sister chromatids with stretched kinetochores, suggestive of merotelic attachments. The C-terminal PBD domain of Plk1 is required for its anaphase function, although it is dispensable for forming a bipolar spindle. The ultimate effect of partial inhibition of Plk1 is formation of micronuclei, increase in tetraploid progeny, and senescence. These results demonstrate that different thresholds of Plk1 activity can elicit distinct phenotypes, illustrating a general method for separating pleiotropic functions of a protein kinase, even when these are executed close in time.

Introduction

Polo-like kinase 1 (Plk1) is a key regulator of human mitosis. Its function is essential for multiple mitotic processes, including centrosome maturation, formation of a bipolar mitotic spindle, chromosome attachment, loss of cohesion between sister chromatids, and cytokinesis[53,112]. On a molecular level, Plk1 interacts with many of its substrates via its C-terminal Polo-box domain (PBD), a phosphopeptide-binding domain. Binding via the PBD requires substrates to be previously phosphorylated ('primed') by protein kinases such as CDK1, and can elicit positive feedback when Plk1 itself generates the PBD binding site[39,85]. The PBD binding provides a high local activity of Plk1 that allows it to phosphorylate substrate proteins and elicit its biologic functions.

Despite the importance of Plk1 in cell division, it is difficult to reconcile its mitotic functions with an expanding list of binding partners and substrates. Although hundreds of Plk1 interactors and substrates have been identified[90,113,114], strong links between function and substrates are established for only a handful. Compounding this difficulty, its activities occur almost exclusively within the ~60 minutes of mitosis, making it difficult to isolate individual functional events. A comprehensive understanding of Plk1 will require reconciliation of each mitotic function with its cognate phosphorylation event. Yet, this has been a challenging goal because the many functions of Plk1 are executed in a short interval of time.

We previously reported a chemical genetic system for specific interrogation of Plk1 in immortalized human retinal pigment epithelial (RPE1) cells[86]. In this system, loxP sites were introduced flanking exon 3 in one copy of *PLK1* and deleted from the other, generating a $PLK1^{flox/\Delta}$ conditional knockout cell line. An EGFP-tagged Plk1

construct was reintroduced followed by Cre-mediated excision of the flox-*PLK1* locus. In this manner, cells were reconstituted with wildtype Plk1 to create $Plk1^{wt}$ RPE1 cells, or by analog-sensitive Plk1 (C67V/L130G) to generate $Plk1^{as}$ RPE1 cells. In these cell lines, EGFP-$Plk1^{wt}$ and EGFP-$Plk1^{as}$ transgenes were expressed at similar levels to endogenously expressed Plk1; however, $Plk1^{as}$ was modestly elevated, possibly due to its decreased catalytic efficiency[86]. In the analog-sensitive cell line, $Plk1^{as}$ can be selectively inhibited by the bulky ATP-analog, 3-MB-PP1, resulting in loss of Plk1 functions with the expected phenotypes. Importantly, wildtype Plk1 is unaffected by 3-MB-PP1, allowing explicit controls for on- versus off-target effects[86,115]. Moreover, BI-2536, an inhibitor of wildtype Plk1 does not affect activity of $Plk1^{as}$, allowing these two functional alleles to be orthogonally controlled independently with these chemicals[110].

We previously used this system to identify the role of Plk1 in triggering cytokinesis concordant with late mitosis and identified the cognate molecular substrate, HsCyk4/RacGAP1[53,86]. This work demonstrates the power of chemical biology to rapidly and specifically inactivate an enzyme to resolve functions that are separable in time.

Here, we seek to extend the chemical genetic system to allow dissection of discrete kinase functions that are not separable in time. We hypothesized that kinase functions that occur close together may be separable by *activity thresholds*. In this model, distinct enzyme functions may be interrupted at different Plk1 thresholds due to differences in local kinase activity, in counteracting phosphatases, or in different phosphorylation requirements to elicit downstream functions. Indeed, we show here that careful titration of Plk1 activity in human cells undergoing mitosis reveals several

discrete functions that are separable at thresholds of Plk1 activity and, in one testable case, this threshold matches that of the cognate molecular phosphorylation.

We demonstrate the power of this method for dissecting pleomorphic enzymatic functions that are close in time and space. Moreover, the phenotypes observed with partial loss of function presage *in vivo* effects of Plk1-targeted drugs which will cross these thresholds of inhibition in human subjects at times dictated by pharmacology.

Results

We surveyed the thresholds of activity required for several known functions of Plk1 using synchronization strategies (Figure 3.1A) and a range of 3-MB-PP1 concentrations up to 10 μM. This maximum concentration was chosen because the observed phenotype matches the effects of knockdown, knockout, and antibody microinjection[86]. The survey of Plk1-dependent phenotypes revealed a graded effect in Plk1 function on mitotic entry (Figure 3.1B), bipolar spindle formation (Figure 3.1C), and formation of a cleavage furrow in anaphase (Figures 3.1D-E). Each Plk1-dependent phenotype had a distinct 50% inhibitory concentration (IC_{50}) ranging from 400 nM to 2.3 μM (Table 3.1). These results demonstrate that individual Plk1 functions are separable, as they have distinct thresholds for inactivation.

We hypothesized that the inhibitory concentration for molecular phosphorylation events will match that of the associated phenotypic events. To test this, we measured the known Plk1-dependent phosphorylation of HsCyk4/RacGAP1 at the spindle midzone, an event known to trigger cytokinesis (Figure 3.1E-F)[53,116]. Indeed, we found that the IC_{50} for HsCyk4 phosphorylation closely matches that seen for furrow formation

(0.36 vs. 0.40 μM). We conclude that graded inhibition of a kinase such as Plk1 can resolve and link individual sets of cognate molecular and biologic events.

To calibrate these biologic IC_{50}'s with biochemical inhibitory concentrations, we performed in vitro kinase assays using $Plk1^{as}$. Using a range of 3-MB-PP1 concentrations and 1μM total ATP, we measured biochemical IC_{50} of 0.15 μM (Figure 3.2). This allows us to estimate the residual kinase activity needed to elicit biologic functions (Table 3.1, right). The actual residual intracellular catalytic activity depends on local concentrations of Plk1, ATP, and the protein substrate, which may differ from that selected in our biochemical assay. However, if intracellular concentrations of these are uniform, relative values are as reported in Table 3.1.

Our survey revealed that spindle polarity is relatively insensitive to loss of Plk1 function (IC_{50} 2.3 μM, Fig 3.1B). This allowed us to evaluate detailed spindle-independent phenotypes associated with loss of Plk1 function. Previous work has demonstrated the presence of such spindle-independent Plk1 functions using other approaches[51,117]. To evaluate these in detail, we inhibited Plk1 at levels below this threshold and observed the effect on division of live cells by timelapse videomicroscopy (Figure 3.3A and Supplementary movies). Three phenotypes were observed: (i) Normal-appearing divisions (top), typically completed within an hour is seen frequently with 0 – 0.25 μM 3-MB-PP1. (ii) Mitotic arrest (bottom) is seen frequently at high levels of 3-MB-PP1, even when there is evidence of bipolar spindle formation. (iii) At intermediate levels of Plk1 inhibition, we observed a distinct phenotype, which we term 'impaired segregation.' These phenotypes were observed with frequencies that depended on level of Plk1 inhibition (Figure 3.3B). Importantly, these phenotypes are not due to an

off-target effect of 3-MB-PP1 or associated solely with Plk1^{as} cells; a similar phenotype was observed with RPE1 cells harboring wild-type Plk1 when interrogated with low levels of BI-2536, a pharmacologic inhibitor of wildtype Plk1[66,110], but no effect in this cell line was observed with the Plk1^{as}-specific inhibitor, 3-MB-PP1 (Figure 3.3B, Right). In addition to impaired chromosome segregation, we also found that chromosomes frequently aligned at the metaphase plate followed by loss of alignment (Figure 3.3A insets in 3rd and 4th row). This loss of alignment occurs with increasing frequency as 3-MB-PP1 is escalated. Again, controls demonstrate that this phenotype is specific to loss of Plk1 function as it was recapitulated with BI-2536 but not 3-MB-PP1 in cells with wildtype Plk1 (Figure 3.3C). We conclude that partial loss of Plk1 catalytic activity impairs chromosome segregation during mitosis in human cells.

Careful observation of cells with impaired segregation revealed additional abnormalities. In the most striking example, chromosomes congressed at the metaphase plate followed by loss of alignment and onset of anaphase with poor separation of chromosome masses (Figure 3.3A, 3rd row, time-point 64; Movie 3.S3). To characterize the misalignment and anaphase segregation defects, we analyzed cells by IF (Figure 3.4). We found that chromosomes frequently were misaligned (distinctly separated from midline-oriented chromosomes) on bipolar spindles at 0.5 and 1 μM 3-MB-PP1, but this was less common at concentrations <0.5 μM (IC_{50} 0.5 μM, Figure 3.4A). The number of misaligned chromosomes and their spindle position varied, but the severity increased with degree of Plk1 inhibition. In many cases, chromosomes appeared detached from microtubules, judged by α-tubulin staining, and remained paired, as indicated by the presence of two distinct CREST signals (Figure 3.4A,

arrowheads). We considered that this chromosome misalignment could simply reflect a delay in chromosome congression during prometaphase; however, timelapse videomicroscopy revealed a significant fraction of cells exhibit loss of chromosome alignment *after* initial midline congression (Figure 3.3C and Movie 3.S4). We conclude that maintenance of chromosome alignment requires high activity of Plk1.

Compared with chromosome misalignment in metaphase, impaired segregation in anaphase was more sensitive to loss of Plk1 function (Figure 3.4B). Anaphase chromosomes frequently lagged in as little as 0.125 μM 3-MB-PP1. Consistent with timelapse observations, impaired segregation is sometimes severe with a large number of chromosomes remaining at the midline spindle (Figure 3.4B, top right panel). We were nevertheless able to confirm that such cells were in anaphase due to both polar-oriented CREST signals and re-localization of Plk1 at the spindle midzone. Thus, among the phenotypes observed with loss of Plk1 function, the anaphase chromosome segregation is most sensitive to partial loss of function, suggesting the existence of a required substrate that is either not readily accessible to this kinase or is influenced by high local phosphatase activity.

To ensure that the anaphase segregation defect could be directly attributed to Plk1, we again analyzed cells with wildtype Plk1. As expected, BI-2536 but not 3-MB-PP1 elicited the segregation defect in cells with wildtype Plk1 (Figure 3.4C-D). This was not specific to any one subline as similar observations were obtained with both wildtype RPE1 cells (with endogenous Plk1) and $Plk1^{wt}$ cells ($PLK1^{-/-}$ knockout cells complemented with EGFP-$Plk1^{wt}$). Moreover, these findings were not specific to RPE1 cells as they were also observed in MCF-10A, MCF-7, and T47D cells (Figure 3.4D).

We conclude that anaphase chromosome missegregation is a directly related to loss of Plk1 activity.

We reasoned that impaired chromosome segregation could be attributable to either poor chromosome migration in anaphase A or to dysfunction of spindle elongation in anaphase B, which is known to require Plk1 function[84]. To distinguish these, we performed a detailed analysis of spindle elongation and chromosome segregation after partial impairment of Plk1 activity (Figure 3.5). Under these conditions, we were able to confirm anaphase and visualize other Plk1-dependent processes including its own localization to the spindle midzone and initiation of cytokinesis, consistent with the higher IC_{50} associated with these processes. As expected, we observed a shortening in average spindle length as was previously reported with complete inhibition of Plk1 at anaphase onset (Figure 3.5A-B)[84]. We next surveyed kinetochore position relative to poles (Figure 3.5C). Using this scheme we evaluated kinetochore position and spindle length in 12 $Plk1^{as}$ cells by spindle length for each condition: DMSO control and 0.25 μM 3-MB-PP1 (Figure 3.5D). As illustrated, chromosome laggards (0.8-1.0 fractional distance) were absent in control cells but present in the majority of cells after partial loss of Plk1 activity; no correlation was seen between presence of laggards and spindle length. We confirmed this finding by comparing 3 cells with similar spindle lengths (Figure 3.5E-F). This demonstrated that, even controlling for spindle length, there is impaired chromosome segregation to poles with Plk1 inhibition. We conclude that both chromosome segregation and spindle elongation are sensitive to modest losses of Plk1 activity.

Most known functions of Plk1 are dependent on a functional C-terminal PBD domain, which localizes the kinase activity to specific locales or substrates that are primed by phosphorylation, often by CDK1 or by Plk1 itself[39,51,113,114]. In the prevailing model, the PBD binds to substrates to generate a high local Plk1 concentration[39], although some kinase functions may not require the cis-acting PBD[51]. We considered that, in principle, PBD-dependent binding could buffer loss of Plk1 activity by providing a high local concentration. If so, the PBD-independent substrates may be exquisitely sensitive to partial Plk1 kinase inhibition because of the absence of this buffering activity. We therefore tested if the PBD is dispensable for chromosome segregation. To do this, we employed a chemical genetic complementation assay using either wildtype or a mutant PBD that is nonfunctional (PBD^{AA}; Figure 3.6A)[39,53]. We developed cell lines where $Plk1^{as}$ is complemented by a separate Plk1 allele with a wildtype kinase domain and either wildtype PBD or nonfunctional PBD^{AA}. We confirmed that both are expressed at similar levels and that the $Plk1^{AA}$ fails to localize to kinetochores and centrosomes as expected (Figures 3.6B-C). Next, we performed the rescue experiment. Whereas Plk1 with wildtype PBD readily rescued the anaphase missegregation phenotype, the allele with PBD^{AA} failed to rescue this activity (Figure 3.6C right, D). We conclude that the anaphase functions of Plk1 require its cis-acting PBD-localizing function and reject the hypothesis that its buffering activity is dispensable for sensitive substrates.

Hanisch and coworkers[51] reported that the PBD is not required for formation of bipolar spindles. We confirmed this result using complementation: Plk1 with the mutant PBD^{AA} is capable of preserving bipolar spindles (Figure 3.6E-F), even though this mutant fails to localize to centrosomes (Figure 3.6C). These results demonstrate that a

functional PBD is required to execute Plk1 functions that require high catalytic activities, but is dispensable for at least one function that requires only a small amount of activity.

We next considered four mechanisms by which loss of Plk1 function could impair chromosome segregation in anaphase (Figure 3.7, top). We first considered the possibility that anaphase was triggered prematurely due to an inactive mitotic checkpoint with partial loss of Plk1 activity (Figure 3.7A). The mitotic checkpoint has been proposed to detect chromosome attachment to microtubules and possibly inter-kinetochore tension[118]. We tested whether partial inhibition of Plk1 could interrupt the checkpoint by challenging cells with nocodazole, which precludes both attachment and tension. This revealed that loss of Plk1 activity does not impair activation of the mitotic checkpoint (not shown). Similarly, the checkpoint is active with Taxol, which activates the mitotic checkpoint by a more subtle effect of loss of attachment and/or tension on kinetochores (Figure 3.7A). We conclude that the mitotic checkpoint is intact with partial loss of Plk1 activity.

We turned to the possibility that lagging chromosomes arise from impaired DNA de-catenation on anaphase onset. During replication, sister chromatids become intertwined and these topologic links are sundered in mitosis by topoisomerase II[119]. When these links are not resolved, protein-coated, DNAse-sensitive ultrafine bridges can be observed in anaphase. Plk1 has a possible function in resolving DNA catenation because it is known to regulate both topoisomerase II and PICH (Plk1-interacting helicase), which is found on ultrafine bridges[81,120]. To test this, we treated cells with either 3-MB-PP1 or ICRF-193, an inhibitor of topoisomerase II (Figure 3.7B). For each, we quantified anaphase cells with ultrafine bridges, detected through staining of the

Bloom helicase (BLM)[121]. As expected, ICRF-193 frequently yielded lagging anaphase chromosomes with BLM-coated bridges. In contrast, 3-MB-PP1-induced laggards rarely harbored ultrafine bridges. Similar results were obtained when visualizing ultrafine bridges with an antibody detecting PICH (not shown). We conclude that partial loss of Plk1 activity does not impair resolution of DNA catenation.

In budding yeast, the polo-kinase homolog, Cdc5, phosphorylates cohesin subunits at kinetochores, promoting its removal upon anaphase onset[122]. We considered the possibility that loss of Plk1 activity impairs cohesin removal for some sister chromatid pairs. To test this, we evaluated CREST signals from kinetochores to determine if they were singlet or doublet by comparing with paired signals seen in prometaphase (Figure 3.7C). We found that signals on lagging chromosomes were single, demonstrating successful separation of sister chromatids in anaphase. This is consistent with the finding that phosphorylation of cohesin subunits by Plk1 is dispensable for its cleavage by separase in human cells[71].

Finally, we considered the possibility that partial inhibition of Plk1 induces merotelic attachments of a single kinetochore to both spindle poles. Merotelic attachments arise when a single kinetochore is simultaneously linked to both spindle poles, precluding its migration to either pole at anaphase onset. Although difficult to observe directly, merotelic attachments can be identified by stretching of a kinetochore, which occurs in anaphase as it is pulled simultaneously to both spindle poles[123]. To test this, we measured width of CREST signals on lagging kinetochores and compared with nocodazole washout, which increases lagging chromosomes and merotelic attachments[124] (Figure 3.7D). We observed an increased number of stretched

kinetochores on lagging chromosomes with 0.25 μM 3-MB-PP1, matching the effect of nocodazole washout. We conclude that Plk1 function may be important for resolving merotelic chromosome attachments.

Several Plk1 inhibitors are in clinical development for anticancer therapy[125,126]. In clinical studies, mitotic arrest and abnormal spindle structure are classically used to determine whether Plk1 is actually inhibited *in vivo*. However, treatment doses will frequently result in partial inhibition of Plk1; even at high drug doses this is virtually unavoidable given pharmacologic drug metabolism and washout. We therefore sought to determine the ultimate fate of human cells that encounter partial loss of Plk1 activity. To do this, we challenged $Plk1^{as}$ cells or matched $Plk1^{wt}$ cells with 24-48h treatment of 0.25 μM 3-MB-PP1 and 45 nM BI-2536 (which provides similar effects of inhibition; Figure 2.3B). We immediately identified a large number of cells with abnormal nuclear morphologies, when Plk1 was inhibited (Figure 3.8A). This included not only micronuclei as noted previously[117] but also lobed, binucleate, and multinucleate cells (Figure 3.8A right, not shown). Again, this phenotype was specific to inhibition of Plk1 rather than an off-target effect: similar nuclear morphologies were seen in $Plk1^{wt}$ cells when challenged with BI-2536 but not with 3-MB-PP1. Moreover, blocking cell cycle progression with thymidine reduced the effect, consistent with it being the result of an abnormal prior mitosis.

Based on the findings above, we suspected a loss in genomic integrity in normal cells that traverse mitosis with partial loss of Plk1. To evaluate this directly, we made chromosome spreads of cells that experienced reduced Plk1 during proliferation for 48 hours. This revealed a large increase in tetraploid cells (Figure 3.8B), consistent with

the observation of lobed and binucleated cells and the prior observations of failed cytokinesis. Thus, modest losses of Plk1 activity result in loss of genomic integrity with formation of tetraploid progeny, consistent with failed cytokinesis.

To observe the ultimate effect of persistent partial loss of Plk1 function, we treated Plk1^{as} cells for up to 12 days with 3-MB-PP1 (Figures 3.8C-D). This revealed interruption of cell proliferation and stable cell number over the entire time observed (Figure 3.8C). Morphologically, cells were often enlarged, granular, binucleate, and demonstrated pH-dependent β-galactosidase activity, consistent with senescence (Figure 3.8D). Thus, partial loss of Plk1 function can have significant effect on viability of nonmalignant human cells, leading to impaired chromosome segregation, secondary failure of cytokinesis, and loss of genomic integrity, and senescence. This can occur in spite of normal spindle structure and minor mitotic delays. We conclude that mitotic arrest and spindle morphologies are insensitive biomarkers of Plk1 inhibition.

Discussion

It is difficult to decode complex intracellular signaling networks that regulate homeostasis and proliferation of human cells. Yet such a comprehensive understanding is required to rationally utilize enzymatic inhibitors for medical therapy. In cancer, antimicrotubule antimitotics represent a validated therapeutic paradigm; yet less success has been realized to date with newer inhibitors of mitotic protein kinases. One proposed reason for this is that newer antimitotic drugs have an all-or-none effect, rather than a graded effect observed with antimicrotubule agents such as Taxol[127]. This is not true for Plk1; we demonstrate here that Plk1 inhibition, like Taxol, exhibits a

graded effect. Indeed such concentration-dependent effects of a Plk1 inhibitor have been reported, with differences in spindle structure and mitotic index as a function of inhibitor concentration[117]. This may support the hypothesis that a graded effect is desirable for anticancer therapy since promising results have been reported in a recent Phase I clinical study of the Plk1 inhibitor, BI-6727[126].

Activity thresholds. Our results support a model in which different thresholds of Plk1 activity are required to execute discrete functions that occur throughout mitosis (Figure 3.9). Accurate chromosome segregation in anaphase is the most sensitive function related to loss of Plk1 activity. Additional functions require lower levels of residual Plk1 activity for proper execution.

Isolating kinase functions with thresholds may assist identification of substrates that elicit these functions. One current strategy to isolate Plk1 functions utilizes cell synchronization to separate mitosis into early, middle and late stages. However, synchronization has limitations. For example, releasing cells from a nocodazole block generates lagging chromosomes[124], potentially obscuring effects of Plk1 inhibition.

Our findings indicate that Plk1 functions are separable by careful inhibitor titration (Figure 3.9, Table 3.1) to permit isolation of functions in an asynchronous cell population. Notably, we have observed concordance between the Plk1 activity required for cleavage furrow formation and phosphorylation of HsCyk4 (Figure 3.1E), suggesting a link between biologic function and cognate molecular phosphorylation. Considering the numerous substrates reported for individual Plk1 functions (some shown in Figure 3.9), we propose to use activity thresholds to identify the relevant substrate associated with each.

Using thresholds to isolate functional kinase activities has limitations. First, it will not be able to isolate mitotic functions that require minimal kinase activity (Darkly shaded regions of Figure 3.9). Second, it is possible that the activity threshold for some phenotypes could depend on the assay selected. For example, an assay that detects more subtle errors in anaphase chromosome segregation might yield a lower IC_{50} for this phenotype than we report. This observer effect may be less for robust assays of readily detected dichotomous phenotypes (e.g. spindle polarity). Finally, although we identify cell senescence as a late effect of partial loss of Plk1 activity, we cannot definitively ascribe this to the observed mitotic defect, as a more subtle effect not directly visualized could lead to loss of cell viability.

The role of the PBD. It is interesting to speculate on why nature would link a kinase to a C-terminal phosphopeptide-binding module, the PBD. The PBD domain detects an upstream signal allowing the kinase activity to be recruited at high local concentration. This recruited kinase, in turn, can phosphorylate multiple adjacent proteins, although usually at sites different from the PBD docking site. In effect, Plk1 is a mitotic signal transducer and amplifier, which allows weak upstream molecular signals to be converted into substantial increases in local phosphorylation to mediate major events in cell division. This can even be auto-amplification if the upstream signal is generated by Plk1 itself, as occurs in late mitosis[53,128]. Given this view, it is perhaps unsurprising that transducer/amplifier Plk1 is involved in a multitude of mitotic functions or that many Plk1 functions require a functional PBD. Moreover, our observation that Plk1 functions require different activity thresholds suggests that different degrees of signal amplification are required for each functional event.

Yet, not all Plk1 functions are mediated through a functional PBD (see orange versus yellow boxes in Figure 3.9). Prior studies with dominant-negative PBD expression[51] or competitive PBD binding[129] have demonstrated abnormal chromosome congression, but normal spindle formation. Here we confirmed that the PBD is dispensable for spindle function, suggesting that the Plk1-dependent substrate required to form a bipolar spindle is readily accessible, and is isolated from phosphatases or requires little phosphorylation to elicit spindle bipolarity. Moreover, it suggests that the spindle function of Plk1 might not be mediated by a substrate localized at the centrosome. The substrate could be, for example, a plus-end directed motor required to maintain spindle polarity. If so, the centrosome-localized pool of Plk1 may have a more obscure function, or may simply represent a reservoir of kinase; this idea is supported by the recent discovery that Plk1 function requires dynamic relocalization from the centrosome[130].

In contrast to the effect on spindle polarity, a functional PBD is essential for cells to accurately congress and segregate chromosomes even though these functions can be readily blocked with modest inhibition of Plk1. Thus the PBD domain appears to provide a high local activity of Plk1 to overcome phosphatases and saturate substrates. We speculate that PBD-dependent functions of Plk1 on chromosome congression and segregation emanate from kinetochores, a complex zone of activities of overlapping kinases and phosphatases in which high local kinase activity may be required to elicit effects.

Anaphase function of Plk1. We demonstrate here that Plk1 has a function in chromosome segregation in anaphase. Indeed this function is distinct from the spindle-

elongation defect described previously[84]. Moreover, we and others did not observe impaired chromosome segregation when Plk1 was inhibited specifically upon anaphase onset[84,86,87]. This suggests that the observed anaphase phenotype is related to an earlier mitotic event that requires a high level of Plk1 activity. This is not related to the effect on the mitotic checkpoint or impaired resolution of sister chromatid cohesion or DNA topology. However, the stretched CREST signals at kinetochores suggests merotelic attachment as a likely mechanism[123,131]. Intriguingly, Aurora B, a known mediator of resolving merotelic attachments, has recently been described as a direct activator of Plk1 at the centromere/inner-kinetochore[43]. Moreover, improper syntelic attachments due to kinetochore dysfunction have been reported with Polo depletion in Drosophila S2 cells[132]. These observations suggest a number of intriguing possibilities, but it remains unclear how Plk1 might mediate resolution of merotelic microtubule attachments.

Aside from merotely, weak chromosome attachment is an important alternative explanation for the observed missegregation of chromosomes seen in anaphase. Plk1 is known to mediate stable kinetochore-microtubule attachment in part through phosphorylation of BubR1[58,133]. Consistent with this, misaligned chromosomes are often seen with partial inhibition of Plk1 (Figure 3.3A-C and 3.4A), as expected from the known function of Plk1 promoting stable end-on attachments[58,66]. However, we do not believe that poor kinetochore-microtubule attachment is sufficient to explain poorly segregated anaphase chromosomes. First, residual Plk1 activity is sufficient to silence the mitotic checkpoint and allow cells to proceed into anaphase, suggesting adequate attachment of all kinetochores. Second, poor chromosome congression at the

metaphase plate is a characteristic feature of poor kinetochore-spindle attachment, yet the threshold for this phenotype is distinct from that of impaired anaphase segregation (0.5 vs. 0.2 μM; Figure 3.4A-B). For these reasons, the anaphase phenotype is unlikely to be a product of unstable kinetochore-microtubule attachment.

Clinical implications. We demonstrate here that low levels of Plk1 inhibition lead to loss of genomic integrity. This occurs with the development of micronuclei which can lead to chromosome pulverization and chromothripsis[134]. However, the primary abnormality observed at the chromosome is development of tetraploid progeny, which are known to lead to subsequent chromosome instability[5]. Loss of Plk1 activity can therefore allow progression through a bipolar mitosis, albeit abnormally, and result in loss of genomic integrity and cell senescence.

These results have important implications in the clinical development of Plk1 inhibitors. First, pharmacokinetic endpoints for Plk1 inhibitors should include chromosome segregation errors, which appears to be the most sensitive phenotype related to partial loss of Plk1 function. Second, under some conditions Plk1 inhibitors may lead to a loss of genomic integrity in proliferating healthy cells, similar to classic chemotherapies and radiation, and (unless prevented by senescence) latent second malignancies are a consideration when Plk1 inhibition is used as a component of curative therapy. Third, the therapeutic window for cancer therapy could depend markedly on drug pharmacology as complete Plk1 loss of function for short times (e.g. intravenous dosing with short half-life drug) may produce remarkably different effects than achieved with partial Plk1 loss of function for extended times (e.g. low-dose continual oral dosing of long half-life drug).

Conclusions. A major strength of our study is the use of chemical genetics with explicit controls to ensure that phenotypes are linked to Plk1 inhibition. Although we confirmed similar phenotypes in other cell lines, we cannot rule out the possibility that the relative order of Plk1 activity thresholds may be cell line dependent. This may occur both because of various levels of Plk1 expression, differences in activity of wildtype versus analog sensitive Plk1 alleles, and different intracellular phosphatase activities. Despite limitations, we are able to demonstrate that it is possible to dissect the multiple functions of a kinase through activity thresholds.

In sum, we demonstrate that different thresholds of Plk1 activities are required to execute each specific biologic function of this kinase. We anticipate that this will allow dissection of Plk1 functions and ultimately provide a detailed understanding of how the many substrates of Plk1 mediate its functions in human cell division. Chemical genetics can separate functions in both time and concentration threshold, allowing dissection and mechanistic interrogation of discrete functions of a multifunctional kinase.

Materials and Methods

Cell culture procedures. All cell lines were propagated at 37°C and 5% CO_2 in media supplemented with 10% fetal bovine serum and 100 units/mL penicillin-streptomycin, except MCF-10A cells which were propagated as previously reported[135]. T47-D, hTert-RPE1 (ATCC, Manassas, VA) and RPE1-derived cell lines were propagated in a 1:1 mixture of DMEM and Ham's F-12 medium supplemented with 2.5 mM L-Glutamine. MCF-7 cells were propagated in DMEM supplemented with 4 mM L-Glutamine, 4500 mg/L glucose and 10 μg/mL insulin.

EGFP-Plk1^{as} and EGFP-Plk1^{wt} RPE1 cell lines were previously reported[86]. Plk1^{as} cell lines stably expressing mCherry-Plk1^{wt} constructs with a wild-type (AS/WT) or "pincer mutant" (AS/AA) PBD were derived as reported[53] and clones were obtained by limiting dilutions using 0.4 µg/mL G418 for selection.

To assay cell proliferation with prolonged Plk1 inhibition, 25,000 Plk1^{as} cells were plated in individual wells of 12-well plates, allowed to acclimate for 24 hours and then challenged with DMSO or 0.25 μM 3-MB-PP1 for up to 12 days. Media was replaced every four days. Adherent and non-adherent cells were collected every 24 hrs, incubated with Trypan Blue to exclude dead cells and counted with a hemacytometer. Counts were performed in duplicate and averaged. Cellular senescence was assayed using a pH-dependent β-galactosidase staining kit (Cell Signaling) according to manufacturer's instructions.

Immunoblotting, Immunoprecipitation and Kinase Assays. For immunoblotting, cells were lysed in buffer (50 mM HEPES pH 7.5, 100 mM NaCl, 0.5% NP-40, 10% glycerol) containing phosphatase inhibitors (10 mM sodium pyrophosphate, 5 mM β-glycerolphosphate, 50 mM NaF, 0.3 mM Na_3VO_4), 1mM PMSF, 1x protease inhibitor cocktail (Thermo-Scientific) and 1 mM dithiothreitol. Proteins were separated by SDS-PAGE, transferred to Immobilon PVDF membrane (Millipore), and blocked for 30 min in 4% milk and 0.1% Tween-20 Tris buffered saline ph 7.4 (TBST+milk). Membranes were incubated with gentle agitation for 2 hours at room temperature with primary antibodies diluted in TBST+milk, washed 3x with TBST, incubated for 1 hour at room temperature in secondary antibodies conjugated to horse radish peroxidase in TBST+milk.

Membranes were washed and developed with luminol/peroxide (Millipore) and visualized with film.

For immunoprecipitation and *in vitro* kinase assays, RPE1 cells expressing EGFP-Plk1^{as}, EGFP-Plk1^{wt}, or untagged Plk1 were incubated with nocodazole for 16 hours. Whole cell extracts were incubated with EGFP antibody (Invitrogen) at a concentration of 1μg antibody/1 ml total protein in lysis buffer for one hour on ice. EGFP-bound Plk1 was immunoprecipitated using protein A and protein G sepharose beads (GE Healthcare) in a 1:1 ratio for two hours at 4°C with gentle rotation. Beads were washed three times with lysis buffer, once with kinase buffer (20 mM Tris, pH 7.4, 10 mM $MgCl_2$, 50 mM KCl, 1 mM dithiothreitol), and then incubated in kinase buffer plus 5 μg casein, 1 μM ATP, 50 μCi [γ-^{32}P] ATP and 3-MB-PP1 for 30 minutes at 30°C. ^{32}P incorporation was observed by SDS-PAGE and Typhoon TRIO imager (GE Healthcare) and quantified using ImageJ[136].

Immunofluorescence (IF) and Microscopy. For *IF*, cells were seeded on glass coverslips in 24-well plates and fixed with 100% ice-cold methanol (centrosomal and central spindle epitopes) for 15 min to overnight or 4% paraformaldehyde in PBS (all other epitopes) for 10 min. Fixed cells were then blocked for 30 min in 3% bovine serum albumin (BSA) and 0.1% Triton X-100 in PBS (PBSTx+BSA). Primary antibodies were incubated in PBSTx+BSA for 1 hr at room temperature, washed 3 times in PBSTx, followed by secondary antibody incubation in PBSTx+BSA for 30 min at room temperature and two washes with PBSTx. Cells were counterstained with DAPI and mounted on glass slides with Prolong Gold anti-fade medium (Invitrogen) and allowed to cure overnight.

Image acquisition was performed on a Nikon Eclipse Ti inverted microscope equipped with 10x, 20x, 40x and 100x objectives, temperature-controlled motorized stage with 5% CO_2 support (In Vivo Scientific), and CoolSNAP HQ2 CCD camera (Photometrics). Optical sections were taken at 0.2-μm intervals and deconvolved using Nikon Elements. Where appropriate, the observer was blinded to treatment condition during image acquisition and analysis. For live cell imaging, cells were seeded in 35-mm glass-bottom plates and incubated with media containing DMSO, 3-MB-PP1 or BI-2536 for 1 hr prior to imaging in 5% CO_2 at 37°C. Images were processed and analyzed using Nikon Elements. Panels were cropped using Photoshop CS5 (Adobe) and assembled with overlays using Illustrator CS5 (Adobe).

Calculations and statistics. IC_{50} calculations were performed using BioDataFit 1.02 (Chang Bioscience) using an exponential decay model. Replicate experiments were performed and standard errors are reported as indicated below. Statistical evaluations were performed using Excel (Office 2008, Microsoft) or Mstat (http://www.mcardle.wisc.edu/mstat/). Two-tailed t-tests or Wilcoxon Rank sum tests were used to estimate the likelihood that the observed difference was obtained by chance. No corrections were made for multiple hypothesis testing.

Chemicals and antibodies. Chemicals used in this study include monastrol (100 μM, Tocris), nocodazole (0.2 mg/mL, EMD Biosciences), thymidine (2.5 mM, EMD), ICRF-193 (Enzo Life Sciences), 3-MB-PP1 (Toronto Research Chemicals), and BI-2536 (gift of P. Jallepalli). Antibodies used in this study were β-actin (AC-15, Abcam) 1:15,000; BLM (C-18, Santa Cruz) 1:500; CREST (Immunovision) 1:2500; HsCyk4/RacGAP1 (Genetex) 1:375; DsRed (detects m-Cherry, Clontech) 1:1000; Plk1

(F-8, Santa Cruz) 1:500; α-tubulin (YL1/2, Millipore) 1:1000; γ-tubulin (GTU-88, Thermo Scientific) 1:250. Antibodies against pS170 of Cyk4 were developed as previously reported[53]. Alexa-fluor (Life Technologies) secondary antibodies were used at 1:350.

Acknowledgements

We thank B. Weaver and R. Blank for critical reading of the manuscript, P. Jallepalli for sharing BI-2536, A. Mastrocola and members of the Burkard and Weaver labs for helpful discussions. This work was supported by the Flight Attendant Medical Research Institute 062541_YCSA and NIH grant R01 GM097245 to MEB. Additional support was obtained from the NIH CTSA program of the NCATS 9U54TR000021 (K award to MEB) and from P30 CA014520 (support for RL).

Figures and Tables

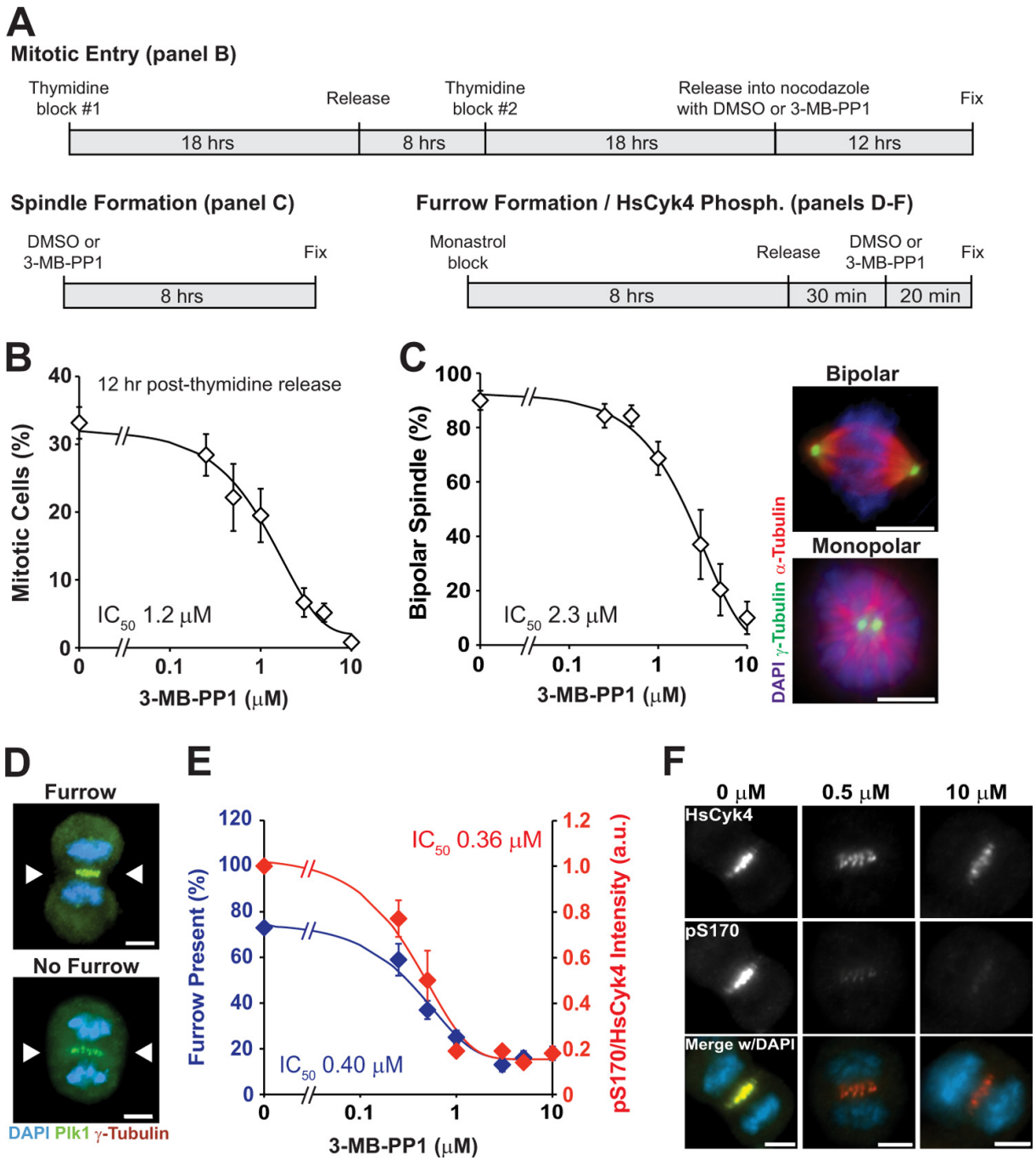

Figure 3.1. Individual Plk1 phenotypes have distinct thresholds of inactivation

RPE-Plk1^{as} cells were challenged with DMSO (0 μM) or 3-MB-PP1 (0.25, 0.5, 1, 3, 5, 10 μM) to determine the IC_{50} for mitotic entry (B), bipolar spindle formation (C), cleavage furrow formation and HsCyk4 phosphorylation (D-F). *A,* Experimental Schemas– Synchronization schemes used to assess phenotypes. *B,* Mitotic Entry– cells were synchronized in S-phase using a double-thymidine block. Upon release, DMSO or 3-MB-PP1 was added to the media with nocodazole (to prevent mitotic exit). After 12 hours, cells were fixed and stained with Hoescht 33258 to visualize nuclei. Percentage of mitotic cells was plotted for each concentration (n=600 cells, 2 independent experiments) to determine the IC_{50}. Data represent averages ± SEM. *C,* Bipolar spindle formation– asynchronously growing cells were challenged with DMSO or 3-MB-PP1 for 8 hours and fixed for IF. Percentage of pre-anaphase mitotic cells exhibiting a normal bipolar spindle was plotted for each concentration (n=300 cells, 3 independent experiments) to determine the IC_{50}. Data represent averages ± SEM. Representative images of cells exhibiting a normal bipolar or monopolar spindle are displayed. Other abnormal spindle structures (i.e. multipolar and unfocused bipolar spindles) were observed infrequently and are not depicted here. *D-F,* Cleavage furrow formation and HsCyk4 phosphorylation– cells were synchronized in prometaphase with a monastrol block, released into fresh media for 30 min to allow cells to enter anaphase, and then challenged with DMSO or 3-MB-PP1 for 20 min prior to fixation. *D*, Late anaphase cells were scored for the presence (top) or absence (bottom) of a cleavage furrow (arrowheads). *E*, Graph indicating the percentage of cells exhibiting a cleavage furrow (blue plot, n=300 cells/concentration) and the ratio of phosphorylated (pS170) to total

HsCyk4 intensity (red plot, n=100 cells/concentration). Data represent averages from 3 independent experiments ± SEM. *F,* Representative images of single optical z-sections through cells demonstrating decreased serine 170 phosphorylation (pS170) with increasing Plk1 inhibition as compared to total HsCyk4 intensity. Scale bars, 5 μm.

Phenotype	IC_{50} 3-MB-PP1 (μM)	% Residual Activity[a]
Bipolar spindle formation	2.3	0.4
Mitotic entry	1.2	0.7
Chromosome congression	0.50	11
Formation of cytokinesis furrow	0.40	16
Chromosome segregation	0.21	38

Table 3.1. IC_{50} values for various phenotypes associated with loss of Plk1 activity

[a] *In vitro* inhibition with 1 μM total ATP. For higher intracellular ATP concentrations, absolute residual activities will be greater but the order will be the same.

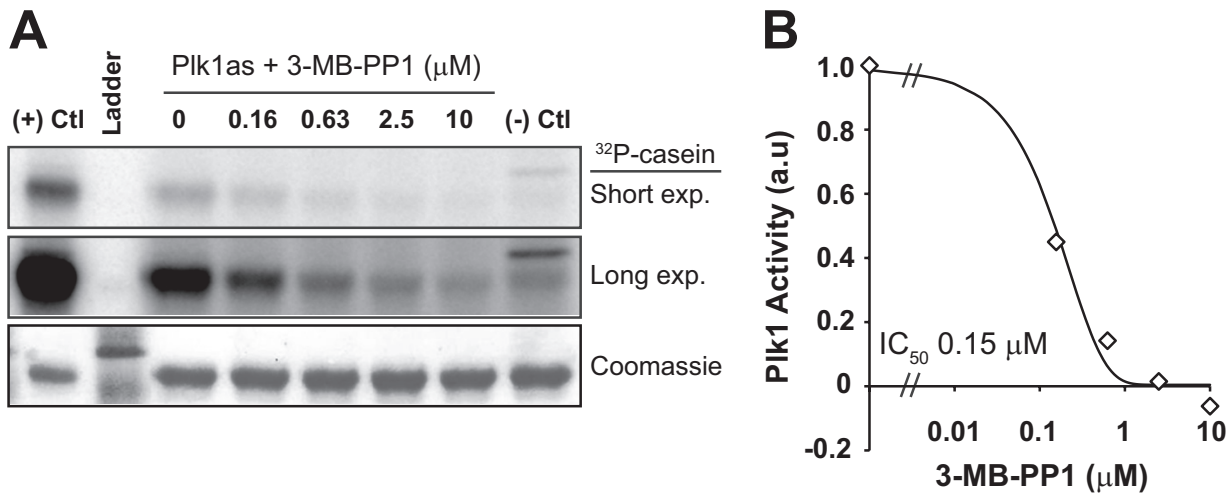

Figure 3.2. Plk1^{as} activity is inhibited by 3-MB-PP1

A, Plk1 was immunoprecipitated from mitotic extracts of RPE1 cells expressing EGFP-Plk1^{as}, EGFP-Plk1^{wt} (positive control), or untagged Plk1 (negative control) using an EGFP antibody and then incubated with casein and [γ-^{32}P] ATP. Where indicated, 3-MB-PP1 was added to the reactions. *B,* Plk1^{as} activity was quantified by casein labeling relative to Plk1^{as} reactions without inhibitor and plotted to determine the IC_{50}.

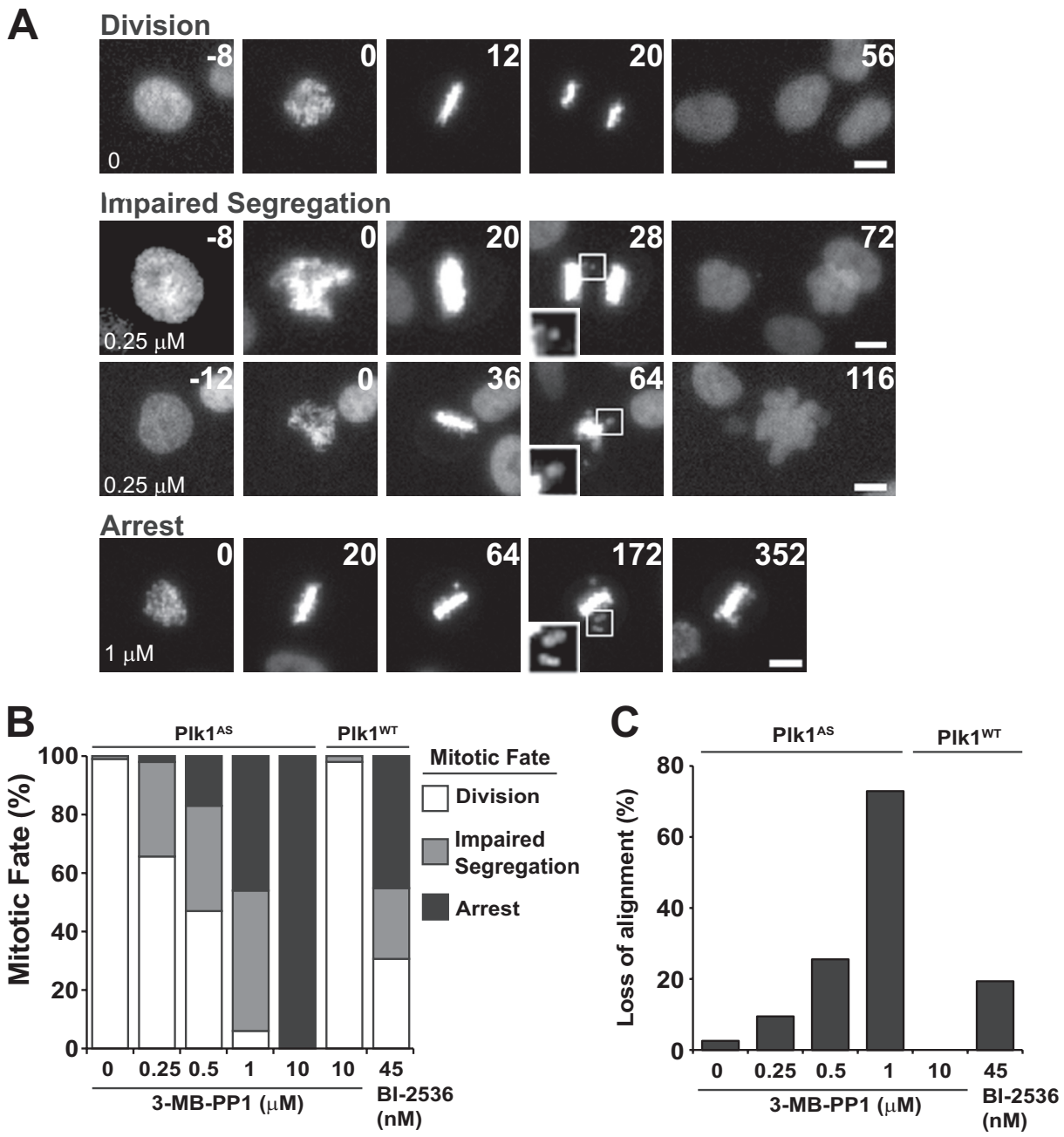

Figure 3.3. Live-cell imaging reveals partial loss of Plk1 activity results in impaired chromosome alignment and segregation

To visualize chromosome movements during mitosis, mCherry-tagged histone 2B (H2B) was expressed in Plk1^{as} and Plk1^{wt} cells. Cells were challenged with DMSO, 3-MB-PP1

or BI-2536 and observed for 10 hours at 4-minute intervals using timelapse videomicroscopy. *A,* Still frames from timelapse movies (*Supplemental Movies S1-S4*) highlighting three observed mitotic fates: a clear separation of chromosomes during anaphase ('Division', top row), anaphase with a few lagging chromosomes (second row, see inset frame 28) or frank failure to separate chromosome masses (third row, see inset frame 64), collectively termed 'Impaired Segregation', and a sustained (≥ 240 min) pre-anaphase mitotic arrest ('Arrest', bottom row). 3-MB-PP1 concentrations indicated in first frame. Time in minutes after nuclear envelope breakdown is shown at upper right. Scale bars, 5 μm. *B*, Cumulative frequency of mitotic fates observed in *A* (n=30-80 cells/concentration). Note $Plk1^{wt}$ cells are resistant to the effects 3-MB-PP1 (> 90% Division with 10 μM exposure), but sensitive to the pharmacological inhibitor BI-2536 (< 40% Division with 45 nM exposure). *C*, Chromosomes frequently lost alignment after initial midline congression (compare inset from frame 172 with frame 20 in 'Arrest', panel *A*). The frequency of cells exhibiting loss of chromosome alignment after establishing midline congression was recorded for each concentration (as in *B*). $Plk1^{as}$ cells challenged with 10 μM 3-MB-PP1 are excluded because initial midline congression did not occur.

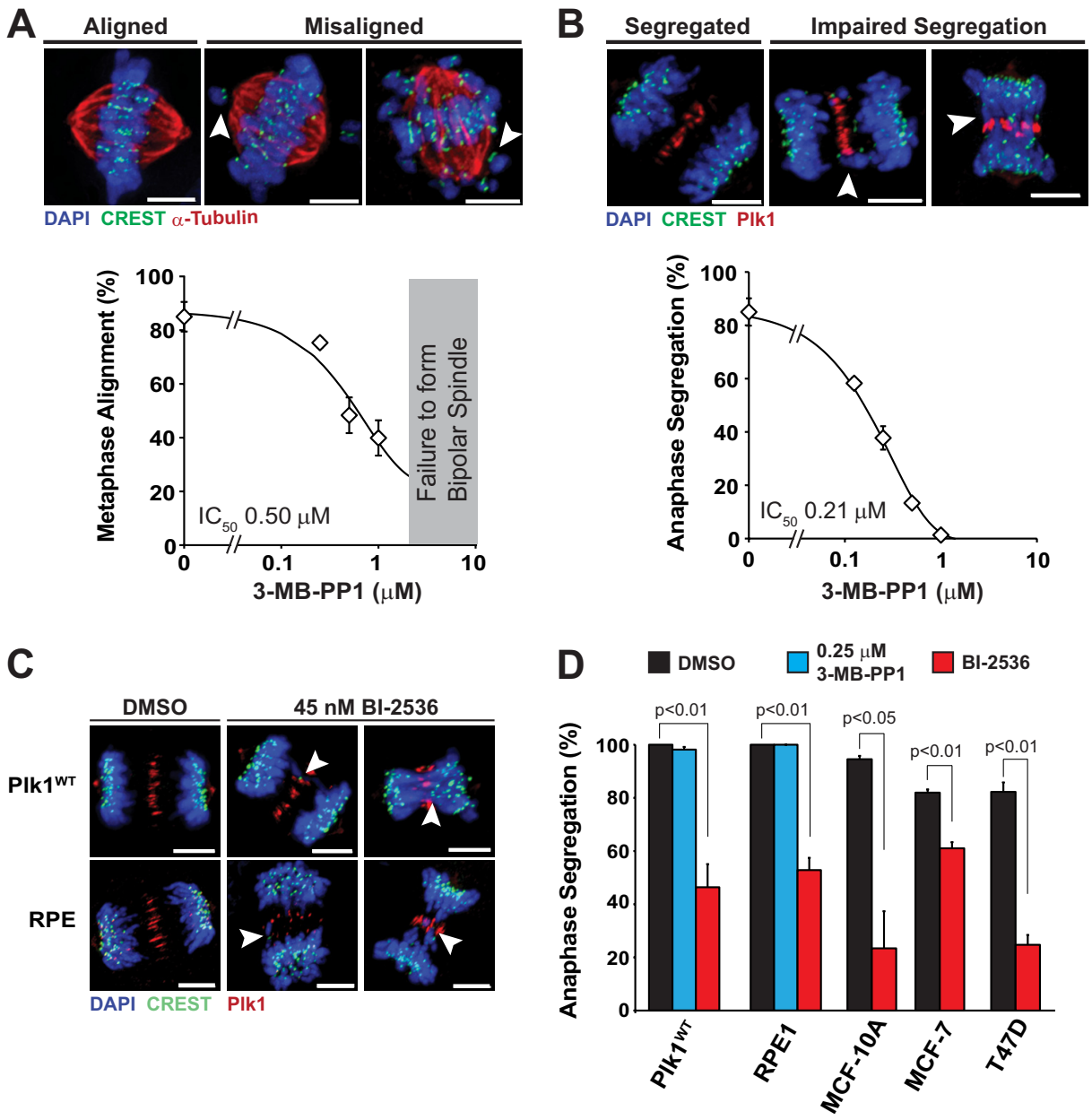

Figure 3.4. Anaphase chromosome segregation is most sensitive to Plk1 inhibition and impairment is associated with shortened spindles and lagging chromosomes

A-B, To determine the IC_{50} for metaphase chromosome alignment and anaphase chromosome segregation, asynchronously growing $Plk1^{as}$ cells were challenged with

DMSO (0 μM) or 3-MB-PP1 (0.125, 0.25, 0.5, 1 μM) for 8 hours and fixed for IF. *A*, For chromosome alignment, pre-anaphase cells exhibiting distinct midline chromosome alignment (n= 300 cells/condition, 3 independent experiments) were scored as having midline alignment of all chromosomes ('Aligned', top left) or misalignment of a few (top center) or many (top right) chromosomes (indicated by arrowheads), collectively termed 'Misaligned'. Percentage of metaphase cells with aligned chromosomes was plotted for each inhibitor concentration to determine the IC_{50}. Data represent averages ± SEM. *B*, For chromosome segregation, anaphase cells (n=75-100 cells/condition from 3 independent experiments) were identified by central-spindle localization of Plk1 (in red) and scored as having separated chromosome masses without midline-localized chromosomes ('Segregated') or lagging/poorly segregated chromosomes (arrowheads, 'Impaired Segregation'). Percentage of anaphase cells with segregated chromosomes was plotted for each inhibitor concentration to determine the IC_{50}. Data represent averages ± SEM. *C and D,* Impaired chromosome segregation is specific to Plk1 inhibition but independent of cell type. *C*, $Plk1^{wt}$ and hTert-RPE1 cells were challenged with DMSO, BI-2536 for 8 hours prior to fixation for IF, revealing defects in anaphase chromosome segregation with lagging chromosomes (arrowheads). *D*, Anaphase cells (n=120-150/condition, 3 independent experiments) were identified and scored by IF for anaphase segregation after 8 hours treatment as shown. Data represent averages ± SEM. Significance determined by t-test. Scale bars, 5 μm.

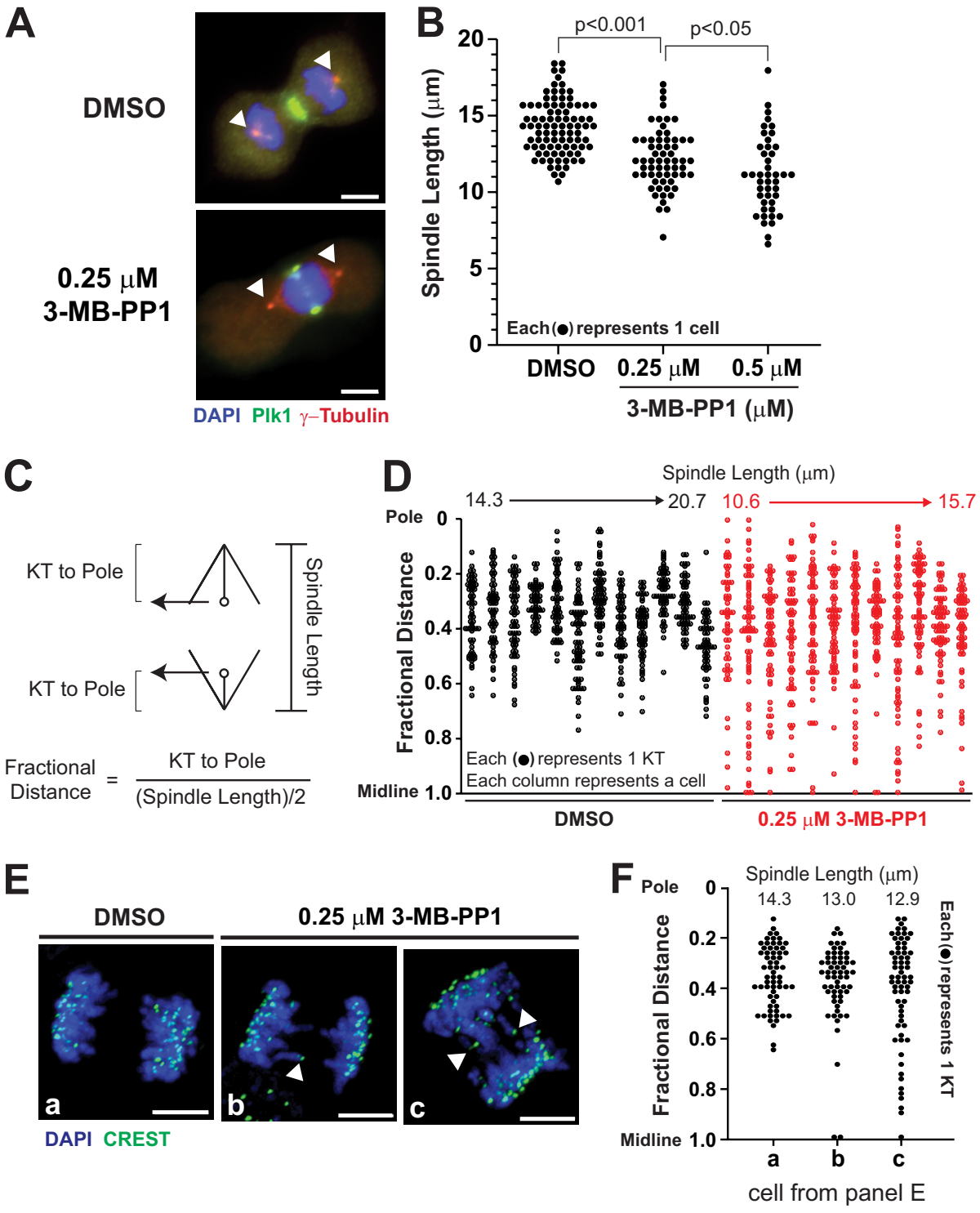
A
DMSO
0.25 μM
3-MB-PP1
DAPI Plk1 γ–Tubulin
B
p<0.001
p<0.05
Spindle Length (μm)
20
15
10
5
0
Each (●) represents 1 cell
DMSO
0.25 μM
0.5 μM
3-MB-PP1 (μM)
C
KT to Pole
KT to Pole
Spindle Length
Fractional Distance = KT to Pole / (Spindle Length)/2
D
Spindle Length (μm)
14.3
20.7
10.6
15.7
Pole
Fractional Distance
0
0.2
0.4
0.6
0.8
Midline 1.0
Each (●) represents 1 KT
Each column represents a cell
DMSO
0.25 μM 3-MB-PP1
E
DMSO
0.25 μM 3-MB-PP1
a
b
c
DAPI CREST
F
Pole
Spindle Length (μm)
14.3
13.0
12.9
Fractional Distance
0
0.2
0.4
0.6
0.8
Midline 1.0
Each (●) represents 1 KT
a
b
c
cell from panel E

Figure 3.5. Spindle elongation and chromosome segregation are impaired with partial loss of Plk1 activity

To characterize impaired chromosome segregation, asynchronously growing Plk1^{as} cells were challenged with DMSO or 3-MB-PP1 (0.25, 0.5 μM) for 8 hours and fixed for IF. *A,* Anaphase spindle lengths were determined by measuring the distance between the peak γ-tubulin intensities at each centrosome (arrowheads). *B,* Spindle lengths of individual cells were plotted for each inhibitor concentration. p-values were determined by Wilcoxon rank sum test. *C-F,* Spindle position of individual chromosomes was determined using a fractional distance calculation, adapted from Lampson et al.[137], where the distance of the chromosome's kinetochore (KT) from the spindle pole is divided by half the length of the spindle axis. Fractional distance is then plotted to visualize KT positions relative to the spindle midline (1.0) and pole (0). *D,* Fractional distance plots in twelve control cells (black) and twelve 3-MB-PP1 treated Plk1^{as} cells (red). Cells are ordered by spindle length from shortest to longest (top). *E-F,* Fractional distance plots of KTs for three cells with similar spindle lengths. *E,* Images of cells presented in *F* (arrowheads identify midline positioned KTs). Scale bars, 5 μm.

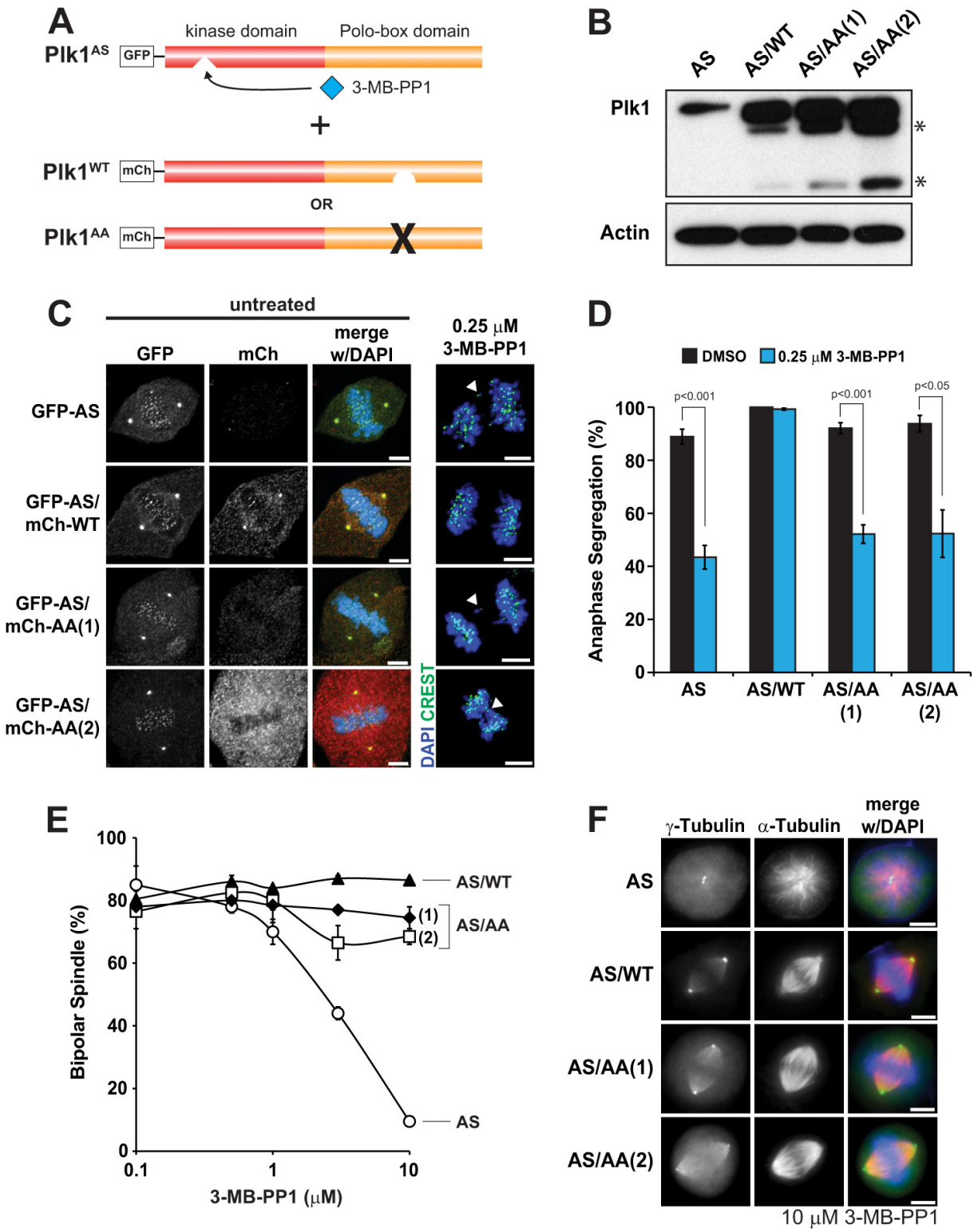
A
kinase domain
Polo-box domain
Plk1AS
GFP
3-MB-PP1
+
Plk1WT
mCh
OR
Plk1AA
mCh
X
B
AS
AS/WT
AS/AA(1)
AS/AA(2)
Plk1
Actin
C
untreated
0.25 μM 3-MB-PP1
GFP
mCh
merge w/DAPI
GFP-AS
GFP-AS/ mCh-WT
GFP-AS/ mCh-AA(1)
GFP-AS/ mCh-AA(2)
DAPI CREST
D
DMSO
0.25 μM 3-MB-PP1
Anaphase Segregation (%)
p<0.001
p<0.001
p<0.05
AS
AS/WT
AS/AA (1)
AS/AA (2)
E
Bipolar Spindle (%)
AS/WT
(1)
(2)
AS/AA
AS
3-MB-PP1 (μM)
F
γ-Tubulin
α-Tubulin
merge w/DAPI
AS
AS/WT
AS/AA(1)
AS/AA(2)
10 μM 3-MB-PP1

Figure 3.6. The Polo-box domain (PBD) is required for chromosome segregation, but dispensable for bipolar spindle formation

A, GFP-Plk1^{as} (AS) cells were transduced with retroviruses expressing mCherry-tagged wild-type Plk1 (WT) or Plk1 with a mutated PBD (AA) to and clonal populations (2 for AS/AA) were selected for experiments. *B,* Total Plk1 expression was determined by immunoblotting mitotic cell lysates for Plk1 and β-actin (loading control). *indicates proteolysis products. *C,* Clonal cells were challenged with 3-MB-PP1 or left untreated for 8 hours and fixed for IF. Localization of each Plk1 allele was determined by GFP (AS) or mCh (WT or AA) in untreated metaphase cells. Images scaled identically for each channel. Note the Plk1 AA allele fails to localize to kinetochores and centrosomes. Representative images of anaphase chromosome segregation in clonal cells challenged with 3-MB-PP1. Arrowheads indicate lagging chromosomes. *D,* Percentage of cells with segregated chromosomes was determined (as in *Fig. 3B*) for each clone challenged with DMSO or 3-MB-PP1 (n=100 cells/condition, 3 independent experiments). Data represent averages ± SEM. p-values determined by t-test. *E-F,* For bipolar spindle formation, clonal cells were challenged with DMSO (0 μM) or 3-MB-PP1 (0.5, 1, 3, 10 μM) for 8 hours and fixed for IF. *E,* Percentage of cells with normal bipolar spindles was determined (as in *Fig. 1C*) for each clone (n=200 cells/concentration, 2 independent experiments). Data represent averages ± SEM. *F,* Representative images of pre-anaphase mitotic spindles observed for each clone challenged with 10 μM 3-MB-PP1. Scale bars, 5 μm.

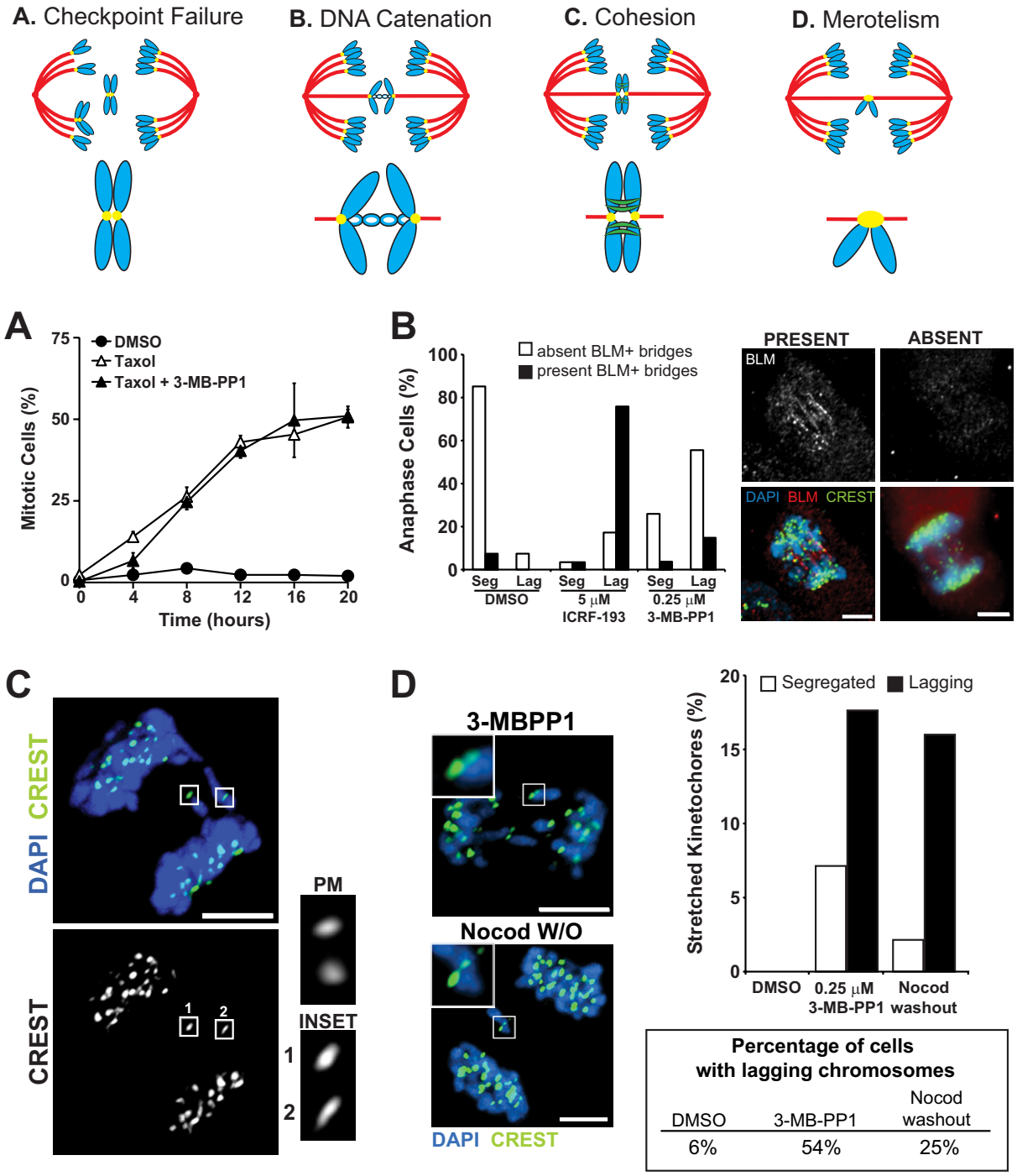

Percentage of cells with lagging chromosomes

DMSO	3-MB-PP1	Nocod washout
6%	54%	25%

Figure 3.7. **Impaired chromosome segregation is not caused by a mitotic checkpoint failure or persistent topologic linkages, but includes merotelic attachments**

Top, Schematic illustrating four potential sources of impaired segregation with Plk1 inhibition. *A,* Checkpoint Failure–Plk1^{as} were challenged with Taxol (to activate the mitotic checkpoint) and 0.5 μM 3-MB-PP1 and then collected at 4-hour intervals for 20 hours. Percentage of mitotic cells was determined at each timepoint. Data points represent averages (3 sets of 100 cells) ± SEM. *B,* DNA catenation– Plk1^{as} cells were synchronized for 8 hours with monastrol, released into fresh media for 30 min and then challenged with DMSO or ICRF-193 (topoisomerase II inhibitor) for 20 min before fixation. For 3-MB-PP1 exposure, asynchronous Plk1^{as} cells were challenged with 0.25μM 3-MB-PP1 for 8 hours prior to fixation. Anaphase cells (n=25 cells/condition) were identified (as in *Fig. 3B*) and scored for BLM(+) bridges in cells exhibiting segregated or mis-segregated chromosomes. Scale bars, 5 μm. *C,* Persistent cohesion– Plk1^{as} cells were challenged with 0.25μM 3-MB-PP1 for 8 hours and fixed. CREST(+) kinetochores (magnified in insets) depict single lagging chromosomes during anaphase instead of paired sisters as seen during prometaphase (PM). Scale bars, 5 μm. Inset, 0.5 μm. *D,* Merotelism– Asynchronous Plk1^{as} cells were challenged with DMSO, 3-MB-PP1 (8 hours) or nocodazole (7 hours + 60 min washout) prior to fixation. Anaphase cells were identified (as in *Fig. 3B*). CREST(+) kinetochores of segregated and lagging chromosomes were measured along their longest dimension. Images illustrate cells with stretched CREST signals, magnified 300X in insets. Scale bars, 5 μm. Graph depicts percentage of segregated and lagging kinetochores in each

condition that exceeded the maximal segregated kinetochore width (0.74 μm) observed in DMSO-treated cells. Table indicates frequency of cells exhibiting lagging chromosomes for each condition (n=120 cells/condition, 3 independent experiments).

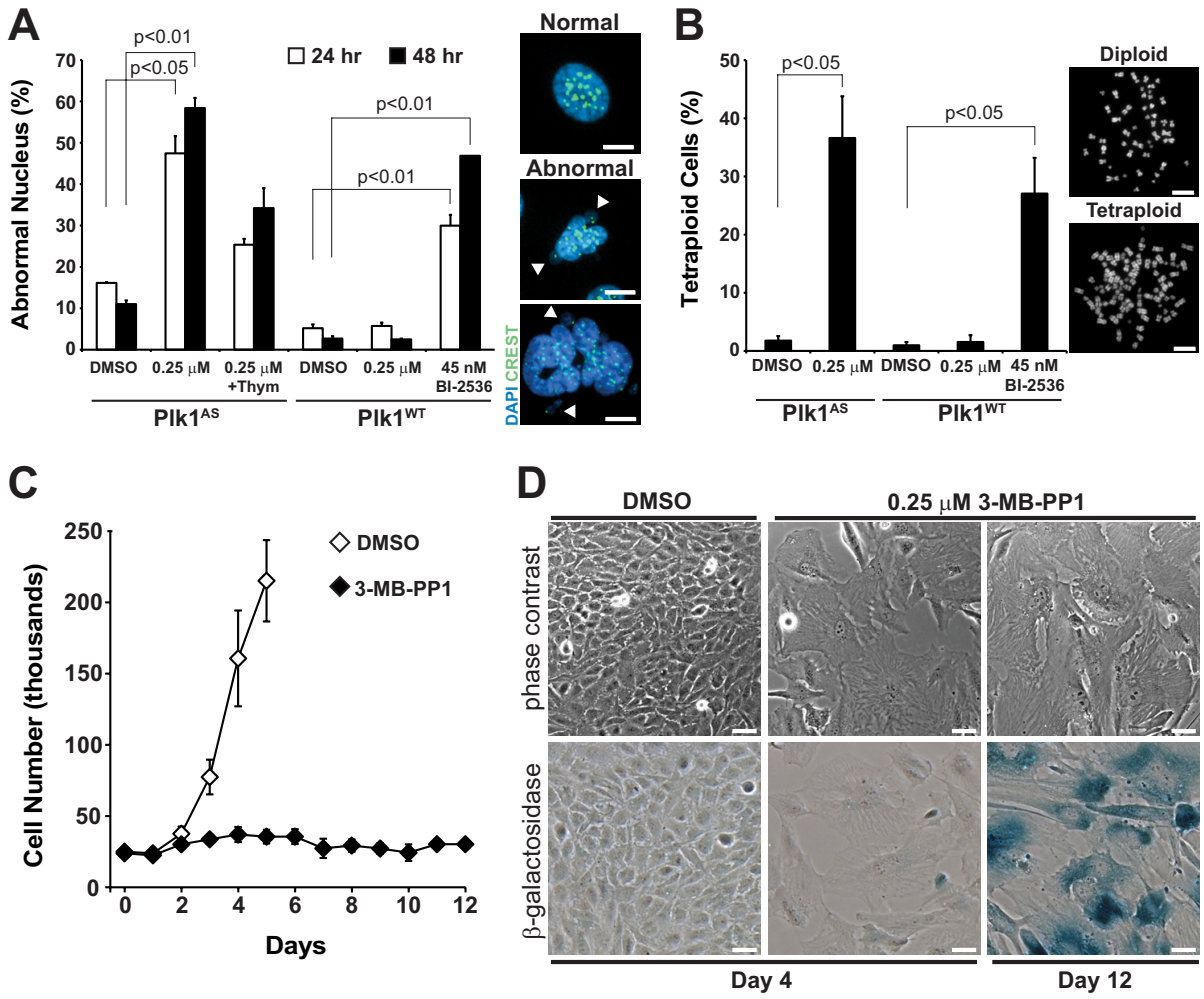

Figure 3.8. Impaired chromosome segregation produces progeny that exhibit abnormal nuclear morphologies, are tetraploid, and fail to proliferate

A, Plk1^{as} and Plk1^{wt} cells were challenged with DMSO, 3-MB-PP1 or BI-2536 for 24 or 48 hours prior to fixation. Interphase cells were scored for normal or abnormal nuclear morphology. Graph represents average percentage (± SEM) of interphase cells (n=300 cells/timepoint/condition, 3 independent experiments) with abnormal nuclei. p-values determined by t-test. Thymidine was added in one condition to verify that effects require cell cycle progression. Representative images of normal and abnormal nuclei with

arrowheads indicating micronuclei. Scale bars, 5 μm. *B,* Plk1^{as} and Plk1^{wt} cells were challenged with DMSO, 3-MB-PP1 or BI-2536 for 48 hours, released and incubated with nocodazole for 5 hours. Mitotic cells were collected by shake-off and chromosome spreads were performed to determine the incidence of tetraploidy. Graph represents average percentage (± SEM) of tetraploid cells (> 80 chromosome pairs) for each condition. n=120 cells/condition, 3 independent experiments. Representative images of diploid or tetraploid chromosome spreads. Scale bars, 10 μm. *C-D,* 25,000 Plk1^{as} cells were seeded in 12-well plates and challenged with DMSO or 0.25 μM 3-MB-PP1 for up to 12 days to determine the effects of prolonged Plk1 inhibition. *C,* Live cells (excluding Trypan Blue) were counted daily and plotted to determine cell proliferation. Data represent average cell counts (± SEM) from 2 independent experiments. *D,* Imaging of DMSO- and 3-MB-PP1-challenged cells at days 4 & 12 indicate that Plk1-inhibited cells become enlarged, flattened (top) and senescent as evidenced by pH-dependent β-galactosidase activity (bottom, blue staining). Scale bars, 50μm.

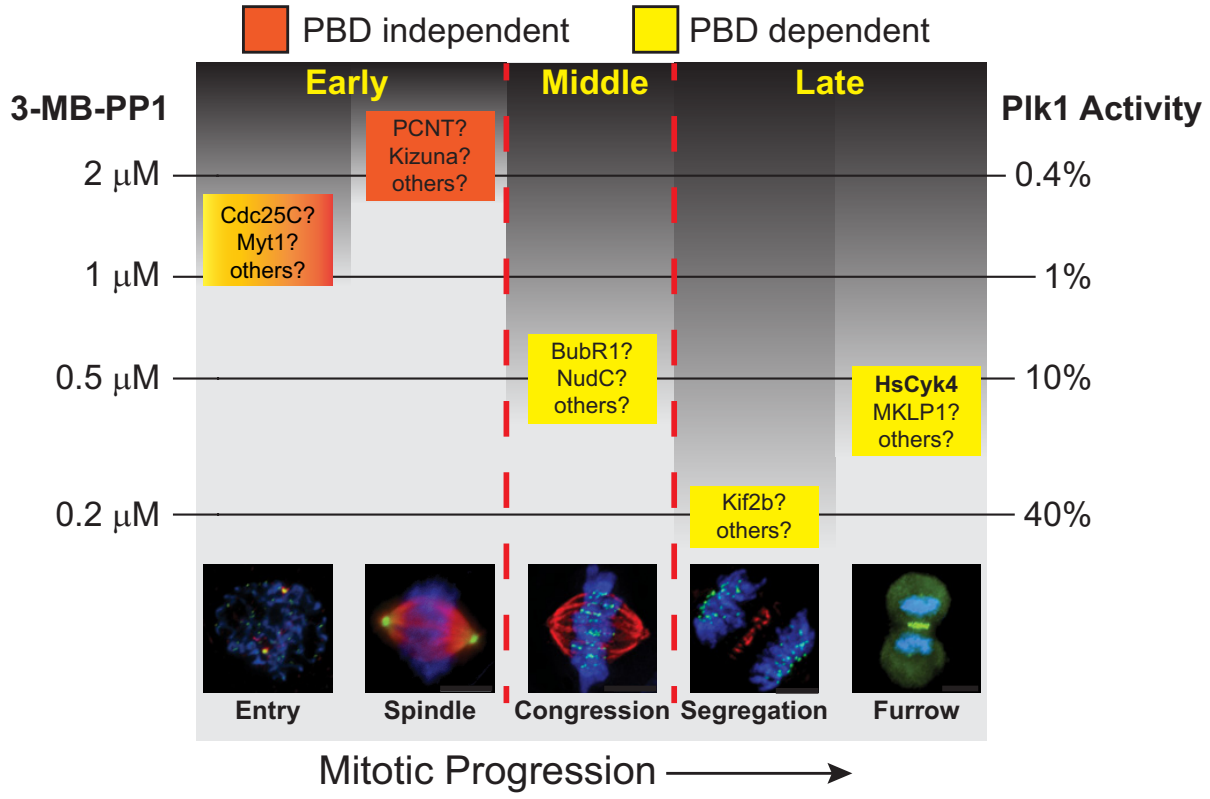

Figure 3.9. Separation of Plk1 function by activity threshold reveals its most sensitive functions and may help link these to substrates

Each box represents an observable phenotype seen at a specific time in mitosis (horizontal axis) and the IC_{50} for this phenotype (vertical axis). The box is colored by dependence on the PBD of Plk1 (mixed for mitotic entry– not tested). Within each box, substrates that may mediate the observed function are shown. HsCyk4 is shown in bold because we confirmed here that molecular and biologic effects have similar IC_{50} thresholds. The dark background represents regions in the schematic in which additional kinase functions and substrates may exist but are not readily isolated by activity thresholds. Residual Plk1 kinase activity estimated from *in vitro* assay is displayed at right.

Movies

Location of movies are provided in parentheses beneath legends

Movie 3.S1. H2B-mCherry expressing Plk1^{as} cell undergoing a normal division

Related to Figure 2A, top row. 3-MB-PP1 concentration: 0 μM.

(http://www.jbc.org/content/suppl/2012/10/27/M112.412544.DC1/jbc.M112.412544-1.mov)

Movie 3.S2. H2B-mCherry expressing Plk1^{as} cell dividing with a lagging chromosome

Related to Figure 2A, second row. 3-MB-PP1 concentration: 0.25 μM.

(http://www.jbc.org/content/suppl/2012/10/27/M112.412544.DC1/jbc.M112.412544-2.mov)

Movie 3.S3. H2B-mCherry expressing Plk1^{as} cell exhibiting severely impaired chromosome segregation during anaphase

Related to Figure 2A, third row. 3-MB-PP1 concentration: 0.25 μM.

(http://www.jbc.org/content/suppl/2012/10/27/M112.412544.DC1/jbc.M112.412544-3.mov)

Movie 3.S4. H2B-mCherry expressing Plk1^{as} cell exhibiting initial chromosome congression with subsequent loss of chromosome alignment

Related to Figure 2A, fourth row. 3-MB-PP1 concentration: 1μM.

(http://www.jbc.org/content/suppl/2012/10/27/M112.412544.DC1/jbc.M112.412544-4.mov)

Chapter IV—Decoding Polo-like kinase 1 signaling along the kinetochore-centromere axis

---

Adapted from: Lera RF, Potts GK, Suzuki A, Johnson JM, Salmon ED, Coon JJ, and Burkard ME (in revision) *Nat Chem Biol.*

Abstract

Protein kinase signaling along the kinetochore-centromere axis is crucial to assure mitotic fidelity, yet its spatial coordination is obscure. Here, we examined how pools of Polo-like kinase 1 (Plk1) within this axis control signaling events to elicit mitotic functions. To do this, we restricted active Plk1 to discrete subcompartments within the kinetochore-centromere axis using chemical genetics and decoded functional and phosphoproteomic signatures of each. We observe distinct phosphoproteomic and functional roles, suggesting that Plk1 exists and functions in discrete pools along this axis. Deep within the centromere, Plk1 operates to assure proper chromosome alignment and segregation. Thus, Plk1 at the kinetochore is a conglomerate of an observable bulk pool coupled with additional functional pools below the threshold of microscopic detection/resolution. Although complex, this multiplicity of locales provides an opportunity to decouple functional and phosphoproteomic signatures for a comprehensive understanding of Plk1's kinetochore functions.

Introduction

During mitosis, macromolecular kinetochores assemble upon centromeric chromatin to attach chromosomes to spindle microtubules. In addition to its structural role, the kinetochore generates signals to promote proper attachment of sister chromatids to opposite spindle poles (biorientation) to ensure accurate segregation into daughter cells. Several protein kinases regulate kinetochore signaling, including Aurora B, Bub1, BubR1, Mps1, Haspin and Polo-like kinase 1 (Plk1)[138–140]. How these mitotic kinases operate within the kinetochore is obscure, but spatial cues are clearly important. For

example, one model for Aurora B function is based on a tension-generated loss of spatial access to its substrates[141,142]. It is unclear if the spatial distributions of mitotic kinases within the kinetochore control accessibility of substrates and functions. Here, we investigated how spatial distribution of Plk1 along the kinetochore contributes to its function and access to substrates.

Polo-like kinase 1 (Plk1) is a core regulator of mitosis required for centrosome maturation, bipolar spindle formation, chromosome arm resolution, chromosome alignment and segregation, and cytokinesis[112]. Plk1 localizes to several mitotic structures, including centrosomes, chromosome arms, kinetochores and the anaphase spindle midzone[112,143]. Its localization is established primarily via its C-terminal Polo-box domain (PBD), a phosphopeptide binding domain, which requires its direct binding partner to be primed through phosphorylation[39,49]. Preventing Plk1 localization impairs its functions, resulting in failure to align and segregate chromosomes[51,144–146] and impaired cytokinesis[53].

The spatial regulation of Plk1 signaling at the kinetochore remains enigmatic due to a multiplicity of interactors and substrates that are located at distinct sites along the entire kinetochore-centromere axis (Figure 4.S1). During mitosis, Plk1 is recruited to the outer kinetochore by Bub1[57], NudC[73], and BubR1, where it phosphorylates BubR1[58,78] and CLASP[77] to stabilize kinetochore-microtubule attachments, promoting chromosome alignment, and Kif2b[82] to correct microtubule attachment errors, facilitating accurate chromosome segregation. At the inner kinetochore, Plk1's role in chromosome alignment and segregation also requires recruitment by and phosphorylation of CENP-U/50[56] (also called PBIP) and CENP-Q[83]. Surprisingly, Plk1 is also reported to function

at the inner centromere, approximately 500 nm from the outer kinetochore, and normal chromosome dynamics depend on its binding to INCENP[147] and phosphorylation of Survivin[76,148], members of the chromosome passenger complex (CPC). Microscopically, Plk1 is visualized as a single kinetochore focus, and its kinase domain is only 5 nm in length[149], so it is difficult to envision how a it could span the ~500 nm distance to access these substrates. The alternative is that multiple pools of Plk1 exist at distinct kinetochore subcompartments. If so, we would expect kinetochore functions to be functionally separable by precise spatial control of Plk1 activity.

A detailed understanding of Plk1 signaling at the kinetochore has remained elusive for several reasons. First, most previous inhibitor and depletion studies abrogate all Plk1 activity, resulting in prometaphase-arrested cells with monopolar spindles. This prevents direct evaluation of mitotic activities that require a bipolar spindle, including chromosome alignment, segregation, and cytokinesis. Second, Plk1's localization to multiple mitotic structures necessitates uncoupling its kinetochore activity from other locales[150]. Finally, phosphoproteomic studies have identified hundreds of Plk1-regulated phosphorylation sites on mitotic proteins, many of which appear direct[46,47,90,91]. Yet the depth and richness of these findings have impaired efficient assignment of Plk1 phosphorylation events to their biologic functions. To circumvent the first obstacle, we recently used inhibitor titration to uncouple chromosome alignment and segregation from bipolar spindle formation[145]. Here, we address the second and third obstacles through chemical genetic complementation combined with high-resolution microscopy and quantitative phosphoproteomics. These data reveal that Plk1 operates in pools within the kinetochore and, surprisingly, the bulk pool is at the inner

kinetochore/centromere. Moreover, Plk1 operates at chromatin and in the inner centromere, in a manner that is distinct and separable from Plk1's role to stabilize microtubule attachments at the outer kinetochore[58,77,78]. The separability of Plk1 operation within the kinetochore provides an opportunity to match functional and phosphoproteomic signatures, and to identify protein phosphorylation events that are likely to contribute to specific aspects of mitotic progression.

Results

Diffusible Plk1 fails to function at the kinetochore.

To interrogate Plk1 signaling at the kinetochore, we employed a chemical genetic system wherein each of two distinct Plk1 alleles is separately controlled by chemical inhibitors. Briefly, human RPE1 cells had the endogenous *PLK1* exon 3 deleted and rescued by GFP-Plk1^{as}, which encodes chemical sensitivity to 3-methylbenzyl-pyrazolopyrimidine (3-MB-PP1) through two point mutations[86]. When wild type Plk1 (Plk1^{wt}) is co-expressed in cells with Plk1^{as}, these complement, and either allele can execute the essential functions of this kinase. However, Plk1^{wt} and Plk1^{as} can be separately controlled: Plk1^{wt} is sensitive to the pharmacologic inhibitor, BI-2536 and resistant to 3-MB-PP1, whereas Plk1^{as} is resistant to BI-2536[110] (Figure 4.1A). This empowers exquisite spatial and temporal chemical control of Plk1 activity at specific subcompartments along the kinetochore-centromere axis.

We first considered that Plk1 signaling at the kinetochore might not require binding to specific kinetochore proteins to exert its functions. To test this, we generated RPE1 cell lines that stably co-express GFP-Plk1^{as} and either Plk1^{wt}, or Plk1^{aa}, which

has a wild type kinase domain but is delocalized by virtue of a mutant PBD (Figure 4.1B). The PBD of Plk1^{aa} contains two point mutations (H538A/K540M), which are sufficient to disrupt Plk1 localization[39,53]. We generated two lines expressing the delocalized construct: one with an N-terminal Flag tag (Plk1^{aa}), the other with an N-terminal mCherry tag (Ch-Plk1^{aa}) (Figure 4.1B). Both constructs are expressed and exhibit catalytic activity similar to Plk1^{wt} (Figure 4.S2A-B). As expected, both fail to localize to centrosomes, kinetochores and the spindle midzone (Figure 4.2C). Notably, both constructs (Ch-Plk1^{aa} > Plk1^{aa}) partially rescue mitotic bipolar spindles with inhibition of Plk1^{as} (Figure 4.1C-D), consistent with previous findings that substrate binding via the PBD is dispensable for spindle formation[51,145].

We next tested if delocalized Plk1 could restore functions that are likely to arise from the kinetochore. Because Plk1 affects both spindle polarity and kinetochore function, it is challenging to decouple these phenotypes to isolate effects specifically attributable to kinetochore dysfunction. To meet this challenge, we previously titrated low levels of inhibitor to observe Plk1 loss-of-function phenotypes in which a bipolar spindle was preserved[145]. With modest losses of kinase activity (500 nM 3-MB-PP1), bipolar spindles form but chromosomes fail to fully align at the spindle midline, presumably due to impaired function at the kinetochore. We first complemented with cells expressing Plk1^{wt}, which localizes properly (Figure 4.S2C). As expected, Plk1^{wt} restores chromosome alignment (81% vs. 28% with vector, $p<0.0001$) (Figure 4.1E-F). Next, we complemented with Plk1^{aa} or Ch-Plk1^{aa}, but chromosome alignment was commonly impaired similar to the vector control (both 26% vs. 28%). We conclude that

a functional PBD of Plk1 is required for proper alignment of mitotic chromosomes, consistent with earlier reports[51,151].

We previously identified a second loss-of-function phenotype of Plk1 that is also likely to arise from the kinetochore—lagging anaphase chromosomes, which occur at very modest losses of Plk1 activity (250 nM 3-MB-PP1) in which cells properly form a bipolar spindle, align chromosomes and silence the mitotic checkpoint[145]. We therefore tested if delocalized Plk1 was sufficient to restore accurate anaphase chromosome segregation. As expected, $Plk1^{wt}$ localized and restored chromosome segregation compared to uncomplemented (vector) cells (94% vs. 47%, $p<0.0001$), yet both $Plk1^{aa}$ and Ch-$Plk1^{aa}$ failed to do so (54% and 40%, respectively) (Figure 4.1G-H). We conclude that, although partly dispensable for bipolar spindle formation, PBD-dependent kinase localization is required for both chromosome alignment and segregation.

Recapitulating Plk1 at the kinetochore

We next considered how localization of Plk1 within the kinetochore might control function. At the extremes, Plk1 could bind each substrate directly (processive operation) or it could bind a single partner and have sufficient reach that allow it to signal throughout the kinetochore (distributive operation), or it could be intermediate between these extremes, binding multiple partners each with limited distributivity to reach adjacent substrates. To test these models, we artificially tethered Plk1 to discrete subcompartments within the kinetochore axis, by replacing the C-terminal PBD with cDNAs encoding proteins that localize to the outer kinetochore (Dsn1), to chromatin (H2B), or to the inner centromere (Kif2c) (Figure 4.2A). We initially selected these

because of their diversity of localization and we found them superior to other tether partners that were unsuitable due to inadequate localization, expression, or activity. We selected clonal lines in which these fusion proteins localized appropriately without observable non-physiologic localization (Figure 4.S3A). Typically, the kinetochore-tethered Plk1 constructs were expressed at lower levels than full-length Plk1 ($Plk1^{wt}$) but had a higher specific activity (Figure 4.S3B-C). These constructs were recruited efficiently to the kinetochore, as evidenced by a low level of delocalized extractable protein compared with $Plk1^{wt}$ or Ch-$Plk1^{aa}$ (Figure 4.S3D-F).

To precisely localize Plk1 and the kinetochore-tethered constructs, we employed high-resolution microscopy of metaphase cells to map mean positions relative to CENP-I/CENP-C standards as described previously[152,153] (Figure 4.2B-D). Surprisingly, endogenous Plk1 mapped approximately 37 nm inside of the CENP-I probe, within the inner kinetochore at the centromere periphery (Figure 4.2D). This finding is unexpected because it spatially isolates bulk Plk1 from known outer kinetochore targets, such as CENP-U/50 and BubR1, which mapped approximately 64 nm and 80 nm outward from Plk1, respectively (Figure 4.2B,D). Importantly, we observed similar Plk1 localization in HeLa cells and with antibodies targeting tagged Plk1 (Figure 4.S4), indicating that these findings were not an artifact of cell type or antibody. For the tethered constructs, we observed two distinct pools of Plk1ΔC-Kif2c: one located as expected in the inner centromere, and a second pool 34 nm outside the inner kinetochore CENP-C probe, placing it in the region of the Ndc80 complex within the outer kinetochore (Figure 4.2C-D). Because of the proximity to the Ndc80 complex, this outer kinetochore pool likely represents Kif2c bound to microtubule tips[153–155]. The Plk1ΔC-Dsn1 construct localized

an average of 24 nm outside of the CENP-C probe, consistent with endogenous Dsn1 localization[152,153], validating the localization of the fusion constructs.

It was initially unclear whether these re-localized kinases could access Plk1 substrates, and if so, whether they would operate with sufficient distributivity to usefully separate function. Therefore, to assess substrates accessed, we compared phosphoproteomic signatures of each with that of Plk1^{wt} and Ch-Plk1^{aa} (Figure 4.3). To do this, we conducted a multiplexed quantitative high-resolution mass spectrometry phosphoproteomic analysis. We used 5 constructs: Plk1^{wt} (normal localization) and Plk1^{AA} (delocalized) controls, plus each of the three constructs tethered to Dsn1 (outer kinetochore), H2B (chromatin), and Kif2c (inner kinetochore and microtubule tips). For each, we examined phosphoproteomics with tethered/control Plk1 both on (-BI-2536) and off (+BI-2536) for a total of 5 cell lines/2 conditions using 10-plex tandem mass tags (TMT)[156] (Figure 4.S5A-B). We detected 531 phosphopeptides decreased >2x by inhibition of Plk1^{wt}, corresponding to 396 proteins (Figure 4.3A, Supplementary Dataset), similar to those found in other Plk1 phosphoproteomic analyses[46,47,90,91]. We next considered whether these sites would be partitioned by locale (Figure 4.3B**)**. Of the 531 Plk1-regulated phosphopeptides, the kinetochore-tethered constructs together restored 94 (Figure 4.3C). These 94 phosphopeptides met three criteria: (i) >2x decrease when Plk1^{wt} was inhibited by BI; (ii) >2x increase with the tethered construct vs. Plk1^{wt}+BI; (iii) >2x decrease when the tethered construct was inhibited with BI. Although some phosphorylation events could be indirect, 47 of these 94 phosphopeptides share the Plk1 consensus motif [D/E/N/Q-X-pS/pT][46], demonstrating many are likely direct and the reach of tethered Plk1 is significant. Additionally, there is

minimal overlap in phosphopeptides reached by the 3 tethered constructs, with 63/119 unique to one construct and only 7 restored by all. Thus tethered Plk1 effectively partitions kinase signaling within kinetochore subcompartments.

The phosphopeptides accessed within the kinetochore are largely consistent with the localization of constructs (Figure 4.4A). For example, Plk1ΔC-Dsn1 enhances phosphorylation of proteins that interact with microtubules and cytoskeleton, consistent with its known function at the outer kinetochore. Further validating outer-kinetochore activity of this construct, we were able to detect restored Plk1-regulated phosphorylation of Dsn1 itself. By contrast, Plk1ΔC-H2B regulated phosphorylation of multiple substrates involved in DNA repair and transcription. Moreover, overlapping phosphopeptides were found between Plk1ΔC-Kif2c with both Plk1ΔC-Dsn1 and with Plk1ΔC-H2B, consistent with the known localization of Kif2c at both the outer kinetochore (near Dsn1) and inner centromere (near chromatin), but no overlap was found between Plk1ΔC-Dsn1 and Plk1ΔC-H2B, demonstrating these are spatially isolated. We next considered phosphopeptides from kinetochore proteins that are likely direct; they match the minimal Plk1 (D/E/N/Q-X-pS/pT) consensus (Figure 4.S5C**)**. $Plk1^{wt}$ is capable of reaching targets at the outer kinetochore (CENPE, CENPF, CDC27), along chromatin (KIF4A, ERCC6L/PICH) and at the inner centromere (INCENP). $Plk1^{aa}$ successfully phosphorylated targeted proteins both at the outer kinetochore (CENPE, CENP-F) and the inner centromere (INCENP). This may occur, for example, if low levels of delocalized Plk1 activity are sufficient to phosphorylate proteins protected from phosphatases. Alternatively, delocalized Plk1 could phosphorylate soluble substrates in early mitosis, before kinetochore assembly. Analysis of the tethered Plk1 constructs

revealed additional remarkable findings. First, Plk1 tethered to the outer kinetochore (Plk1ΔC-Dsn1) failed to target kinetochore proteins other than those also targeted by $Plk1^{aa}$. Second, Plk1ΔC-Kif2c targeted some, but not all, proteins along the kinetochore-centromere axis. As expected, chromatin-bound Plk1 (Plk1ΔC-H2B) was limited to proteins along chromatin (Kif4A, USP16). These data suggest that Plk1 localized to discrete sites within the kinetochore have restricted regions of activity that overlap minimally, yet are sufficiently distributive to elicit ~40 phosphorylation events each.

Plk1 operates at chromatin and the inner centromere

To evaluate where Plk1 operates functionally, we tested the kinetochore-tethered constructs for complementation. In considering functions of Plk1 that might arise from the kinetochore, we again turned to chromosome alignment and segregation as in Figure 4.1, because these phenotypes are separable and elicited by gently titrating inhibition of $Plk1^{as}$. Indeed, we found that Kif2c-tethered Plk1, but not Dsn1-localized or H2B-localized kinase restored accurate chromosome alignment compared to uncomplemented (vector) cells (48% vs. 19%, $p<0.0001$) (Figure 4.4B, left; Fig. 4.S6A). This rescue was substantial, but incomplete compared to $Plk1^{wt}$, possibly due to insufficient activation of the requisite substrate, or perhaps, complete rescue requires additional substrate phosphorylation beyond the tethered construct's reach. Importantly, this rescue is reversed by inhibiting tethered Plk1 with BI-2536 (Figure 4.4A, right), demonstrating that activity of re-localized Plk1, not Kif2c expression, facilitates normal alignment. Additionally, this is unlikely to arise from a soluble pool of $Plk1^{\Delta C}$-Kif2c because active delocalized $Plk1^{aa}$ is unable to rescue (Figure 4.1E). We conclude that

Kif2c-tethered Plk1 rescues the chromosome alignment function, either due to activity at microtubule tips or at the inner centromere.

Similarly, we anticipated that impaired chromosome segregation in anaphase could originate from Plk1 dysfunction at the kinetochore. As before, Plk1ΔC-Kif2c rescued accurate chromosome segregation whereas outer-kinetochore Plk1 (Plk1ΔC-Dsn1) failed to restore function (Figures 4.4D-E, 4.S6B). However, in this case, chromatin-localized Plk1 also restored its function in anaphase chromosome segregation. Again, rescue requires active kinase, as it is reversed with BI-2536 (Figure 4.4B, right). Moreover, soluble Plk1^{aa} is unable to rescue (Figure 4.1G). Tethered constructs do not disrupt chromosome alignment or segregation in the absence of inhibition of Plk1^{as} by 3-MB-PP1 (Figure 4.S6C-D**)**. Thus Plk1 acts at either chromatin or at Kif2c sites to elicit its function required for proper chromosome segregation in anaphase. Moreover, the functionally distinct behavior of Plk1ΔC-H2B from Plk1ΔC-Kif2c in chromosome alignment suggests that Plk1 phosphorylates one or more unique substrates to execute the disparate functions.

Re-evaluating Plk1 function at the outer kinetochore

We have identified kinetochore functions that appear to arise from Plk1 signals at chromatin or the inner centromere, where the bulk of Plk1 is located. However, two caveats are that Plk1ΔC-Kif2c could operate at the microtubule tips near the outer kinetochore, and that Plk1ΔC-Dsn1 could fail to restore activity merely due to impaired access to key outer kinetochore substrates. To address the first question, we asked which particular pool of Plk1ΔC-Kif2c restored its functions. The Kif2c N-terminus is

important for inner centromere targeting[157] and the SxIP sequence within the N-terminus promotes microtubule tip-tracking[154,155] (Figure 4.5A, top). To address this, we generated Kif2c localization mutant constructs (Figure 4.5A, bottom) and repeated the complementation assay. Both the N-terminal deletion mutant (ΔN) and the microtubule tip-tracking mutant (SKNN) were expressed as Plk1 fusions stably in cell lines (Figure 4.S7A) and exhibited catalytic activity similar to Plk1ΔC-Kif2c^{wt} (Figure 4.7B). As expected, the SKNN mutant, but not the ΔN mutant, localized to the inner centromere (Figure 4.5B). Importantly, we could not detect an outer kinetochore localized pool with the SKNN mutant (Figure 4.S7C), verifying that the previously observed outer kinetochore signal (Figure 4.2C) was microtubule tip-bound Kif2c, now abolished. Notably, the SKNN, but not the ΔN mutant, rescued both chromosome alignment and anaphase chromosome segregation phenotypes, and rescue depended on tethered Plk1 activity, as seen by BI-2536-dependent reversal (Figures 4.4E-F and 4.S7D-E). Thus, Plk1ΔC-Kif2c operates in the inner centromere to execute key mitotic functions.

We next considered that Plk1ΔC-Dsn1, though localized correctly and catalytically active, might not be able to access key outer kinetochore substrates, resulting in its failure to restore Plk1 functions. As a measure of Plk1 activity at the outer kinetochore, we tested if any of kinetochore-tethered constructs could phosphorylate BubR1. During mitosis, Plk1 hyperphosphorylation of BubR1 is detectable by a slower migrating band on SDS-PAGE[58,110]. Therefore, we tested BubR1 phosphorylation from mitotic extracts, +/- 3-MB-PP1 to inactivate Plk1^{as} (Figure 4.S8A). Indeed the Plk1ΔC-Dsn1 was unable to reach or only weakly phosphorylated BubR1 in the presence of 3-MB-PP1. Therefore, we generated additional constructs, tethering Plk1 to the outer

kinetochore proteins Bub1, BubR1 and Hec1. We identified stable cell lines exhibiting diverse expression levels including ones expressed at high levels, similar levels to the other tethers with comparable catalytic activity (Figure 4.S8B-D). Moreover, the Plk1ΔC-Bub1 and Plk1ΔC-Hec1 constructs restored a slow-mobility p-BubR1 band (Figure 4.S8A, bottom). Nevertheless, all three constructs failed to rescue either chromosome alignment or segregation (Figure 4.5E-I and Figure 4.S8E-F). Together, these data support the idea that outer kinetochore Plk1 activity is not required for its function in chromosome alignment or segregation. However, we do not exclude the possibility that these four constructs all fail to phosphorylate a critical outer kinetochore protein.

Decoding Plk1 function-substrate matches with spatial signatures

Our results afforded the opportunity to decode Plk1 function at the kinetochore by phenotypic-phosphoproteomic signature. Heretofore, phosphoproteomic analyses of pleiotropic kinases like Plk1 have succeeded in discovering hundreds of new substrates, yet have provided limited information to link substrates to cognate kinase functions. Here, we have identified complex functional signatures for Plk1-dependent phenotypes, which are expected to match a limited set of substrates (Figure 4.6A). To identify potential substrates, we matched these functional signatures with those of phosphopeptides. For example, chromosome alignment is restored by Plk1 tethered to Kif2c, but is not restored by delocalized Plk1^{aa} or Plk1 tethered to Dsn1 or H2B; only 7 of 176 Plk1-dependent phosphopeptides match this signature (Figure 4.6A, left). Similarly, chromosome segregation is restored with Plk1 localized either to H2B or Kif2c, but not to Dsn1 or delocalized Plk1^{aa}; this signature matches that of only 4 of 146

Plk1-dependent phosphopeptides (Figure 4.6A, right). Because Plk1 operates in specific pools within the kinetochore, these data demonstrate that an enlarged set of constructs with restricted localization may effectively decode Plk1 function at the kinetochore. This match of phosphoproteomic signature with functional signature is a unbiased tool to hone in on phosphorylation events that concordantly occur with phenotypic rescue.

Discussion

In this report, we identify the functional and phosphoproteomic signatures of Plk1 tethered to discrete locales within the centromere, chromatin, and kinetochore. A major finding is that Plk1 is predominantly located deep within the kinetochore, where it operates to ensure accurate chromosome alignment and segregation. Previous work has reported that small pools of Plk1 are found in the inner centromere, where it is activated[43]. We find that Plk1 functions at the inner centromere and at chromatin during mitosis. This finding is supported by concordant data, including high-resolution microscopy co-localizing endogenous Plk1 with centromeric chromatin, by phosphoproteomic data identifying chromatin-bound and inner centromere substrates, and by rescue of Plk1 functions when it is artificially tethered to chromatin or to the inner centromere. Although the central binding partner of Plk1 at chromatin is unclear, one candidate is Plk1-Interacting Checkpoint Helicase (PICH), a known binding partner[120].

Although our functional rescue data are limited to active kinase at the chromatin and inner-centromere, our findings do not exclude the possibility of Plk1 functions outside of this zone. Indeed, Plk1 phosphorylation at the outer kinetochore mediates its

function in attaching chromosomes to the microtubule spindle[58,78]. Our assays do not capture the outer kinetochore functions of Plk1, likely because they are observed with *partial* loss-of-function[145], in which residual activity may be sufficient to retain phosphorylation of BubR1 and other outer kinetochore substrates. Moreover, we do identify a number of physiologic phosphorylations that are elicited with Plk1 tethered to the outer kinetochore (Figures 4.3, 4.4A). Thus, our findings do not conflict with other strong evidence that Plk1 operates at the outer kinetochore[58,78,151].

A second key finding of this study is that Plk1 function at the kinetochore can be uncoupled with distinct functions and phosphorylation events from the inner centromere, chromatin, and outer kinetochore, suggesting Plk1 operates in distinct pools within the kinetochore (Figure. 4.6B). A canonical model for Plk1 function is that it directly engages substrates through its C-terminal PBD[49,114] (Figure 4.6B, extreme right), and discovery of a new substrate is often coupled with an assay for direct binding (processive operation). Consistent with this model, Plk1 is known to bind many substrates within the kinetochore, including BubR1 and others[56,58,73,120]. We are aware of only one counter-example—endogenous Plk1 engages CENP-U/50 to reach CENP-Q[158]. Yet, our data powerfully demonstrate that direct binding of substrates via the PBD is not only unnecessary, but that it should not be routinely expected. For example, Plk1^{aa} lacks phosphopeptide-binding activity, yet phosphorylates 21% of the peptides reached by wild type kinase. Second, Plk1 tethered to each discrete kinetochore subcompartment restores ~40 phosphopeptides (Figure. 4.3). Thus, Plk1 function at the kinetochore cannot be accounted for by a processive model where it engages each substrate directly.

Conversely, Plk1 operation in the kinetochore is not purely distributive (Figure 4.6B, extreme left). First, delocalized Plk1^{AA} is incapable of rescuing chromosome alignment or segregation (Figure 4.1E-H) even though it elicits phosphorylation of more peptides than any tethered construct (Figure 4.3). Indeed, the scale from inner centromere to outer kinetochore exceeds the ~5 nm width of the Plk1 kinase domain[149] by two orders of magnitude, making it difficult to imagine how a single focus of kinase could reach throughout the kinetochore without at least limited diffusion. In addition to the theoretical considerations, we observe minimal overlap of phosphoproteomic profiles and ability to rescue Plk1 functions (Figures 4.3, 4.4). Thus, our data support a pool model, wherein Plk1 engages, perhaps, a small number of interactors that allow regional distributivity of phosphorylation signals within the kinetochore (Figure 4.6B). Although a single dominant focus of Plk1 is observed microscopically at each kinetochore, this can be explained by limited sensitivity and diffraction limit, making it likely that some pools are not detected or not resolved. Thus, our data converge on a model that is complex in that it requires both a diversity of interactors and distinct requirements for operation for each pool of Plk1, depending, perhaps, on accessibility to phosphatases. A complex interplay of highly regulated kinase and phosphatase activities are consistent with recent observations that proper kinetochore attachment is regulated by access and activity of phosphatases[159–161].

Our tethered Plk1 constructs cannot fully recapitulate the dynamic nature of Plk1, which is important for proper mitosis. For example, during transition from prometaphase to metaphase, CUL3-KLHL22 ubiquitylation removes Plk1 from the kinetochore[162], coincident with decline of phosphorylated targets[151]. Furthermore, non-ubiquitylatable

Plk1^{162} and Plk1 tethered to Hec1^{151} can produce similar aberrant phenotypes—impaired kinetochore-microtubule attachments and mitotic delay—suggesting that dampened activity of Plk1 at the outer kinetochore is important for proper mitotic progression. We do not exclude a requirement for similar dynamics of Plk1 at the inner centromere and chromatin. If removal of Plk1 is required, the lack of dynamic activity in our tethered constructs could account for the inability to completely restore function. Alternatively, we may have inadvertently mimicked the dynamic localization of inner centromere Plk1 because Kif2c is removed at the proper time.

In principle, it is possible that rescue is afforded by phosphorylation of a non-physiologic substrate by tethered Plk1; however it is implausible that a chance phosphorylation event happens to rescue a specific phenotype by a novel mechanism. It is possible that Plk1 does not operate at the inner centromere: although we observe Kif2c at the inner centromere, it is possible that another pool, not readily observable, exists at centromeric chromatin, where tethered Plk1 operates. Additionally, our conclusions from the phosphoproteomic data are limited by the small number of kinetochore peptides detected. Indeed, well-documented substrates such as BubR1 are absent from our list. It is possible that peptide abundance for these proteins were below our level of detection and different protein enrichment strategies may identify additional kinetochore targets which would better illuminate the phosphoproteomic signatures of our Plk1-tethered constructs. Nevertheless, we are able to identify phosphoproteomic evidence of Plk1 function across the kinetochore.

In conclusion, concordant microscopic, phosphoproteomic, and functional evidence places Plk1 deep within the kinetochore and centromere where it executes

key mitotic functions. The data best support a ‘pool model’ of Plk1 function at the kinetochore. Thus, Plk1 exists and operates at multiple locations within the kinetochore. For full function, Plk1 needs to engage the kinetochore in discrete pools via its PBD, but it need not engage each substrate individually. Moreover, such engagement is dispensable altogether for certain phosphorylations, such as on CENPE, CENPF or INCENP, which are phosphorylated well by soluble kinase. Although this complicated picture challenges our ability to decode functions of Plk1 at the kinetochore, it simultaneously provides a tool to meet the challenge—Plk1 kinase restricted to discrete regions of activity within the kinetochore can match functional and phosphoproteomic signatures. In principle, this approach can be employed to decode function of any spatially regulated pleiotropic kinase, and enforced control of spatial activity can resolve kinase signaling at the kinetochore.

From the molecular point of view, the landscape of a kinetochore is finer than can be appreciated by conventional light microscopy. This molecular point of view is crucial for accurate models of molecular signaling within small, complex biologic structures.

Materials and Methods

Cell Line Derivation and Culture Procedures

Cell Culture. All cell lines were maintained at 37 °C and 5% CO_2 in a humidified incubator and propagated in the following media supplemented with 10% fetal bovine serum and 100 units/mL penicillin-streptomycin: Phoenix retroviral packaging line, Dulbecco’s Modified Eagle’s Medium (DMEM) supplemented with 4.0 mM L-Glutamine and 4500 mg/L glucose; hTERT-RPE1 derived cell lines, 1:1 mixture of DMEM and

Ham's F-12 media supplemented with 2.5 mM L-Glutamine. EGFP-Plk1^{as} RPE1 cell lines[86] and Plk1^{as} cell lines stably expressing mCherry-Plk1 constructs with a "pincer mutant" Polo-Box domain (Ch-Plk1^{aa})[145] were derived as previously reported.

Plasmid Construction. All DNA plasmids were cloned into pQCXIN (Clontech) retroviral vector. Human Kif2c (MHS1010-73945), Dsn1 (MHS1010-9205748), and Hec1 (MHS1010-7508250) were purchased from Open Biosystems. Bub1 and BubR1 were gifts from B.A. Weaver. Flag-tagged Plk1 constructs with a wild-type (Plk1^{wt}) or pincer mutant Polo-Box domain (Plk1^{aa}) were generated by PCR amplification of Plk1 from mCherry-tagged constructs and cloned into pQCXIN-Flag (pQCFIN) using standard restriction digest and ligation procedures. Plk1 fusion constructs were made using a modified USER cloning strategy (New England Biolabs). First, the Plk1 kinase domain (Plk1ΔC, 1-1056aa) was PCR amplified and inserted into pQCFIN using standard restriction digest and ligation procedures. Next, the XbaI restriction site was removed by digest with XbaI, overhang removal by T4 DNA polymerase and blunt-end ligation. A 55-base double-stranded USER acceptance sequence (Table 4.S1) containing XbaI and Nt.BbvCI restriction sites was inserted c-terminal to Plk1 (pQCFIN-Plk1ΔC-USER). The plasmid was then linearized by XbaI and NtBbvCI digest, creating 8-base overhangs. Kif2c, H2B and Dsn1 were PCR amplified with primers containing 8-base complementary sequences with a terminal uracil. Products were digested with USER enzyme and ligated into pQCFIN-Plk1ΔC-USER vectors according to manufacturer's protocol. Kif2c localization mutants were made by PCR amplification of amino acids 140-726 (ΔN) or site-directed mutagenesis (SKNN) using a QuikChange

protocol (Stratagene). Constructs were fully sequenced to verify integrity. See Table 4.S1 for primer list.

Retroviral Transgenesis. For stable retroviral transduction, constructs were co-transfected with a VSV-G envelope plasmid into Phoenix cells. Fresh medium was applied and 24 h post-transfection and harvested 24 h later, clarified by centrifugation and filtration through a 0.45 μm membrane to remove cell debris, and diluted 1:1 with complete medium containing 10 μg/ml polybrene (Millipore). Target cells were infected at 40-60% confluence for 24 h, then selected with 0.4 mg/ml G418 for 10-14 d. Polyclonal transductants were further purified by limiting dilution to obtain individual clones.

Chemicals. Chemicals used in this study include 3-MB-PP1 (Toronto Research Chemicals), BI-2536 (Selleck), MG-132 (Enzo Life Sciences), nocodazole and thymidine (both EMD Biosciences).

Immunoblotting, Immunoprecipitation and Kinase Assays

For all experiments, cells were challenged with 0.2 μg/ml nocodazole for 19 h and mitotic cells were collected by shakeoff, pelleted, frozen down and stored at -80°C prior to use. For detection of BubR1, both mitotic and non-mitotic cells were collected after 19 h nocodazole treatment.

Immunoblotting. Cell pellets were lysed in buffer (50 mM HEPES pH 7.5, 100 mM NaCl, 0.5% NP-40, 10% glycerol) containing phosphatase inhibitors (10 mM sodium pyrophosphate, 5 mM β-glycerolphosphate, 50 mM NaF, 0.3 mM Na_3VO_4), 1mM PMSF, 1x protease inhibitor cocktail (Thermo-Scientific) and 1 mM dithiothreitol. Proteins were

separated by SDS-PAGE, transferred to Immobilon PVDF membrane (Millipore), and blocked for 30 min in 4% milk and 0.1% Tween-20 Tris buffered saline ph 7.4 (TBST+milk). Membranes were incubated with gentle agitation for 2 hours at room temperature with primary antibodies (Table 4.S2) diluted in TBST+milk, washed 3x with TBST, incubated for 1 hour at room temperature in secondary antibodies conjugated to horse radish peroxidase in TBST+milk. Membranes were washed and developed with luminol/peroxide (Millipore) and visualized with film.

All results were obtained from single gels. To simultaneously probe for the protein of interest and the loading marker, the membrane was divided in two after transfer and incubated in separate antibody solutions. When identical-sized proteins prevented membrane division, the membrane was first probed for the protein of interest, stripped in an acidic glycine wash (100 mM glycine pH 2, 500 mM NaCl, 2% SDS), rinsed in deionized H_2O, and then reprobed for the loading marker.

Immunoprecipitation and in vitro kinase assays. Cell lysates were prepared as above with up to 1 mg total protein used for pulldown. Protein inputs were adjusted to promote equivalent quantities after pulldown. Flag-construct lysates were immunoprecipitated with anti-Flag affinity gel (Biotool) for 1 h at 4°C. mCherry-construct lysates were incubated for 3 h with 5 μg/mL dsRed antibody, followed by immunoprecipitation with a 1:1 mixture protein A and protein G sepharose beads (GE Healthcare) for 1 h at 4°C with gentle rotation. The beads/gel were washed three times with lysis buffer and then once with kinase buffer (20 mM Tris, pH 7.4, 10 mM $MgCl_2$, 50 mM KCl). Fifteen percent of immunoprecipitated complexes were removed for detection of bound constructs by Flag or Plk1 immunoblotting. The remainder was then divided

and incubated in kinase buffer, with or without 200 nM BI-2536, plus 5 μg GST-S (substrate), 10 μM ATP, 10 mM dithiothreitol and 2.5 μCi [γ-^{32}P] ATP for 40 min at 30°C. ^{32}P incorporation was observed by SDS-PAGE and Typhoon TRIO imager (GE Healthcare). Three kinase assays were performed from two independent pulldowns. Signal intensity quantification was performed in ImageJ[136] by calculating area underneath the curve for each lane after background subtraction. Final construct intensities were determined by subtracting signal with BI-2536 from signal without BI-2536 and expressed as a percentage of the control.

To prepare the Plk1-specific substrate (GST-S) used in the kinase assays, a single nucleic acid sequence combining 6 known, serine-only, Plk1-specific peptide sequences identified from PhosphositePlus[163] was synthesized by Integrated DNA Technologies (IDT) and cloned into the pGEX-6P1 vector (GE Healthcare) by Gibson assembly (New England Biolabs). Vector expression was induced in *E. coli* (BL21DE3) by addition of 400 μM IPTG for 3 hours at 37 °C. Bacteria were resuspended in PBS containing 250 mM NaCl, 10mM EGTA, 10 mM EDTA, 0.1% Tween-20, 1 mM dithiothrietol, 1 mM PMSF, and 1 mg/ml lysozyme prior to sonication. GST-S was purified from lysates using Glutathione Sepharose 4B beads (GE Healthcare) and eluted in 50 mM Tris-HCL pH 8.0.

Immunofluorescence Microscopy

General procedures. Cells were seeded on glass coverslips at low density in 24-well plates and allowed to grow until 80-90% confluence. For chromosome alignment experiments, cells were challenged for 2 h with 10 μM MG-132 to prevent anaphase

onset and 500 nM 3-MB-PP1 ± 200 nM BI-2536. For chromosome segregation experiments, cells were challenged for 6 h with 200 nM 3-MB-PP1 ± 200 nM BI-2536. For extraction experiments, cells were challenged overnight with 0.2 μg/mL nocodazole.

For pre-extraction, coverslips were initially incubated for 15 s at room temperature (RT) in PHEM buffer (60 mM PIPES, 25 mM HEPES, 10 mM EGTA, 2 mM magnesium chloride) with 0.5% Triton X-100. Otherwise, coverslips were fixed in 4% paraformaldehyde in PHEM buffer for 10 min at RT, washed 3 times in PBS, and then blocked for 30 min at RT in 3% bovine serum albumin (BSA) and 0.1% Triton X-100 in PBS (PBSTx+BSA). Primary antibodies (Table 4.S2) were pooled and diluted in PBSTx+BSA. Coverslips were incubated in primary antibodies for 1 h at RT and washed 3 times in PBSTx. Alexa Fluor (Invitrogen) secondary antibodies were pooled and diluted at 1:350 in PBSTx+BSA. Coverslips were incubated in secondary antibodies for 30 min at RT and then washed twice with PBSTx. Coverslips were counterstained with DAPI and mounted on glass slides with Prolong Gold anti-fade medium (Invitrogen) and allowed to cure overnight.

Image acquisition was performed on a Nikon Eclipse Ti inverted microscope equipped with a 100x/1.4NA (Plan Apo) DIC oil immersion objective, motorized stage (Prior Scientific), and CoolSNAP HQ2 CCD camera (Photometrics). Optical sections were taken at 0.2-μm intervals and, except for extraction experiments, deconvolved using the AQI 3D Deconvolution module in Nikon Elements. Panels were cropped using Photoshop CS5 (Adobe) and assembled with overlays using Illustrator CS5 (Adobe).

During quantitation of spindle polarity, chromosome alignment and segregation phenotypes, observer blinding was performed by slide label concealment. “Bipolar”

spindles were defined by tubulin staining that exhibited an oval shape, tapered at opposite ends, with pericentrin signal at each end. All other spindle types were considered “abnormal”. For chromosome alignment, all non-prophase pre-anaphase mitotic cells were included for analysis. Cells were scored as exhibiting “aligned” chromosomes if all DNA, visualized by DAPI, was present at the cell equator. All other cells were scored as “misaligned”. For chromosome segregation, anaphase cells were identified by central spindle localization of GFP-Plk1^{as} and chromosome position was determined by DNA (DAPI) and kinetochores (ACA antibody) signals. Cells were scored as exhibiting “segregated” chromosomes if no lagging DNA or ACA signals were observed. “Lagging” chromosomes were defined if single DNA or ACA signals were observed lagging behind the segregating masses or if the two masses were not sufficiently separated despite elongation of the cytoplasm (see Figure 4.5, panel E for an example).

Quantitation of cytoplasmic fluorescence intensity was performed using Nikon Elements. Images of 10 cells were acquired for each condition (pre-extraction vs. no extraction) per Plk1 construct. Threshold levels were equally applied to all images to exclude background intensity. Average volume intensity measurements for each channel were made using a 1.5x1.5 μm box placed in the cytoplasm of each cell. To determine the quantity of construct extracted, the median intensity of the pre-extracted cells was subtracted from individual intensities in the no extraction group. These values were then divided by the amount of GFP-Plk1^{as} extracted to control for cell-cell variability.

Sample size was selected for cell biology experiments based on prior experience and biologically significant effect size. For immunofluorescence, the sample size was typically ~100 cells. Three biologic replicates were performed each with this sample size.

Data analysis was performed using Prism 6 (GraphPad). Statistical significance was determined using an ordinary one-way ANOVA with Dunnett's multiple comparisons test with a single pooled variance when comparing multiple cell lines against the vector control or a two-tailed, unpaired t-test with Welch's correction when comparing a single cell line with different chemical treatments.

High-resolution imaging and Delta analysis. Samples were prepared as previously described[152]. Image acquisition was performed on a Nikon TE300 inverted microscope equipped with a Yokogawa CSU10 spinning disk confocal with image magnification yielding a 65 nm pixel size from the Orca ER cooled CCD camera and an 100X/1.4NA (Plan Apo) DIC oil immersion objective (Nikon). Sixty-five flame 3D stacks of pairs of red and green fluorescent images were obtained sequentially at 200 nm steps along the z-axis through the cell from coverslip surface using MetaMorph 6.1 software (Molecular Devices).

For each metaphase kinetochore pair, 3D centroid positions were measured with a 3D Gaussian fitting function as described previously[153]. The centroids of one color were projected to the axis defined by the centroids of the other color, and the Delta (average separation of the projection distance between the signals of red and green colors for theta pair) was calculated to correct for chromatic aberration. Mean Delta

values were corrected for tilt of the face of the kinetochore relative to the axis between sister kinetochores.

Mass Spectrometry

Cell Culture. EGFP-Plk1^{as} RPE1 cell lines stably expressing Flag-Plk1^{wt}, Ch-Plk1^{aa}, Flag-Plk1ΔC-Kif2c, Flag-Plk1ΔC-H2B, or Flag-Plk1ΔC-Dsn1 were split in half (2 chemical treatments/cell line) and cultured as above. At approximately 60% confluence, cells were synchronized in S-phase with 3 mM thymidine. After 24 h, cells were rinsed twice with Hank's Balanced Salt Solution (HBSS), then replenished with fresh media containing 0.2 μg/ml nocodazole. After 18 h, 3-MB-PP1 (final concentration 10 mM) was added to all cells to inhibit Plk1^{as}. To half of the cells, BI-2536 (final concentration 200 nM) was also added to inhibit the complementing Plk1^{wt} allele. One hour later, mitotic cells were collected by shake-off, pelleted, rinsed x 1 with PBS, pelleted again, snap frozen in liquid nitrogen and stored at -80°C. A total of 10 cell pellets (5 cell lines ± BI-2536) were prepared in this manner.

MS Sample Preparation. Cell pellets were lysed in buffer (8 M urea, 50 mM Tris pH 8.0, 100 mM $CaCl_2$) containing dissolved protease and phosphatase inhibitor tablets (Roche) and then sonicated for 20 min. Protein concentrations were determined using a BCA kit (Thermo Pierce). Cell lysates were then reduced by addition of dithiothreitol (final concentration of 5 mM), incubated at 37°C for 45 min, and alkylated by adding iodoacetamide (15 mM final concentration). Next, lysates were incubated for 45 min in the dark at room temperature, and remaining iodoacetamide was quenched by bringing each lysate back to a final 5 mM dithiothreitol concentration. Next, lysates were diluted

to a 1.5 M urea concentration using a 50 mM Tris and 100 mM $CaCl_2$ solution. Trypsin was added to each lysate in a 50:1 (protein: enzyme) ratio and digested overnight at ambient temperature. The 10 samples were desalted using 100 mg C18 Sep-Paks (Waters) and dried down using a vacuum centrifuge to obtain tryptically digested peptides. 1 mg of peptides for each of the 10 samples was incubated with 10-plex tandem mass tags (TMT) reagents (Thermo Scientific) for 3 hours at room temperature. An aliquot of each sample was mixed in a 1:1 ratio and run on an Orbitrap Elite mass spectrometer (Thermo Scientific) to ensure complete TMT peptide labeling. The 10 samples were mixed in a final 1:1 ratio across all 10 TMT channels and desalted using a 500 mg C18 Sep-Pak (Waters) to produce a single pooled sample containing chemically labeled peptides from all 10 samples (5 cell lines ± BI-2536). The pooled sample was fractionated using Strong Cation Exchange (SCX) chromatography to produce 12 total peptide fractions, which were subsequently lyophilized and desalted. The resultant 12 peptide fractions were each enriched using Immobilized Metal Affinity Chromatography (IMAC) Ni-NTA magnetic agarose beads (Qiagen), leading to 12 final SCX fractionated enriched phosphopeptide and unenriched peptide fractions. Each fraction was dried down using a vacuum centrifuge and resuspended in 0.2% formic acid for mass spectrometry analyses.

Nano-LC-MS/MS Methods. Each sample was introduced to an Orbitrap Fusion mass spectrometer (Thermo Scientific) during a 90 min nano-liquid chromatography separation using a nanoAcquity UPLC (Waters). A “Top N” Fusion method was used to analyze eluting peptides, using a 60,000 resolving power survey scan followed by MS/MS scans collected at 60,000 resolving power. Peptides were fragmented using

higher-energy collisional dissociation (HCD) at a normalized collision energy of 35%. Phosphopeptide fractions were analyzed with 200 msec maximum injections times for MS scans and 120 msec maximum injection times for MS/MS scans, while unenriched fractions were analyzed with 100 msec maximum injections times for MS scans and 75 msec maximum injection times for MS/MS scans. Only peptides with charge states from +2 to +8 were selected for MS/MS with an exclusion duration of 30 s. The 12 phosphopeptide samples were run in duplicate.

MS Data Analysis. Data was searched using Proteome Discoverer 1.4.1.14 (Thermo Fisher) with the Sequest search algorithm. Thermo RAW files were searched against a Homo sapiens target-decoy database (UniProt, downloaded 11/06/2014). Peptide and phosphopeptide datasets were searched using a 50 ppm precursor mass tolerance and 0.02 Da fragment tolerance for b and y ions produced by HCD fragmentation. All fractions were searched with static carbadimomethyl of cysteine residues, static TMT 10-plex modifications of peptide N-termini and lysines, dynamic methionine oxidation, and dynamic TMT 10-plex modification of tyrosine residues. Phosphopeptide fractions were searched with additional dynamic phosphorylation modifications of serine, threonine, and tyrosine residues. Resulting peptide identifications were filtered to 1% false discovery rate (FDR) and exported to tab-delimited text files compatible with the COMPASS software suite[164]. COMPASS was used to obtain the 10-plex TMT protein and phosphopeptide quantitation for all the 12 peptide fractions and 12 phosphopeptide fractions. Peptides were mapped back to their parent proteins using COMPASS, and Phospho RS[165] was used to localize phosphorylation to amino acid residues with a fragment tolerance of 0.02 Da

automatically considering neutral loss peaks for HCD and considering a maximum of 200 maximum position isoforms per phosphopeptide. The raw 10-plex reporter ion intensities of localized phosphopeptide isoforms were $\log_2$ transformed and normalized against inhibited $Plk1^{wt}$ (+BI-2536) to obtain the relative phosphopeptide and protein quantitation for each cell line and condition. Phosphopeptides were considered targeted by each cell line (A) if the uninhibited condition exhibited a 2-fold increase over inhibited $Plk1^{wt}$ (i.e. AA vs. WT_BI) and (B) if the phosphopeptide abundance decreased by half when the cell line itself was inhibited by BI-2536 (i.e. AA vs. AA_BI).

Acknowledgements

This work was supported by NIH R01 GM097245 (to M.E.B.), NIH R01 GM080148 (to J.J.C), NIH R01 GM24364 (to E.D.S), Cancer Center Support P30 CA014520 (to M.E.B.), and Effcansah.com. The authors thank I.M. Cheeseman, S.S. Taylor, and T.J. Yen for contributing reagents, and B.A. Weaver and members of the Burkard laboratory for helpful discussions.

Figures and Tables

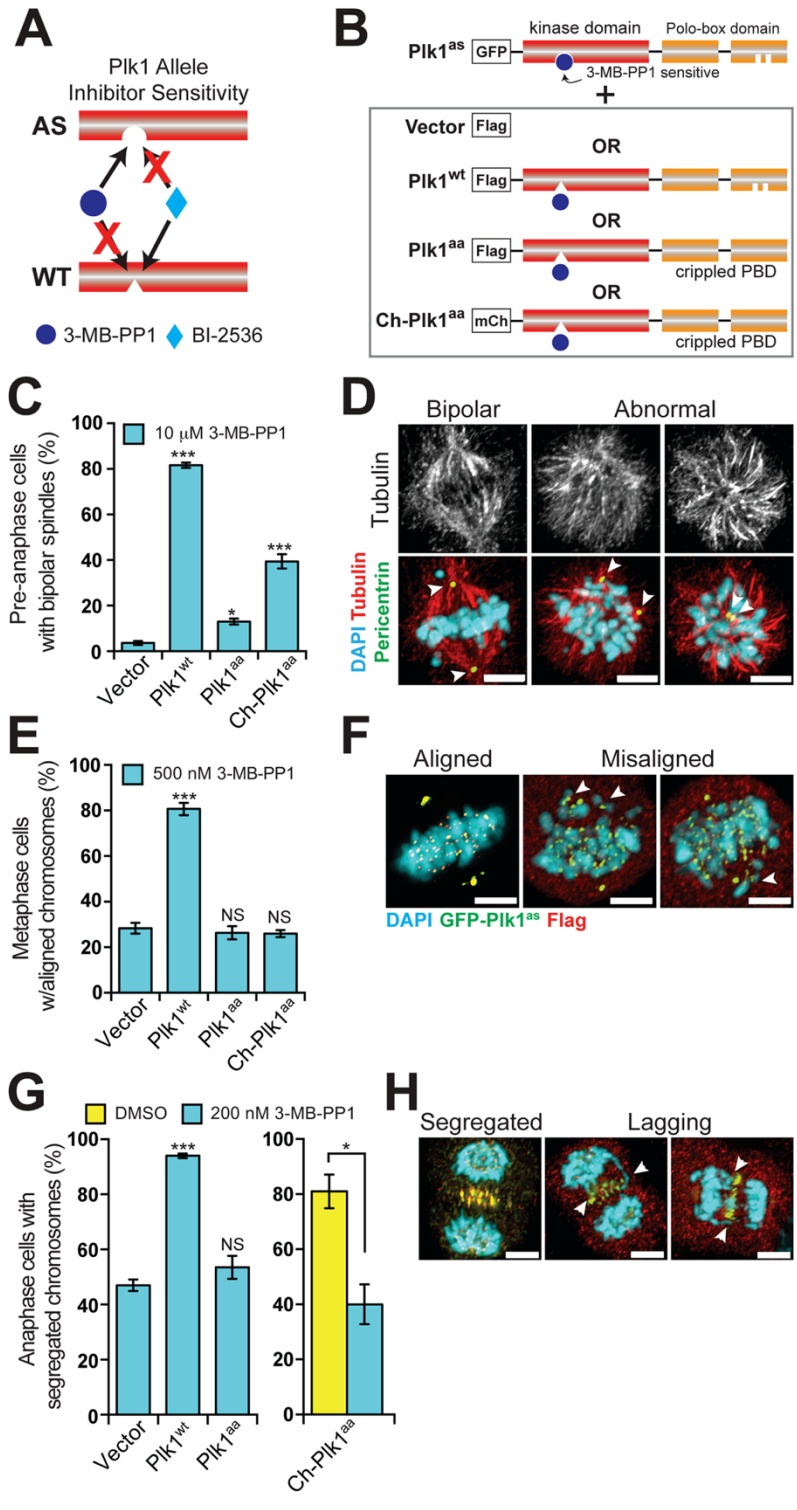

Figure 4.1. Plk1 signaling at the kinetochore requires binding via its PBD

A, Schematic indicating orthogonal control of Plk1 alleles. Analog-sensitive (AS) Plk1 is sensitive to 3-MB-PP1, but not BI-2536, whereas wild-type (WT) Plk1 is the converse. *B,* Schematic of complementation strategy. RPE1 cells expressing GFP-Plk1^{as} (Plk1^{as}) were stably infected with an empty Flag vector (Vector), Flag-tagged wild-type Plk1 (Plk1^{wt}), or Plk1 with a wild-type kinase domain, but crippled Polo-box domain that delocalizes the protein (Plk1^{aa} and Ch-Plk1^{aa}). *C-H,* Delocalized Plk1 (Ch-Plk1^{aa} > Plk1^{aa}) partially restores mitotic bipolar spindles, but fails to restore metaphase chromosome alignment or anaphase chromosome segregation when GFP-Plk1^{as} is inhibited with 3-MB-PP1. *C,* Graph shows average percentage (± SEM) of pre-anaphase cells with bipolar spindles for each cell line challenged with 10 μM 3-MB-PP1 (n=150 cells/experiment; 5 independent experiments). *D,* Representative maximal intensity projection micrographs from *C*. Arrowheads highlight pericentrin-decorated centrosomes. *E,* Graph shows average percentage (± SEM) of pre-anaphase mitotic cells at metaphase with fully aligned chromosomes for each cell line challenged with 500 nM 3-MB-PP1 (n=150 cells/experiment; 3 independent experiments). *F,* Representative maximal intensity projection micrographs from *E*. Arrowheads indicate misaligned chromosomes. *G,* Graph shows average percentage (± SEM) of anaphase cells with fully segregated chromosomes for each cell line challenged with DMSO (yellow bar) or 200 nM 3-MB-PP1 (cyan bars) (n=50 cells/experiment; 4 independent experiments). *H,* Representative maximal intensity projection micrographs from *G*. Arrowheads indicate lagging chromosomes. *P<.05, ***P<0.0001 by one-way ANOVA or unpaired t-test; NS, not significant (panels *C,E,G*). Scale bars, 5 μm (panels *D,F,H*)

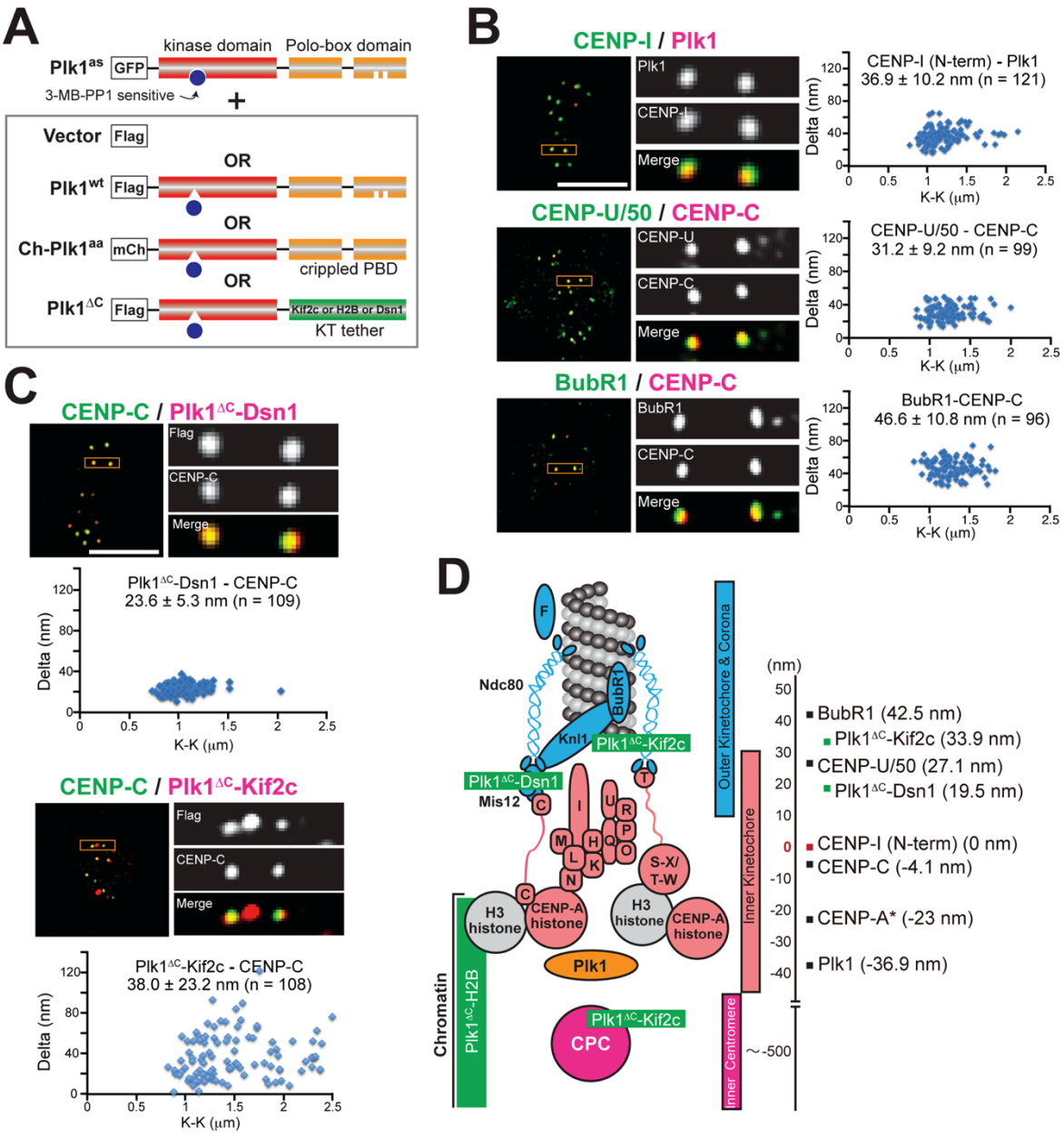

Figure 4.2. High-resolution microscopy identifies discrete localization of endogenous Plk1 and kinetochore-tethered Plk1 constructs along the kinetochore-centromere axis

A, Schematic of complementation strategy. As in Figure 4.1B, except additional Flag-tagged lines were generated to localize the wild-type Plk1 kinase domain (Plk1ΔC) to

discrete locales at the kinetochore. Flag-Plk1ΔC was tethered to proteins localizing to the inner centromere (Kif2c), chromatin (H2B), or to the outer kinetochore (Dsn1). *B,* High-resolution single plane images and Delta analysis of endogenous Plk1, CENP-U/50 (also known as PBIP), and BubR1 used for kinetochore mapping in RPE1 cells. K-K indicates distances between the two centroids for CENP-I, CENP-U/50 or BubR1. *C,* High-resolution single plane micrographs and Delta analysis of kinetochore-tethered Plk1 constructs. K-K indicates distances between the two centroids for the tethered constructs. *D,* Map of kinetochore with summary of Delta measurements from panels *B-C* set relative to the N-terminus of CENP-I (red). Endogenous proteins indicated in black and Plk1 fusion constructs in green. Positive values are outward toward the spindle microtubules and negative values are inward toward the inner centromere. *CENP-A position was reported previously[152]. Scale bars, 5 μm (panels *B-C*).

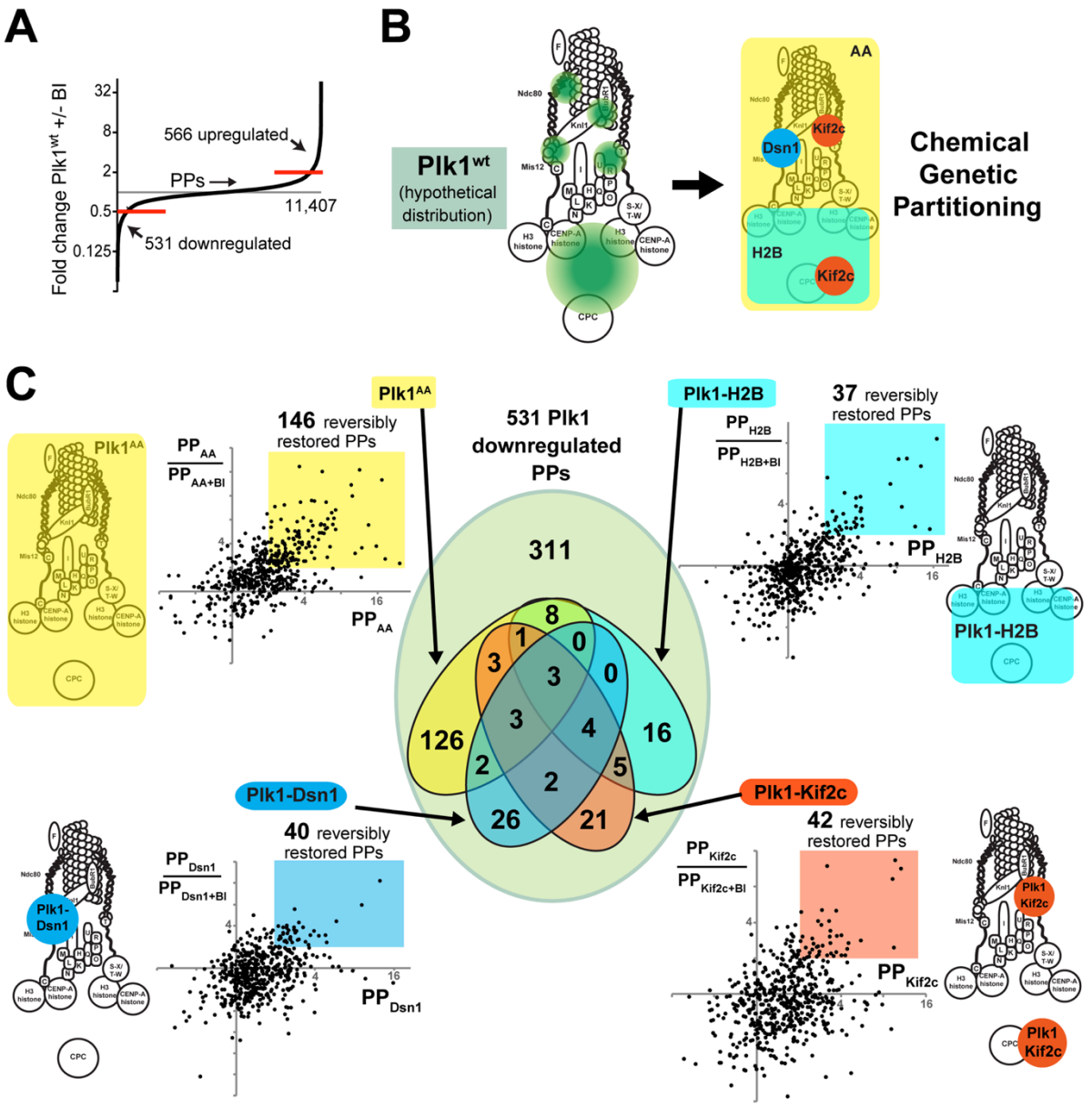

Figure 4.3. 10-plex TMT phosphoproteomic analysis of Plk1 partitioned by locale within the kinetochore-centromere axis

A, Distribution of phosphopeptides (PPs) regulated by Plk1 activity. Out of a total of 11,407 phosphopeptides encountered, 566 PPs were upregulated (> 2-fold increase +BI/-BI) and 531 downregulated (> 2-fold decrease +BI/-BI) with exposure to the $Plk1^{wt}$

inhibitor, BI-2536. *B*, Hypothetical distribution of Plk1^{wt} (green) within the KT axis and partitioning function by locale within the KT axis (Dsn1-outer KT, Kif2c-outer KT/inner centromere, H2B-chromatin) or by a delocalized control, (Ch-Plk1^{AA}). *C*, Identification of phosphopeptides (PPs) that are restored with each tethered Plk1 construct. Each dot on plot represents one of 531 physiologically Plk1-regulated PPs (downregulated >2x with Plk1^{wt}+BI). The X axis displays its abundance relative to control (Plk1^{wt}+BI) with values >2 indicating that phosphorylation is restored by the construct in question. The Y axis indicates the ratio PP/PP+BI, with values >2 indicating that the restored PP is depleted with chemical inactivation of the regionally-restricted construct. Color-coded regions indicate the PPs that are reversibly restored with each regional construct. The Venn diagram at center illustrates the number of PPs that overlap by the distinct color-coded constructs.

A

	Plk1-Dsn1	+	Plk1-Kif2c	+	Plk1-H2B	+ +
Kinetochore	DSN1 INCENP*	CENPF*	CDC27*			
Chromatin/ DNA repair	PBRM1 RFC1 YEATS2*	DLGAP4*	ERCC5* SLX4 TP53BP1*	UBP16* UHRF1BP1*	HMGA2* TNKS1BP1* TOP2B*	
Kinesin				KIF4A*	KIF20B KIF23/MKLP1	
Microtubule/ Cytoskeleton	BICD2* GTSE1 MTCL1 MYO18A NUMA1*	MAP1B* PEAK1 SSFA2*	DPYSL2 VIM		ADD2*	
Cytokinesis/ GTPase	DOCK5 RASGRF2* RASAL2 TBC1D10B		ARHGAP5 ARHGEF17 GIT1*		PDCD6IP*	
Centrosome	CEP131*		PCM1*			CEP55*
Transcription	DIDO1* LMO7*		ZFHX3		CDK13 RLF* HMX2 SSRP1* IWS1 TMF1 PHF6*	TCF12*
Other/ Unknown	CDK11B PNN* ECE1 RAVER1 GTPBP1 STK32C HNRNPA3 ZYX LRRFIP2*		ANO6 LIN9 ARL6IP4* OXTR* EEF1D* PHAX* FEZ2 SRRM2* HUWE1 TRMT1	NHSL1	DDX50* PPP1R7* IPMK SCAF11* LIMD1 SFRS9 NKTR UB2E2 OSBP2*	BCL7C* MAP3K3* METAP2* NAA30 RABL6*

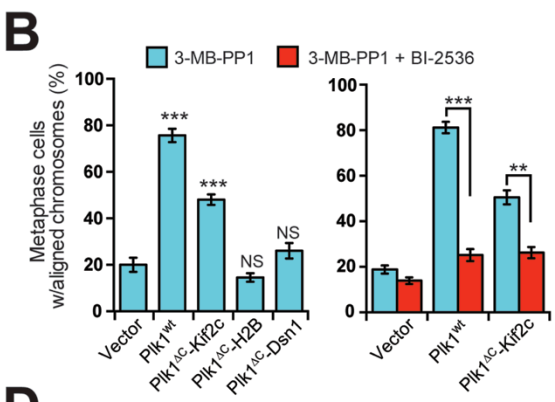

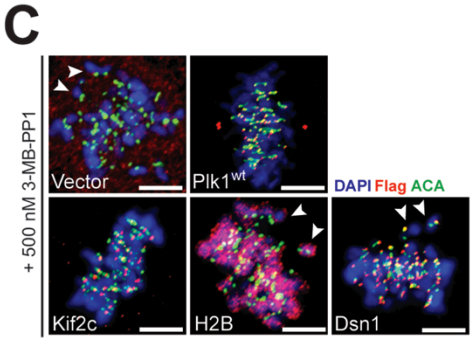

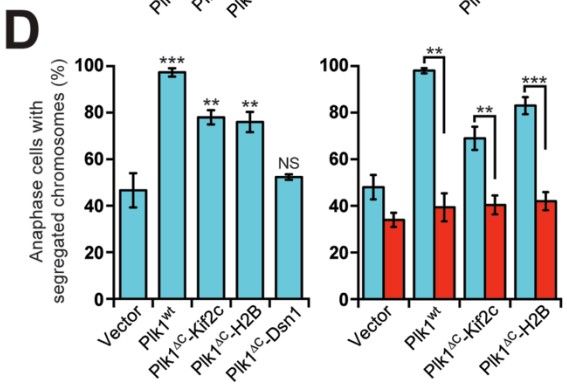

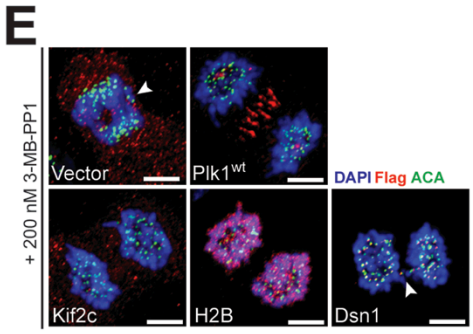

Figure 4.4. Restricting Plk1 activity along the kinetochore-centromere axis produces distinct phosphoproteomic and functional signatures

A, Table of Gene IDs from phosphopeptides regulated by kinetochore-tethered Plk1 constructs. Rows indicate peptide locale or cellular function. Columns indicate peptides with individual or overlapping construct regulation. Peptides also regulated by delocalized Plk1 (Ch-Plk1^{aa}) are listed in red. Asterisk(*) denotes peptides that contain the minimal Plk1 consensus (D/E/N/Q-X-pS/pT) motif. Underline denotes multiple regulated peptides encountered. *B*, Cells expressing GFP-Plk1^{as} and the respective kinetochore-tethered Plk1 constructs were challenged with 3-MB-PP1 (inhibits Plk1^{as}) ± BI-2536 (inhibits Plk1^{wt}/ Plk1ΔC constructs) and assayed for ability of constructs to rescue chromosome alignment during metaphase or segregation during anaphase. *B*, Graphs show average percentage (± SEM) of pre-anaphase mitotic cells at metaphase with fully aligned chromosomes for each cell line (n≥100 cells/experiment; 3 independent experiments). *C*, Representative maximal intensity projection micrographs from *B*. Arrowheads indicate misaligned chromosomes. *D*, Graph shows average percentage (± SEM) of anaphase cells with fully segregated chromosomes for each cell line (n≥40 cells/experiment; at least 3 independent experiments). *E,* Representative maximal intensity projection micrographs from *D*. Arrowheads indicate lagging chromosomes. *P<0.05, **P<0.005, ***P<0.0001 by one-way ANOVA or unpaired t-test; NS, not significant (panels *B*,*D*). Scale bars, 5 μm (panels *C*,*E*).

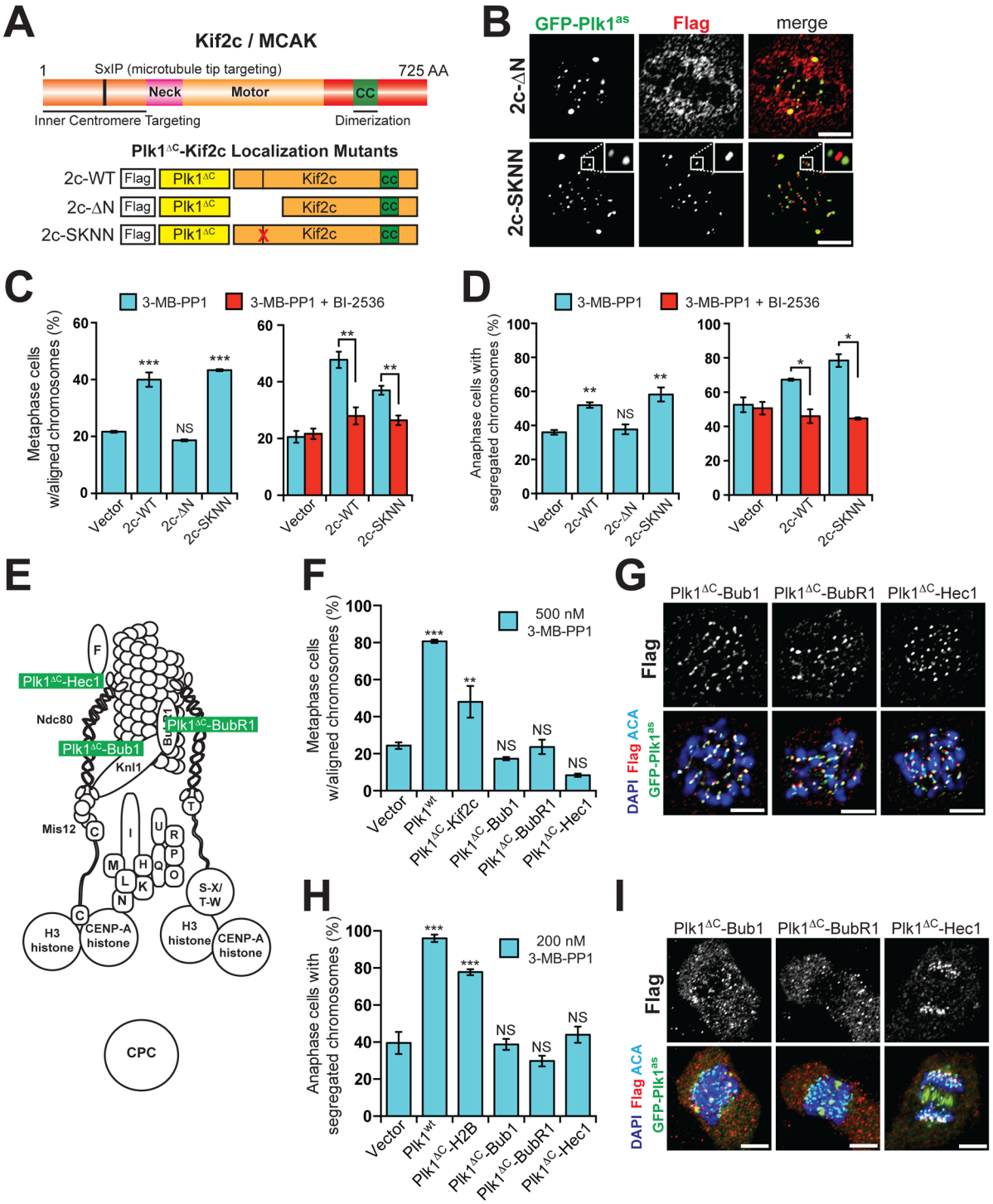
A
Kif2c / MCAK
1
SxIP (microtubule tip targeting)
725 AA
Neck
Motor
CC
Inner Centromere Targeting
Dimerization
Plk1ΔC-Kif2c Localization Mutants
2c-WT
2c-ΔN
2c-SKNN
Flag
Plk1ΔC
Kif2c
B
GFP-Plk1as
Flag
merge
2c-ΔN
2c-SKNN
C
3-MB-PP1
3-MB-PP1 + BI-2536
Metaphase cells w/aligned chromosomes (%)
Vector
2c-WT
2c-ΔN
2c-SKNN
D
Anaphase cells with segregated chromosomes (%)
E
Plk1ΔC-Hec1
Ndc80
Plk1ΔC-BubR1
Plk1ΔC-Bub1
Knl1
Mis12
Bub1
F
I
U
R
P
Q
O
M
H
L
K
N
T
C
S-X/T-W
H3 histone
CENP-A histone
CPC
F
500 nM 3-MB-PP1
Plk1wt
Plk1ΔC-Kif2c
Plk1ΔC-Bub1
Plk1ΔC-BubR1
Plk1ΔC-Hec1
G
Plk1ΔC-Bub1
Plk1ΔC-BubR1
Plk1ΔC-Hec1
Flag
DAPI Flag ACA
GFP-Plk1as
H
200 nM 3-MB-PP1
Plk1ΔC-H2B
I
Plk1ΔC-Bub1
Plk1ΔC-BubR1
Plk1ΔC-Hec1
Flag
DAPI Flag ACA
GFP-Plk1as

Figure 4.5. Outer kinetochore tethering of Plk1 fails to restore chromosome alignment or segregation

A-*D*, Plk1 tethered to the inner centromere-localized pool of Kif2c is important for chromosome alignment and segregation. *Top*, Schematic of Kif2c (also known as mitotic centromere-associated kinesin, MCAK) highlighting important domains. CC, coiled coil. *Bottom*, Schematic of Plk1-tethered to Kif2c localization mutants: ΔN disrupts targeting to both the inner centromere and microtubule tips, whereas SKNN disrupts targeting to the tips only. *B*, Representative single-plane micrographs highlighting diffuse spindle localization of the ΔN mutant and discrete targeting of the SKNN mutant to the inner centromere (insets). *C*-*D*, Cells expressing GFP-Plk1^{as} and Kif2c localization mutants were challenged with 3-MB-PP1 (inhibits Plk1^{as}) ± BI-2536 (inhibits Plk1ΔC constructs) and assayed for ability of constructs to rescue chromosome alignment during metaphase or segregation during anaphase. *C*, Graphs show average percentage (± SEM) of pre-anaphase mitotic cells at metaphase with fully aligned chromosomes for each cell line (n=150 cells/experiment; 3 independent experiments). *D*, Graph shows average percentage (± SEM) of anaphase cells with fully segregated chromosomes for each cell line (n=50 cells/experiment; 4 independent experiments). *E*, Schematic of kinetochore indicating positions of outer kinetochore Plk1 tethers. *F*, As in panel *C* (n=150 cells/experiment; 3 independent experiments). *G*, Representative single-plane micrographs indicating kinetochore localization of Plk1 tethers in cells failing to restore chromosome alignment. H, As in panel *D* (n≥30 cells/experiment; 4 independent experiments). *I*, Representative maximal intensity micrographs indicating localization of Plk1 tethers in cells failing to restore chromosome segregation. *P< 0.05,

**P<0.005, ***P<0.0001 by one-way ANOVA or unpaired t-test; NS, not significant (panels *C*,*D*,*F*,*H*). Scale bars, 5 μm (panel *B*,*G*,*I*).

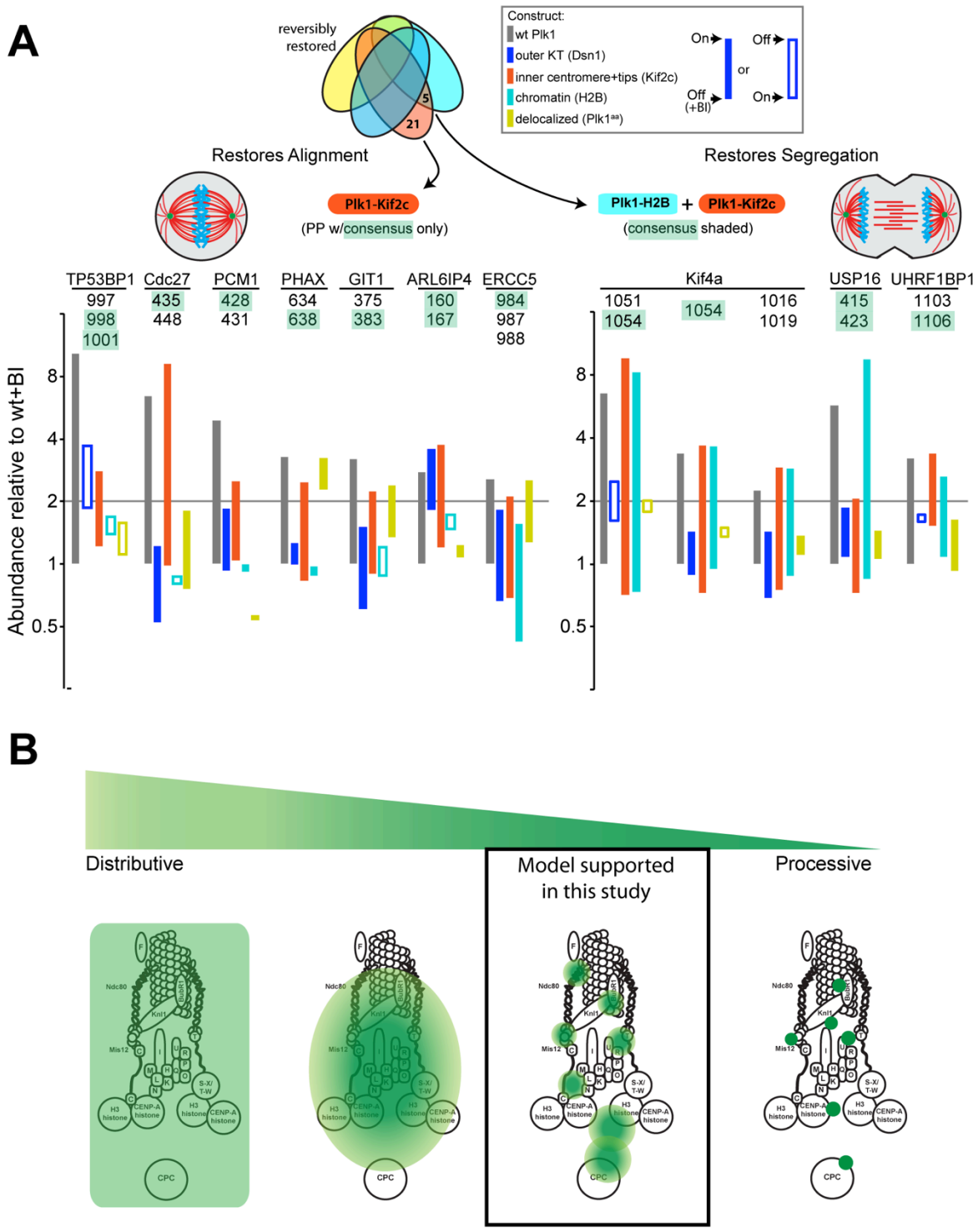
A
reversibly restored
5
21
Construct:
wt Plk1
outer KT (Dsn1)
inner centromere+tips (Kif2c)
chromatin (H2B)
delocalized (Plk1aa)
On
Off
or
Off (+BI)
On
Restores Alignment
Plk1-Kif2c
(PP w/consensus only)
Restores Segregation
Plk1-H2B + Plk1-Kif2c
(consensus shaded)
TP53BP1 997 998 1001
Cdc27 435 448
PCM1 428 431
PHAX 634 638
GIT1 375 383
ARL6IP4 160 167
ERCC5 984 987 988
Kif4a 1051 1054 1054 1016 1019
USP16 415 423
UHRF1BP1 1103 1106
Abundance relative to wt+BI
8
4
2
1
0.5
B
Distributive
Model supported in this study
Processive
Ndc80
Knl1
Bub1R1
Mis12
S-X/T-W
H3 histone
CENP-A histone
CPC

Figure 4.6. Functional/proteomic signatures and a model for Plk1 activity in the kinetochore

A, Phosphopeptides that are restored by constructs concordant with phenotypic rescue of chromosome alignment (*left*) and accurate chromosome segregation (*right*). Phosphopeptides (PPs) containing minimal Plk1 consensus are illustrated for each phenotype with bars illustrating difference between +/- BI-2536 for each construct. *Left*, phosphopeptides that are restored by $Plk1^{wt}$ and Kif2c only. *Right*, phosphopeptides that are restored with $Plk1^{wt}$, H2B, and Kif2c. *B*, A model of Plk1 operation within the kinetochore could range from a highly distributive operation where one binding partner provides access to all substrates (extreme left), versus processive operation, where Plk1 binds each substrate directly (extreme right). Our data support an intermediate model where Plk1 at each sub-compartment can elicit ~40 phosphorylation events, with minimal overlap between inner centromere, chromatin, and the outer kinetochore.

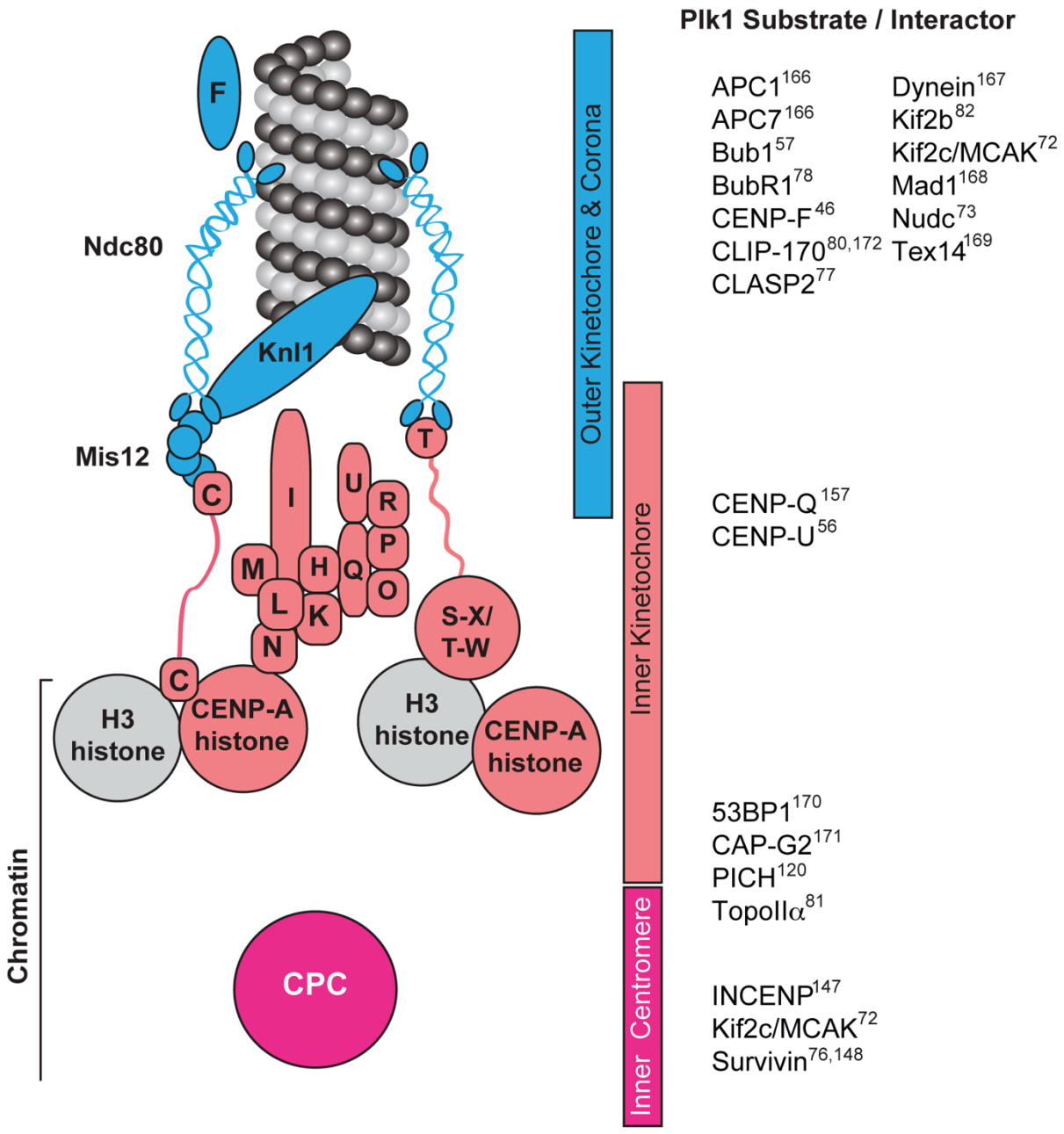

Figure 4.S1. Plk1 substrates and interactors are found along the entire kinetochore-centromere axis

Left, Schematic of the human kinetochore and centromere. Centromere proteins are indicated by their respective letters. CPC, Chromosomal Passenger Complex. *Right*,

List of known mitotic Plk1 substrates and interactors based on reference articles. Locales were determined by referenced articles or inferred based on localization or known binding partners mapped in additional reports, but not referenced here.

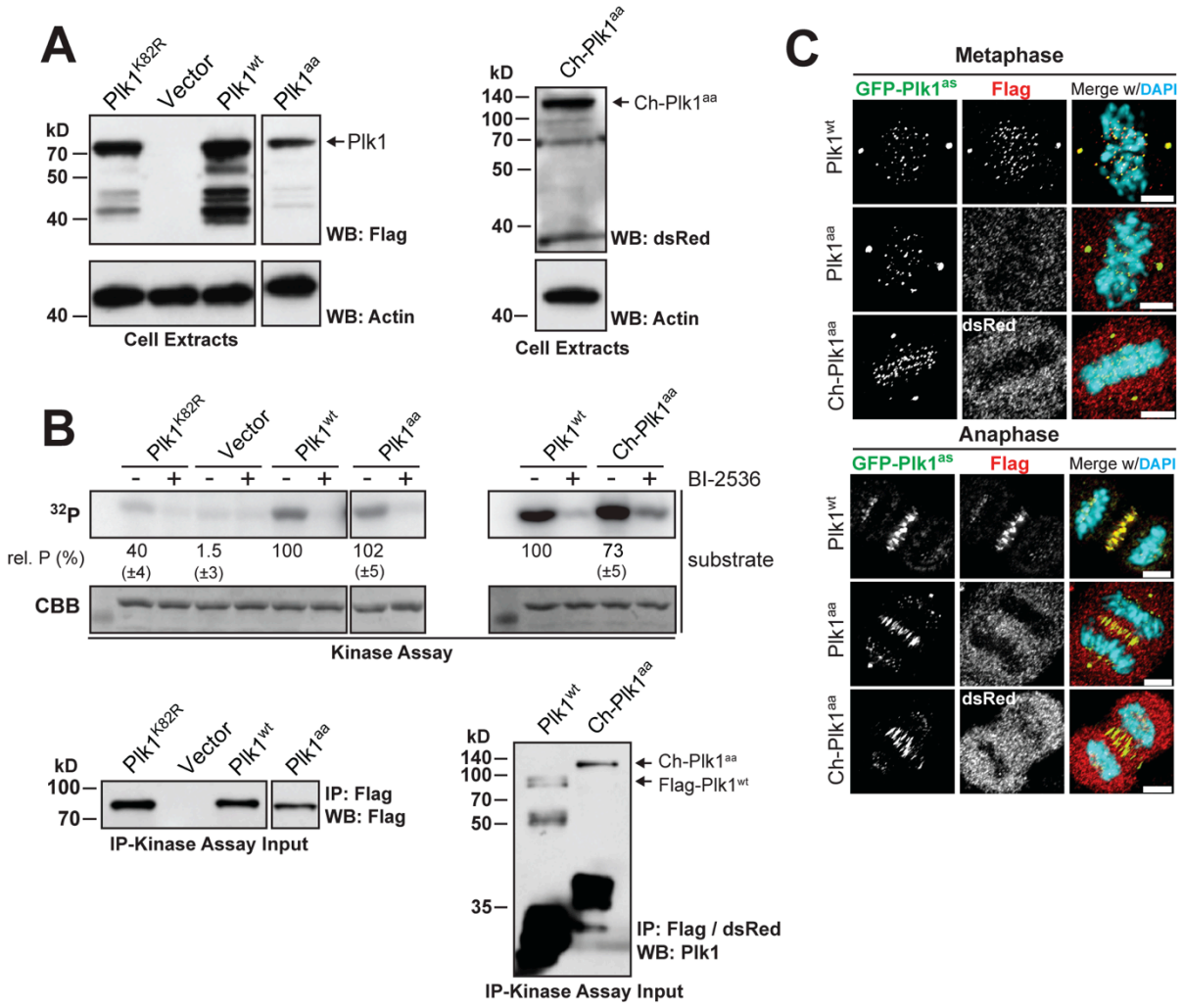

Figure 4.S2. Plk1 signaling at the kinetochore requires binding via its PBD (companion to Figure 4.1)

A, Immunoblot of mitotic protein extracts from RPE1 cell lines co-expressing GFP-Plk1^{as} and the Flag tag (Vector), wildtype Plk1 (Plk1^{wt}), wildtype Plk1 with a mutated PBD (Plk1^{aa} and Ch-Plk1^{aa}) or catalytically inactive Plk1 (Plk1^{K82R}). Membranes probed for Flag-tagged (Flag blot) or mCherry-tagged (dsRed) Plk1 and Actin (loading control). *B*, Plk1 construct activity determined by Flag- or dsRed-immunoprecipitation from mitotic protein lysates, followed by incubation with [γ-^{32}P]-ATP and Plk1-specific substrate.

Where indicated, 200 nM BI-2536 added to reactions to inhibit Plk1. *Top*, autoradiograph (^{32}P) and Coomassie gel (CBB) of substrate from kinase reactions. Average substrate labeling (± SEM) reported relative to Plk1^{wt}. Left-sided membrane in *A* and *B* cropped for presentation- uncropped versions viewable in Figure 4.S3, panels B and C. *Bottom*, immunoblot of kinase reaction input after immunoprecipitation (IP). Plk1 detected by Flag (left) or Plk1 (right) antibodies. *C*, Representative maximal intensity projection micrographs demonstrating normal localization of Plk1^{wt}, but impaired localization of Plk1^{aa}/Ch-Plk1^{aa}, to centrosomes and kinetochores during metaphase and the central spindle during anaphase. Scale bars, 5 μm.

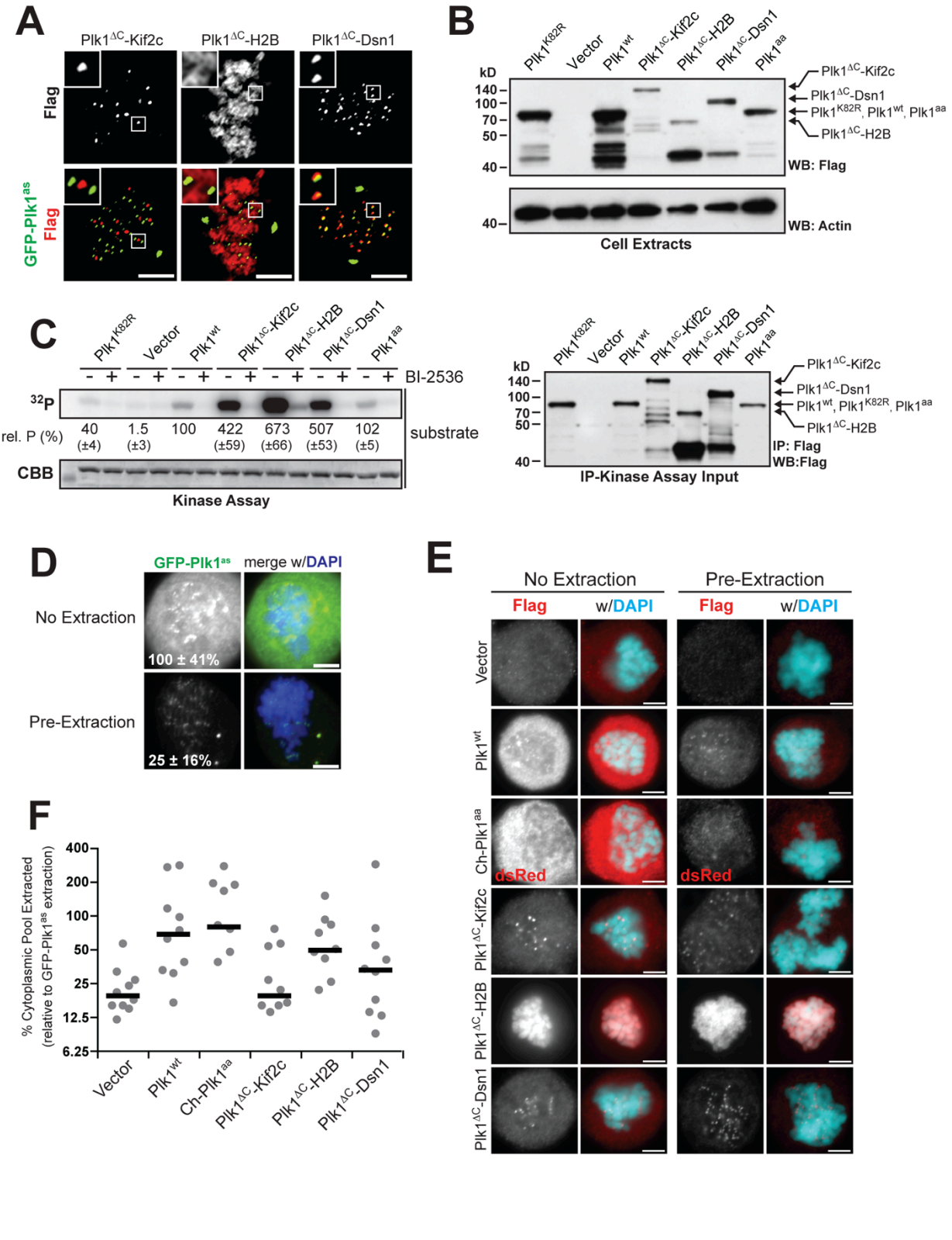
A
Plk1ΔC-Kif2c
Plk1ΔC-H2B
Plk1ΔC-Dsn1
Flag
GFP-Plk1as
Flag
B
Plk1K82R
Vector
Plk1wt
Plk1ΔC-Kif2c
Plk1ΔC-H2B
Plk1ΔC-Dsn1
Plk1aa
kD
140
100
70
50
40
Plk1ΔC-Kif2c
Plk1ΔC-Dsn1
Plk1K82R, Plk1wt, Plk1aa
Plk1ΔC-H2B
WB: Flag
40
WB: Actin
Cell Extracts
C
Plk1K82R
Vector
Plk1wt
Plk1ΔC-Kif2c
Plk1ΔC-H2B
Plk1ΔC-Dsn1
Plk1aa
- + - + - + - + - + - + - + BI-2536
32P
rel. P (%)
40 (±4)
1.5 (±3)
100
422 (±59)
673 (±66)
507 (±53)
102 (±5)
substrate
CBB
Kinase Assay
kD
140
100
70
50
40
Plk1ΔC-Kif2c
Plk1ΔC-Dsn1
Plk1wt, Plk1K82R, Plk1aa
Plk1ΔC-H2B
IP: Flag
WB:Flag
IP-Kinase Assay Input
D
GFP-Plk1as
merge w/DAPI
No Extraction
100 ± 41%
Pre-Extraction
25 ± 16%
E
No Extraction
Pre-Extraction
Flag
w/DAPI
Flag
w/DAPI
Vector
Plk1wt
Ch-Plk1aa
dsRed
dsRed
Plk1ΔC-Kif2c
Plk1ΔC-H2B
Plk1ΔC-Dsn1
F
% Cytoplasmic Pool Extracted
(relative to GFP-Plk1as extraction)
400
200
100
50
25
12.5
6.25
Vector
Plk1wt
Ch-Plk1aa
Plk1ΔC-Kif2c
Plk1ΔC-H2B
Plk1ΔC-Dsn1

Figure 4.S3. Analysis of kinetochore-tethered Plk1 constructs (companion to Figure 4.2)

A, Representative single plane micrographs depicting localization of Flag-tagged Plk1 localized to the inner centromere (Plk1ΔC-Kif2c), to chromatin (Plk1ΔC-H2B), or to the outer kinetochore (Plk1ΔC-Dsn1). *B*, Immunoblot of mitotic protein extracts from RPE1 cell lines co-expressing GFP-Plk1^{as} and the Flag tag (Vector), wildtype Plk1 (Plk1^{wt}), catalytically inactive Plk1 (Plk1^{K82R}), delocalized Plk1 (Plk1^{aa}) or the kinetochore-tethered Plk1 constructs. Membranes probed for Flag-tagged Plk1 (Flag blot) and Actin (loading control). *C*, Plk1 construct activity determined by Flag-immunoprecipitation from mitotic protein lysates, followed by incubation with [γ-^{32}P]-ATP and Plk1-specific substrate. Where indicated, 200 nM BI-2536 added to reactions to inhibit Plk1. Left, autoradiograph (^{32}P) and Coomassie gel (CBB) of substrate from kinase reactions. Average substrate labeling (± SEM) reported relative to Plk1^{wt}. Right, immunoblot of kinase reaction input after immunoprecipitation (IP). Plk1 detected by Flag antibody. *D-F*, Plk1 tethers exhibit soluble (cytoplasmic) fractions within cells. *D*, Representative single-plane, non-deconvolved micrographs of GFP-Plk1^{as} with and without 15 s pre-extraction prior to fixation. Numbers represent average fluorescent intensity (± SD) as a percent of the average intensity in non pre-extracted cells (n=60 cells/condition). *E*, Representative single-plane, non-deconvolved micrographs of Flag-tagged or mCherry-tagged (dsRed) Plk1 constructs with and without 15 s pre-extraction prior to fixation. *F*, Graph indicates percentage of tagged construct extracted relative to amount of GFP-Plk1^{as} extracted in cells. Dots represent single cells and bars indicate median values. Log_2 scale used for Y-axis. Scale bars, 5μm (panels *A*,*D*,*E*).

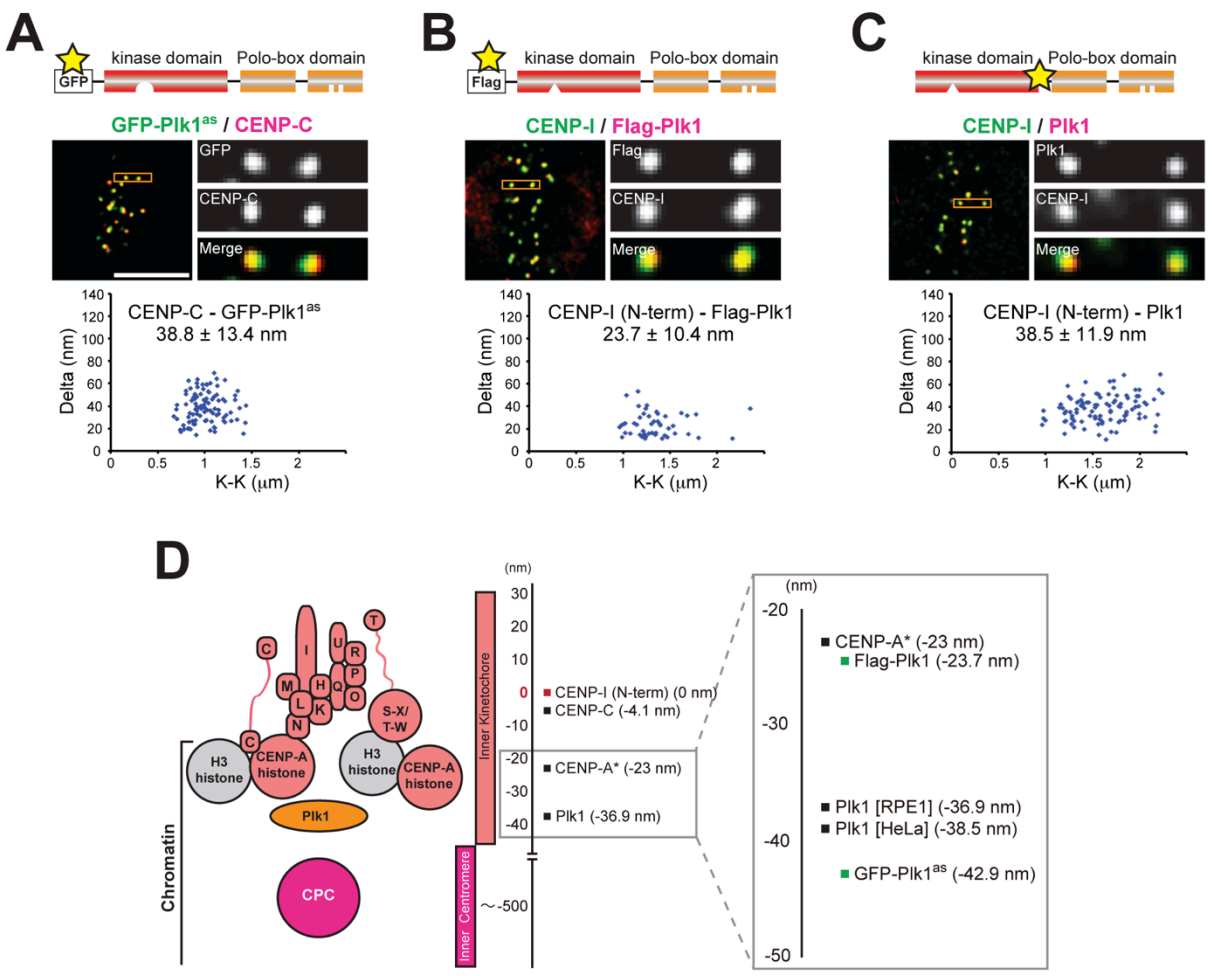

Figure 4.S4. Validation of high-resolution Plk1 localization in cells (companion to Figure 4.2)

A-C, High-resolution single plane micrographs and delta analysis of antibodies targeting GFP tag of the GFP-Plk1^{as} construct (panel *A*), Flag tag of the Flag-Plk1^{wt} construct (panel *B*) in RPE1 cells or endogenous Plk1 in HeLa cells (panel *C*). K-K indicates distance between the two centroids. Yellow stars indicate protein positions targeted by antibodies. *D,* Map of kinetochore plotting distances relative to the N-terminus of CENP-I.

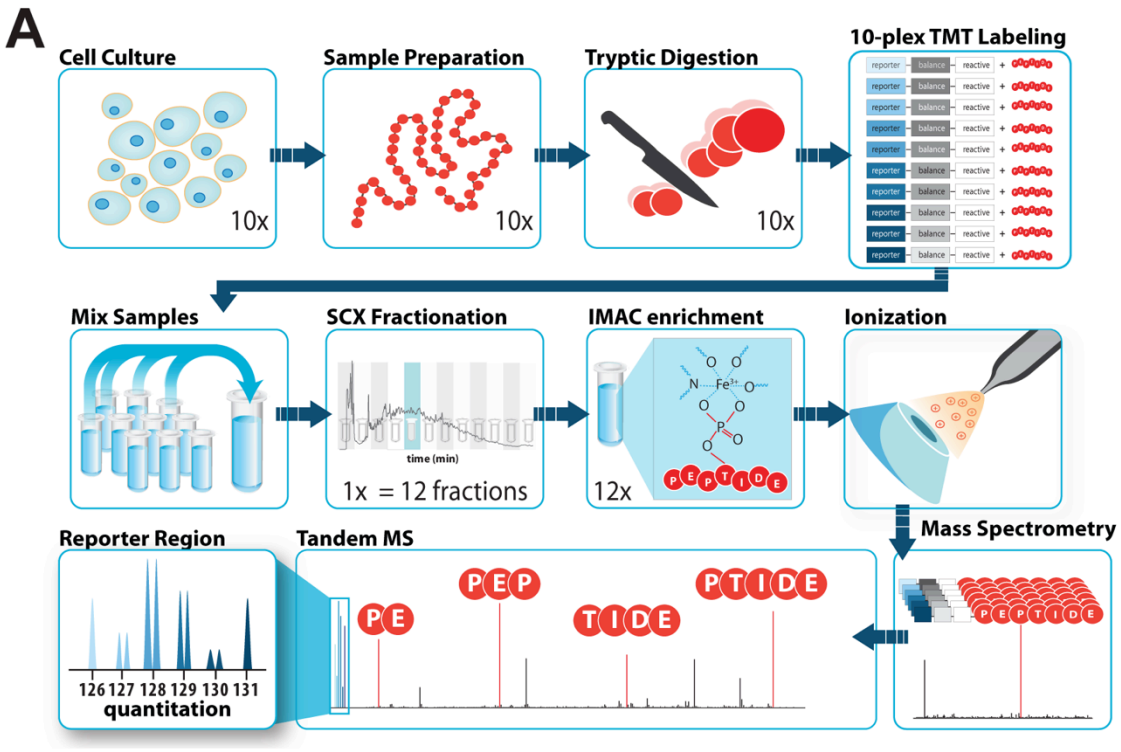

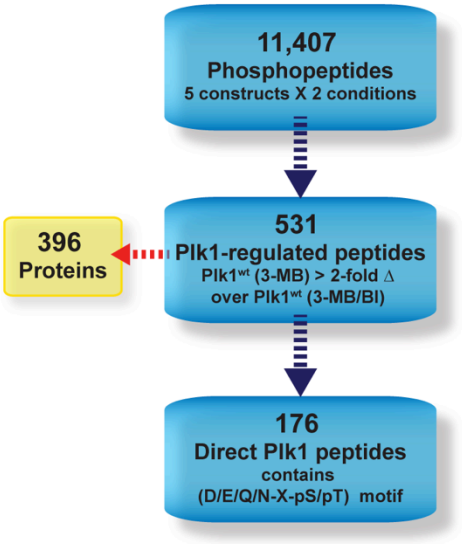

C

Direct Plk1 peptides at kinetochore

	Gene ID (residue)	Fold Δ vs. Plk1^{wt} (BI-2536 inhibited) WT	AA	Kif2c	H2B	Dsn1
outer kinetochore	CENPE (T2601;S2605)	4.6	2.8			
	CENPF (S1747**)	19.8	11.8	3.3	1.8	3.9
	CENPF (S1770;T1781)	2.9	1.1	1.6	1.0	1.4
	CDC27 (S435**)	6.4	1.8	9.2	0.8	1.2
	CDC27 (S387**)	2.1	1.1		1.1	1.9
	ANAPC1 (S372**;S377**)	7.1	0.5	1.0	0.4	1.0
	CHAMP1 (S627)	2.3		1.8	0.9	0.3
	TP53BP1 (S830;831;834)	10.3	1.1	2.8	1.4	1.9
	TP53BP1 (S998**;S1001**)	4.8	0.3	0.5	0.6	0.7
	CHD8 (S2008)	2.0	0.9	1.1	0.3	0.9
	USP16 (S423)	5.7	1.4	2.0	9.5	1.9
	KIF4A (S1054)	6.6	1.8	9.6	8.2	1.6
	ERCC6L (S980)	2.3	0.8	1.6	0.9	1.1
	ERCC6L (S1117;S1118)	2.3	0.6		0.7	1.2
inner centromere	INCENP (S218;T219)	3.2	2.2			2.9

Reversibly Restored
- > 10 fold
- 5-10 fold
- 2-5 fold

Not Reversibly Restored
- 1-2 fold
- < 1 fold
- > 2 fold, but not inhibited by BI-2536

Figure 4.S5. Sample preparation and results for mass spectrometry (MS) of Plk1 cell lines (companion to Figures 4.3 and 4.4)

RPE1 cells coexpressing GFP-Plk1^{as} and Flag-Plk1^{wt}, Ch-Plk1^{aa}, Flag-Plk1ΔC-Kif2c, Flag-Plk1ΔC-H2B, or Flag-Plk1ΔC-Dsn1 were challenged with 10 μM 3-MB-PP1 (inhibits Plk1^{as}) +/- 200 nM BI-2536 (inhibits complementing wildtype Plk1 allele) for a total of 10 samples. Mitotic cells were collected by shake-off. *A*, Pellets were lysed, and their resultant proteins were denatured, reduced, alkylated, and tryptically digested. The 10 samples were each chemically labeled with isobaric 10-plex TMT tags and mixed in equal ratios. The single pooled sample was fractionated by Strong Cation Exchange (SCX) chromatography, and the 12 resultant SCX fractions were enriched for phosphopeptides by immobilized metal affinity chromatography (IMAC). Phosphopeptides from each fraction were chromatographically separated and ionized for MS analysis. Isobaric, chemically labeled peptide species were isolated and fragmented to produce sequencing ions. MS fragmentation also releases non-isobaric reporter ions from the TMT tags, which reveal the relative abundance of each peptide across the 10 cell lines (inset). *B*, A total of 11,407 phosphopeptides were encountered, of which 531 (translating to 396 proteins) were regulated by Plk1 (Flag-Plk1^{wt} cell line exhibited > 2-fold change when comparing 3-MB-PP1 challenged cells with those challenged both with 3-MB-PP1 and BI-2536). 176/531 peptides also contained the D/E/N/Q-X-pS/pT motif, indicating that these were likely direct Plk1 targets. *C*, Quantitative analysis of mitotic kinetochore phosphopeptides directly targeted by wild-type Plk1 (WT) and relative targeting abilities of the PBD mutant (AA) or kinetochore-tethered Plk1 (Kif2c, H2B, or Dsn1). Values indicate fold-change (>2-fold considered

significant) in phosphopeptide abundance of the uninhibited Plk1 constructs compared to inhibition of WT. Phosphopeptides arranged from outer kinetochore to inner centromere.

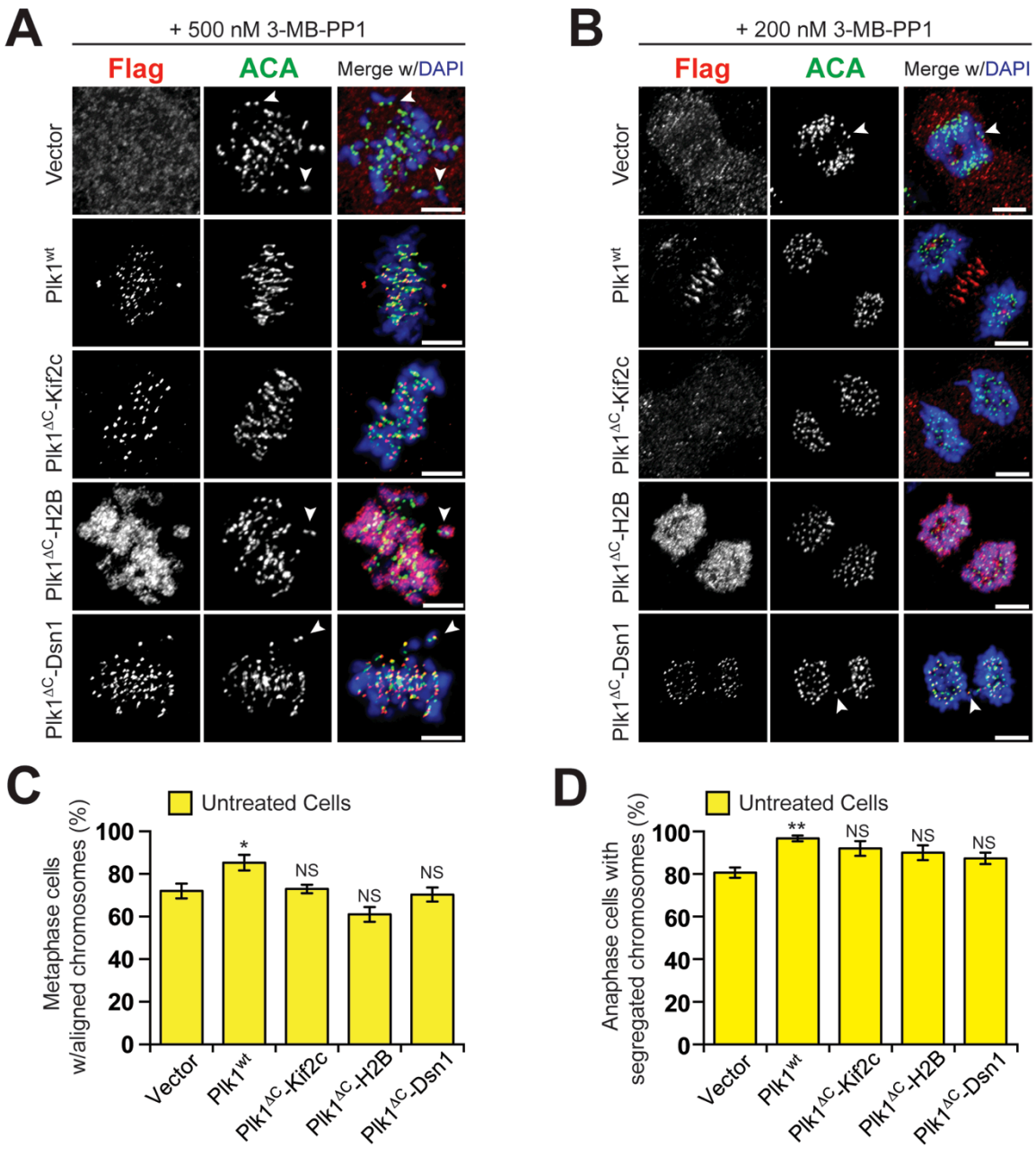

Figure 4.S6. Plk1 activity tethered to chromatin or the inner centromere promotes chromosome alignment and segregation (companion to Figure 4.4)

A, Representative maximal intensity projection micrographs of pre-anaphase mitotic cells challenged with 500 nM 3-MB-PP1. Arrowheads indicate misaligned chromosomes. *B*, Representative maximal intensity projection micrographs of

anaphase cells challenged with 200 nM 3-MB-PP1. Arrowheads indicate lagging chromosomes. ACA, Anti-Centromere Antibody. Scale bars, 5 μm. *C-D*, Plk1 tethered to kinetochore proteins Kif2c, H2B, or Hec1 do not produce mitotic errors in untreated cells. *C*, Graph shows average percentage (±SEM) of pre-anaphase mitotic cells at metaphase with fully aligned chromosomes for each cell line (n=150 cells/experiment; 3 independent experiments). *D*, Graph shows average percentage (±SEM) of anaphase cells with fully segregated chromsomes for each cell line (n≥50 cells/experiment; 3 independent experiments). *P<.05, **P<0.005 by one-way ANOVA; NS, not significant.

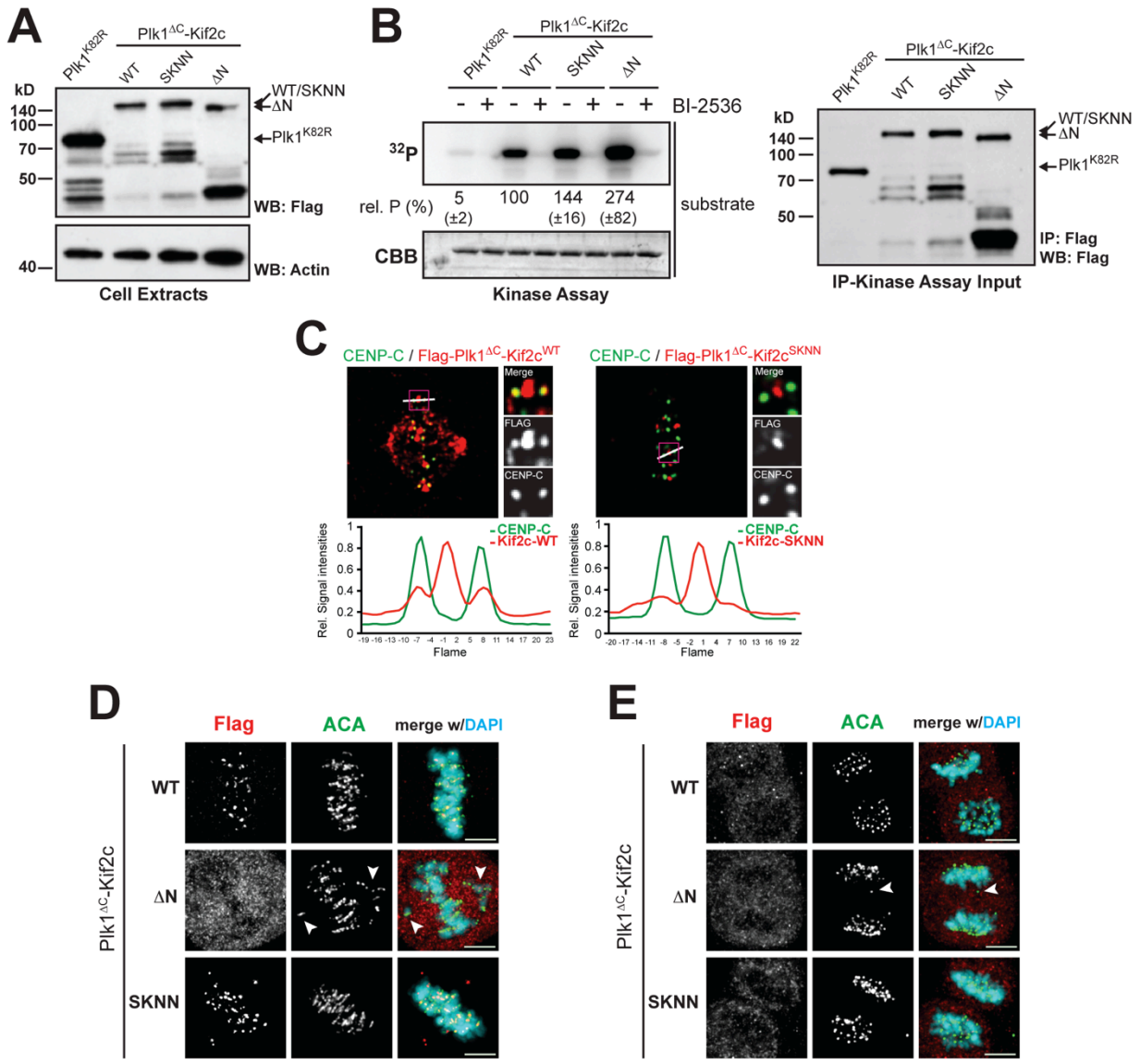

Figure 4.S7. Plk1 activity tethered to the inner centromere pool of Kif2c rescues chromosome alignment and segregation (companion to Figure 4.4)

A, Immunoblot of mitotic protein extracts from RPE1 cell lines co-expressing GFP-Plk1^{as} and catalytically inactive Plk1 (Plk1^{K82R}), or wildtype Plk1 tethered to wildtype Kif2c (WT), Kif2c with an N-terminal deletion that prevents inner centromere and (+)tip targeting (ΔN), or Kif2c with a mutated SxIP domain that prevents (+)tip targeting

(SKNN). Membranes probed for Flag-tagged Plk1 (Flag blot) and Actin (loading control). *B*, Plk1 construct activity determined by Flag-immunoprecipitation from mitotic protein lysates, followed by incubation with [γ-^{32}P]-ATP and Plk1-specific substrate. Where indicated, 200 nM BI-2536 added to reactions to inhibit Plk1. Left, autoradiograph (^{32}P) and Coomassie gel (CBB) of substrate from kinase reactions. Average substrate labeling (± SEM) reported relative to WT. Right, immunoblot of kinase reaction input after immunoprecipitation (IP). Plk1 detected by Flag antibody. *C*, Single-plane, high-resolution micrographs of Kif2c-WT and SKNN mutant showing lack of outer kinetochore Kif2c signal. Linescans indicate relative signal intensities from the CENP-C and Flag antibodies of kinetochore pair highlighted in inset. *D*, Representative maximal intensity projection micrographs of pre-anaphase mitotic cells challenged with 500 nM 3-MB-PP1. Arrowheads indicate misaligned chromosomes. *E*, Representative maximal intensity projection micrographs of anaphase cells challenged with 200 nM 3-MB-PP1. Arrowheads indicate lagging chromosomes. ACA, Anti-Centromere Antibody. Scale bars, 5 μm

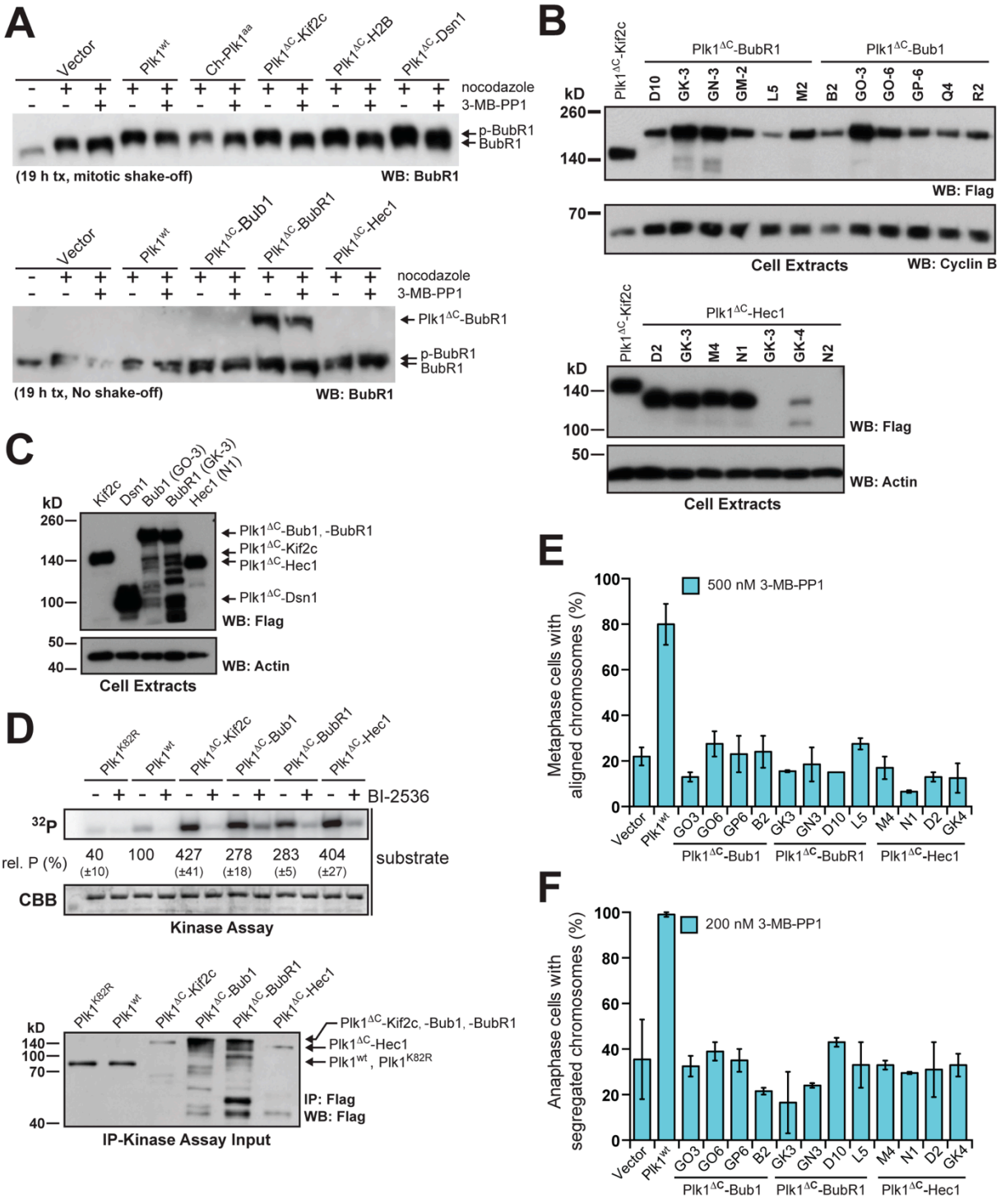
A
Vector
Plk1wt
Ch-Plk1aa
Plk1ΔC-Kif2c
Plk1ΔC-H2B
Plk1ΔC-Dsn1
nocodazole
3-MB-PP1
p-BubR1
BubR1
(19 h tx, mitotic shake-off)
WB: BubR1
Vector
Plk1wt
Plk1ΔC-Bub1
Plk1ΔC-BubR1
Plk1ΔC-Hec1
nocodazole
3-MB-PP1
Plk1ΔC-BubR1
p-BubR1
BubR1
(19 h tx, No shake-off)
WB: BubR1
B
Plk1ΔC-Kif2c
Plk1ΔC-BubR1
Plk1ΔC-Bub1
D10
GK-3
GN-3
GM-2
L5
M2
B2
GO-3
GO-6
GP-6
Q4
R2
kD
260
140
WB: Flag
70
Cell Extracts
WB: Cyclin B
Plk1ΔC-Kif2c
Plk1ΔC-Hec1
D2
GK-3
M4
N1
GK-3
GK-4
N2
kD
140
100
WB: Flag
50
WB: Actin
Cell Extracts
C
Kif2c
Dsn1
Bub1 (GO-3)
BubR1 (GK-3)
Hec1 (N1)
kD
260
140
100
50
40
Plk1ΔC-Bub1, -BubR1
Plk1ΔC-Kif2c
Plk1ΔC-Hec1
Plk1ΔC-Dsn1
WB: Flag
WB: Actin
Cell Extracts
D
Plk1K82R
Plk1wt
Plk1ΔC-Kif2c
Plk1ΔC-Bub1
Plk1ΔC-BubR1
Plk1ΔC-Hec1
BI-2536
32P
rel. P (%)
40 (±10)
100
427 (±41)
278 (±18)
283 (±5)
404 (±27)
substrate
CBB
Kinase Assay
kD
140
100
70
40
Plk1ΔC-Kif2c, -Bub1, -BubR1
Plk1ΔC-Hec1
Plk1wt, Plk1K82R
IP: Flag
WB: Flag
IP-Kinase Assay Input
E
500 nM 3-MB-PP1
Metaphase cells with aligned chromosomes (%)
100
80
60
40
20
0
Vector
Plk1wt
GO3
GO6
GP6
B2
GK3
GN3
D10
L5
M4
N1
D2
GK4
Plk1ΔC-Bub1
Plk1ΔC-BubR1
Plk1ΔC-Hec1
F
200 nM 3-MB-PP1
Anaphase cells with segregated chromosomes (%)
100
80
60
40
20
0
Vector
Plk1wt
GO3
GO6
GP6
B2
GK3
GN3
D10
L5
M4
N1
D2
GK4
Plk1ΔC-Bub1
Plk1ΔC-BubR1
Plk1ΔC-Hec1

Figure 4.S8. Analysis of outer kinetochore-tethered Plk1 constructs (companion to Figure 4.5)

A, Immunoblot for BubR1 in mitotic extracts from cell lines co-expressing GFP-Plk1as and the Flag tag (Vector), wildtype Plk1 ($Plk1^{wt}$), delocalized (Ch-$Plk1^{aa}$) or kinetochore-tethered Plk1 constructs (Top: Kif2c, H2B, Dsn1; Bottom: Bub1, BubR1, Hec1) challenged with nocodazole ± 10 μM 3-MB-PP1. *B*, Immunoblot of mitotic protein extracts from RPE1 cell lines co-expressing GFP-$Plk1^{as}$ and Plk1 tethered to Kif2c, Bub1, BubR1 or Hec1. Each lane represents a clonal cell line. Membranes probed for Flag-tagged Plk1 (Flag blot) and Cyclin B (mitotic fraction, *Top*) or actin (loading control, *Bottom*). *C-D*, Highest expressing cell lines, Bub1 (GO-3), BubR1 (GK-3), and Hec1 (N1) were selected for further characterization. *C*, Immunoblot of mitotic protein extracts comparing expression of kinetochore-tethered Plk1 constructs. *D*, Plk1-tethered construct activity determined by Flag-immunoprecipitation from mitotic protein lysates, followed by incubation with [γ-^{32}P]-ATP and Plk1-specific substrate. Where indicated, 200 nM BI-2536 added to reactions to inhibit Plk1. *Top*, autoradiograph (^{32}P) and Coomassie gel (CBB) of substrate from kinase reactions. Average substrate labeling (± SEM) reported relative to $Plk1^{wt}$. *Bottom*, immunoblot of kinase reaction input after immunoprecipitation (IP). Plk1 detected by Flag antibody. *E-F*, Moderate to low expressing outer kinetochore tethers also fail to restore metaphase chromosome alignment or anaphase chromosome segregation when GFP-Plk1as is inhibited with 3-MB-PP1. *E*, Graph shows average percentage (± SEM) of pre-anaphase cells with bipolar spindles for each cell line challenged with 10 μM 3-MB-PP1 (n=100 cells/experiment; 2 independent experiments). *F*, Graph shows average percentage (±

SEM) of anaphase cells with fully segregated chromosomes for each cell line (n≥30 cells/experiment; 2 independent experiments).

NAME	SEQUENCE
USER INSERT TOP	5'-GAATTGCTGAGGAGACATCTAGAGAATTCTCTAGACTTTCCCTCAGCAATTCCGC-3'
USER INSERT BOTTOM	5'-GCGGAATTGCTGAGGGAAAGTCTAGAGAATTCTCTAGATGTCTCCTCAGCAATTC-3'
Bub1 FWD	5'-GGAGACAUATGGACACCCCGGAAAATG-3'
Bub1 REV	5'-GGGAAAGUTTATTTTCGTGAACGCTTACATTCT-3'
BubR1 FWD	5'-GGAGACAUATGGCGGCGGTGAAGAAGG-3'
BubR1 REV	5'-GGGAAAGUTCACTGAAAGAGCAAAGCCCC-3'
Hec1 FWD	5'-GGAGACAUATGAAGCGCAGTTCAGTTTCCAG-3'
Hec1 REV	5'-GGGAAAGUTCATTCTTCAGAAGACTTAATTAGAGTAGC-3'
Kif2c FWD	5'-GGAGACAUATGGCCATGGACTCGTCGC-3'
Kif2c REV	5'-GGGAAAGUTCACTGGGGCCGTTTCTTG-3'
H2B FWD	5'-GGAGACAUATGCCAGAGCCAGCGAAGTC-3'
H2B REV	5'-GGGAAAGUTAACTTAGCGCTGGTGTACTTGGTG-3'
Dsn1 FWD	5'-GGAGACAUATGACTTCAGTGACTAGATCAGAGATCA-3'
Dsn1 REV	5'-GGGAAAGUTCACTGACAAGATCCAGATCCAGAT-3'
Kif2c-ΔN	5'-GGAGACAUCGCAAGCAGTTTTCAGTTCCTC-3'
Kif2c-SKNN TOP	5'-GTGAATTCCAAAAACAACGCTCCAAAAGAAAGTCTTCGAAG-3'
Kif2c-SKNN BOTTOM	5'-CGTTGTTTTTGGAATTCACGGATCTCCGTTTTTGTTTCTG-3'

Table 4.S1. Table of primers used for USER cloning and mutagenesis

Antibody	Source	Reference
Human anti-ACA	Immunovision (HCT-0100)	145
Sheep anti-BubR1 (SBR1.1)	Steven Taylor	173
Rabbit anti-CENP-I	Tim Yen	174
Rabbit anti-CENP-C	Iain Cheeseman	175
Rabbit anti-CENP-U/50	MBL (PD019)	152
Rabbit anti-DsRed	Clontech (632496)	145
Mouse anti-Flag (M2)	Sigma-Aldrich (F1804)	This Study
Mouse anti-GFP (3E6)	Invitrogen (A-11120)	This Study
Mouse anti-Plk1 (F8)	Santa Cruz Biotechnology (sc-17783)	145
Rat anti-Tubulin (YL1/2)	EMD Millipore (MAB1864)	145

Table 4.S2. Table of antibodies used for immunofluorescence and immunoblotting

Chapter V—Perspectives

Polo-like kinase 1 (Plk1) regulates many critical activities during mitosis, including spindle assembly, chromosome alignment, chromosome segregation, and cytokinesis. Ironically, this multi-functionality limits the ability to interrogate many of Plk1's individual functions. Current genetic tools have provided important insights into Plk1 function by identifying a host of substrates and binding partners. Yet these findings remain somewhat disconnected. The focus of this dissertation was to develop new investigative strategies to complement traditional techniques, so we could develop a comprehensive understanding of Plk1. Here, I highlight several important findings from my work and suggest future directions for study.

Partitioning Plk1 function by chemical titration elucidates its role in maintaining genomic fidelity

A major finding from the inhibitor titration experiments was that chromosome segregation was the most sensitive of the Plk1 functions surveyed (Figure 3.9). Moreover, impaired segregation was characterized by both lagging chromosomes and decreased spindle elongation (Figure 3.5). Previously, decreased spindle elongation was the only anaphase defect identified with chemical inhibition[84,86,87]. Thus, my results suggest that Plk1 operates via two distinct mechanisms to promote proper chromosome segregation during anaphase and these mechanisms likely involve separate substrate pools. To my knowledge, no Plk1 substrate has been implicated spindle elongation and only one substrate, Kif2b[82], is directly linked to lagging chromosomes. Therefore, inhibitor titration provides an avenue to probe the mechanisms underlying these activities.

The findings from this work have important clinical implications as well. Numerous Plk1 inhibitors are in clinical development. Chromosome missegregation will be encountered if these inhibitors are delivered in low doses to limit toxicity or after pharmacologic washout, which dictates that low drug levels will be traversed (Figure 5.1). Moreover, chromosome missegregation with Plk1 inhibition is associated with tetraploidy, impaired proliferation and senescence (Figure 3.8B-D) in non-transformed RPE1 cells. Cancer cells with deregulated cell cycle controls may exhibit markedly different effects. Therefore, mechanistic understanding of Plk1 inhibitor-induced chromosome missegregation may be crucial for selection of optimal cancer subtypes and dosing regime.

Partitioning Plk1 function by kinetochore locale reveals that Plk1 operates at the inner centromere and chromatin

Isolation of Plk1 functions by inhibitor titration afforded me the opportunity to develop a chemical genetic complementation strategy to partition Plk1 functions by subcellular locale. In doing so, I learned that Plk1 operates within centromeric chromatin and at the inner centromere. Notably, matching functional profiles of the kinetochore-tethered Plk1 constructs with their phosphoproteomic signatures revealed two substrates potentially important for chromosome segregation: Kif4a and Usp16 (Figure 4.6A). Kif4a has documented roles in chromosome segregation[176] and central spindle assembly[177] and elongation[178], whereas Usp16 has recently been identified as a *bona fide* Plk1 kinetochore substrate[179]. One area of future investigation will be to determine if either Kif4a or Usp16 are Plk1-specific effectors of chromosome segregation.

A novel role for Plk1 in maintaining kinetochore architecture

The prevailing model for Plk1 activity at the kinetochore is that it promotes chromosome alignment and segregation by stabilizing microtubule attachments to the kinetochore. Several lines of evidence support this concept. First, microscopic analysis reveals that chemical inhibition of Plk1 prevents the establishment and maintenance of stable microtubule attachments to the kinetochore[66]. Second, Plk1 stabilizes attachments, promoting chromosome alignment, by phosphorylating BubR1, which in turn recruits Protein phosphatase 2A (PP2A) to counteract attachment destabilization by Aurora B[78]. Finally, Plk1 phosphorylates the microtubule depolymerase Kif2b to destabilize incorrect attachments, which results in proper chromosome segregation[82]. Both BubR1 (Figure 4.2B, 4.2D) and Kif2b[82] localize to the outer kinetochore; however, my findings suggest that Plk1 also operates at the inner kinetochore. Microscopic evidence localizes Plk1 at the inner kinetochore, internal to the centromere-specific histone variant CENP-A (Figure 4.2B, 4.2D) and functional analyses using kinetochore-tethered Plk1 indicate that chromatin- or inner centromere-tethered activity promotes chromosome alignment and segregation. So how is Plk1 mediating chromosome alignment and segregation?

My previous attempts to answer this question using inhibitor titration have been largely unsuccessful, notable only for circumstantial evidence implicating merotelic attachments (Figure 3.7). Recently, however, I have observed that lagging chromosomes generated by Plk1 inhibition are largely devoid of major kinetochore proteins, including CENP-A (Figure 5.2). Notably, this loss is specific to Plk1 inhibition

as generating lagging chromosomes by nocodazole washout fails to recapitulate this phenotype (Figure 5.2A-B,D-F). Because CENP-A provides the foundation for kinetochore assembly[180,181], a simple explanation is that Plk1 mediates CENP-A loading at centromeric nucleosomes- a finding recently reported by Iain Cheeseman's group[182]. Failure to properly load CENP-A results in impaired kinetochore assembly, preventing correct microtubule attachment, which leads to impaired chromosome segregation. There are several critical limitations to this explanation, however. First, CENP-A loading occurs exclusively during G1[183–185]. The anaphase defects I have observed occur within 6 hours of inhibitor challenge, meaning Plk1 inhibition occurs during G2 at the earliest. Second, CENP-A is stably associated at the centromere with a 50% reduction occurring during S-phase as the nucleosomes are equally partitioned between the sister DNA strands[185,186]. Therefore, only a 50% signal reduction would be expected with failure to load CENP-A. My findings demonstrate almost complete loss of CENP-A signal on lagging chromosomes (Figure 5.2C-D). Moreover, I observe similar reductions in CENP-C and CENP-T levels (Figure 5.2E-F), which is in contrast to a previous report that CENP-C and CENP-T reduction at kinetochores is delayed following CENP-A knockout[186]. Thus, my findings do not support a model whereby Plk1 inhibition perturbs kinetochore loading of CENP-A. Rather, they suggest perturbation in retention of CENP-A and other kinetochore proteins. How this occurs is an important area of future investigation, because it establishes a mechanistic link of how Plk1 promotes proper chromosome segregation during anaphase.

Conclusion

The findings presented in this dissertation highlight the power of an orthogonal chemical genetic system to interrogate the functions of a pleiotropic kinase, such as Plk1. Major findings include: the discovery that Plk1 localizes to the inner kinetochore and that some of its signaling activities are mediated within this region, and the characterization of its role in chromosome segregation and the identification of two substrates that may mediate this activity. Additionally, the strategies developed herein provide opportunities to interrogate other known Plk1 functions (e.g. chromosome alignment), or to use activity tethering to elucidate new functions (e.g. cytokinesis functions with membrane tethering). Moreover, they may be adapted to study other multifunctional kinases. Finally, this works reinforces the importance of investigating cellular biology to inform rational development of kinase inhibitors as cancer therapies.

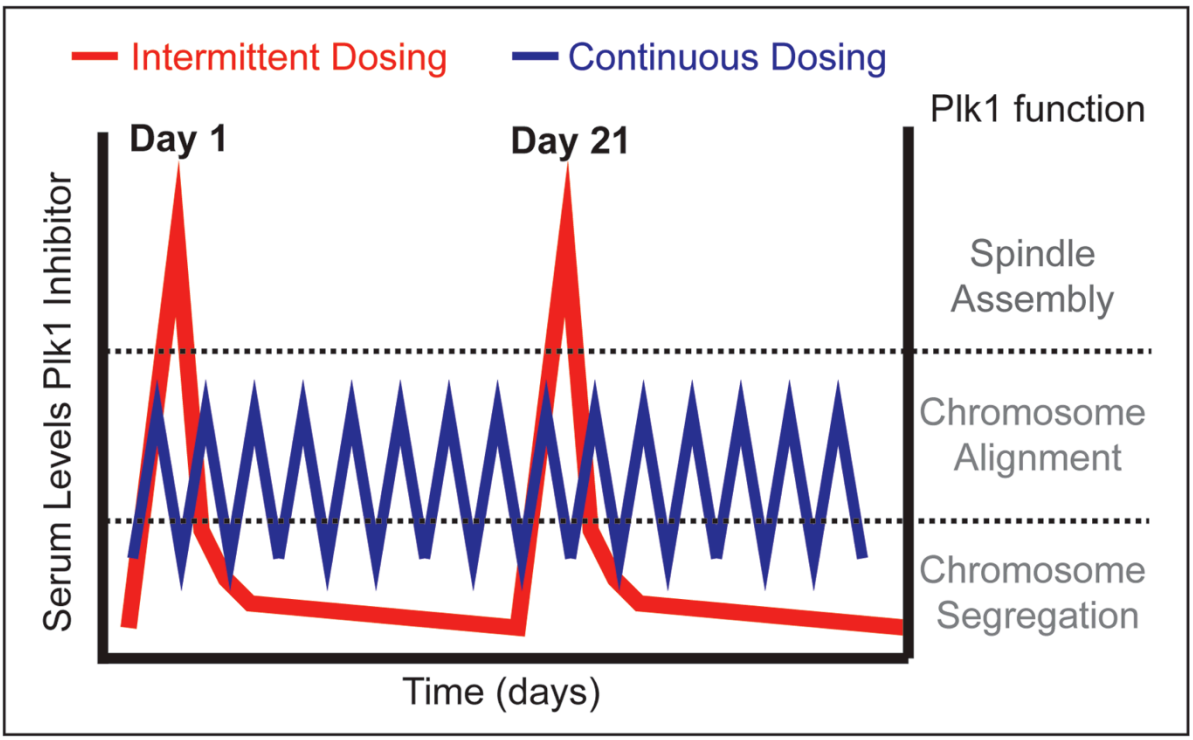

Figure 5.1. Schematic demonstrating differential clinical effects of Plk1 inhibitors

Clinical effects from Plk1 inhibition will likely vary based on serum levels of inhibitor. Serum levels of Plk1 inhibitors used in a traditional 3-week Intermittent dosing schedule (red line) will peak initially, affecting spindle assembly in mitotic cells. As the inhibitor washes out, bipolar spindles will form, but chromosome alignment and segregation defects may be encountered. To limit toxicity, a continuous dosing schedule may be used (blue line). In this case, spindle assembly defects may not be observed, however alignment and segregation defects will be the primary phenotype encountered.

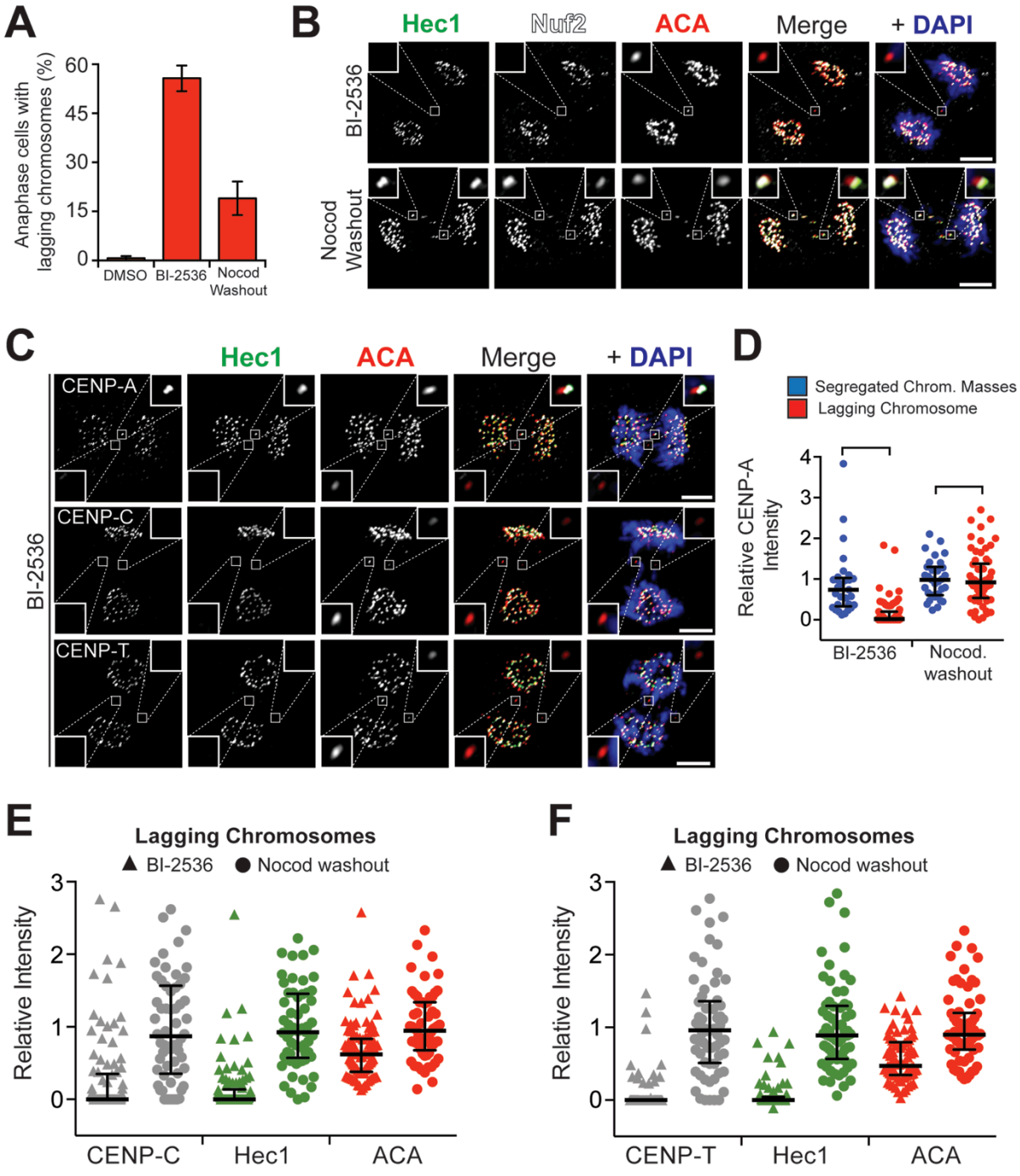
A
Anaphase cells with lagging chromosomes (%)
60
45
30
15
0
DMSO
BI-2536
Nocod Washout
B
Hec1
Nuf2
ACA
Merge
+ DAPI
BI-2536
Nocod Washout
C
Hec1
ACA
Merge
+ DAPI
CENP-A
CENP-C
CENP-T
BI-2536
D
Segregated Chrom. Masses
Lagging Chromosome
Relative CENP-A Intensity
4
3
2
1
0
BI-2536
Nocod. washout
E
Lagging Chromosomes
BI-2536
Nocod washout
Relative Intensity
3
2
1
0
CENP-C
Hec1
ACA
F
Lagging Chromosomes
BI-2536
Nocod washout
Relative Intensity
3
2
1
0
CENP-T
Hec1
ACA

Figure 5.2. Plk1 inhibition induces lagging chromosomes characterized by loss of kinetochore proteins

Human RPE1 cells were challenged for 6 h with DMSO or 40 nM BI-2536, or for 5 h with 0.2 μg/mL nocodazole followed by a 45 min washout. Cells were fixed and processed for immunofluorescence analysis of the kinetochore proteins Hec1, Nuf2, CENP-A, CENP-C, and CENP-T during anaphase. *A,* Graph depicting the average percentage of anaphase cells (± SEM) exhibiting lagging chromosomes (n=50 cells/condition, 3 independent experiments. *B,* Representative maximal intensity projection micrographs of anaphase cells challenged with BI-2536 or from nocodazole washout. Insets highlight absence of outer kinetochore proteins Hec1 and Nuf2 with BI-2536 challenge, but not with nocodazole washout. *C,* Representative maximal intensity projection micrographs of anaphase cells challenged with BI-2536. Insets highlight absence of inner kinetochore proteins CENP-A, CENP-C, and CENP-T. *D,* Graph of relative CENP-A intensity at kinetochores of lagging chromosomes or segregated chromosome masses (n=10 cells/condition, 3 independent experiments). Each dot represents an individual lagging chromosome or segregated chromosome mass. Bars indicate the median and interquartile range. *E-F,* Graphs of relative CENP-C (panel *E*) or CENP-T (panel *F*), Hec1 and ACA intensities at kinetochores of lagging chromosomes after BI-2536 challenge (triangles) or nocodazole washout (circles) (n=10 cells/condition, 3 independent experiments). Each symbol represents an individual lagging chromosome. Bars indicate the median and interquartile range. ACA, Anti-Centromere Antibody. Scale bars, 5 μm (panels *B* and *C*).

References

1. Weinberg, R. A. *One Renegade Cell: How Cancer Begins*. (1st ed. New York, NY : Basic Books, c1998., 1998).

2. Choudhary, A. *et al.* Interphase cytofission maintains genomic integrity of human cells after failed cytokinesis. *Proc. Natl. Acad. Sci. U. S. A.* **110,** 13026-31 (2013).

3. Zasadil, L. M., Britigan, E. M. C. & Weaver, B. A. A. 2n or not 2n: Aneuploidy, polyploidy and chromosomal instability in primary and tumor cells. *Semin Cell Dev Biol.* **24,** 370–379 (2013).

4. Siegel, J. J. & Amon, A. New Insights into the Troubles of Aneuploidy. *Annu. Rev. Cell Dev. Biol.* **28,** 189-214 (2012).

5. Ganem, N. J., Godinho, S. A. & Pellman, D. A mechanism linking extra centrosomes to chromosomal instability. *Nature* **460,** 278–282 (2009).

6. Davoli, T. & de Lange, T. The causes and consequences of polyploidy in normal development and cancer. *Annu. Rev. Cell Dev. Biol.* **27,** 585–610 (2011).

7. Orr, B. & Compton, D. A. A double-edged sword: how oncogenes and tumor suppressor genes can contribute to chromosomal instability. *Front Oncol* **3,** 164 (2013).

8. Lera, R. F. & Burkard, M. E. The Final Link: Tapping the Power of Chemical Genetics to Connect the Molecular and Biologic Functions of Mitotic Protein Kinases. *Molecules* **17,** 12172–12186 (2012).

9. Parsons, G. G. & Spencer, C. A. Mitotic repression of RNA polymerase II transcription is accompanied by release of transcription elongation complexes. *Mol Cell Biol* **17,** 5791–5802 (1997).

10. Manning, G., Whyte, D. B., Martinez, R., Hunter, T. & Sudarsanam, S. The protein kinase complement of the human genome. *Science* **298,** 1912–1934 (2002).

11. Dulla, K., Daub, H., Hornberger, R., Nigg, E. A. & Körner, R. Quantitative site-specific phosphorylation dynamics of human protein kinases during mitotic

progression. *Mol. Cell. Proteomics* **9,** 1167–1181 (2010).

12. Daub, H. *et al.* Kinase-selective enrichment enables quantitative phosphoproteomics of the kinome across the cell cycle. *Mol Cell* **31,** 438–448 (2008).

13. Nigg, E. A. Mitotic kinases as regulators of cell division and its checkpoints. *Nat Rev Mol Cell Biol* **2,** 21–32 (2001).

14. Ma, H. T. & Poon, R. Y. C. How protein kinases co-ordinate mitosis in animal cells. *Biochem. J.* **435,** 17–31 (2011).

15. Marzo, I. & Naval, J. Antimitotic drugs in cancer chemotherapy: promises and pitfalls. *Biochem. Pharmacol.* **86,** 703–710 (2013).

16. Golsteyn, R. M. *et al.* Cell cycle analysis and chromosomal localization of human Plk1, a putative homologue of the mitotic kinases Drosophila polo and Saccharomyces cerevisiae Cdc5. *J. Cell Sci.* **107,** 1509–1517 (1994).

17. Hamanaka, R. *et al.* Cloning and characterization of human and murine homologues of the Drosophila polo serine-threonine kinase. *Cell Growth Differ* **5,** 249–257 (1994).

18. Lu, L.-Y. *et al.* Polo-like kinase 1 is essential for early embryonic development and tumor suppression. *Mol Cell Biol* **28,** 6870–6876 (2008).

19. Sunkel, C. E. & Glover, D. M. polo, a mitotic mutant of Drosophila displaying abnormal spindle poles. *J. Cell Sci.* **89,** 25–38 (1988).

20. Llamazares, S. *et al.* polo encodes a protein kinase homolog required for mitosis in Drosophila. *Genes Dev.* **5,** 2153–2165 (1991).

21. Clay, F. J., McEwen, S. J., Bertoncello, I., Wilks, A. F. & Dunn, A. R. Identification and cloning of a protein kinase-encoding mouse gene, Plk, related to the polo gene of Drosophila. *Proc. Natl. Acad. Sci. U. S. A.* **90,** 4882–4886 (1993).

22. Lake, R. J. & Jelinek, W. R. Cell cycle- and terminal differentiation-associated regulation of the mouse mRNA encoding a conserved mitotic protein kinase. *Mol Cell Biol* **13,** 7793–7801 (1993).

23. Holtrich, U. *et al.* Induction and down-regulation of PLK, a human serine/threonine kinase expressed in proliferating cells and tumors. *Proc. Natl. Acad. Sci. U. S. A.* **91,** 1736–1740 (1994).

24. Kumagai, A & Dunphy, W. G. Purification and molecular cloning of Plx1, a Cdc25-regulatory kinase from Xenopus egg extracts. *Science* **273,** 1377–1380 (1996).

25. Hartwell, L. H., Mortimer, R. K., Culotti, J. & Culotti, M. Genetic Control of the Cell Division Cycle in Yeast: V. Genetic Analysis of cdc Mutants. *Genetics* **74,** 267–286 (1973).

26. Zitouni, S., Nabais, C., Jana, S. C., Guerrero, A. & Bettencourt-Dias, M. Polo-like kinases: structural variations lead to multiple functions. *Nat Rev Mol Cell Biol* **15,** 433–452 (2014).

27. Bettencourt-Dias, M. *et al.* SAK/PLK4 is required for centriole duplication and flagella development. *Curr. Biol.* **15,** 2199–2207 (2005).

28. Habedanck, R., Stierhof, Y.-D., Wilkinson, C. J. & Nigg, E. A. The Polo kinase Plk4 functions in centriole duplication. *Nat. Cell Biol.* **7,** 1140–1146 (2005).

29. Warnke, S. *et al.* Polo-like kinase-2 is required for centriole duplication in mammalian cells. *Curr. Biol.* **14,** 1200–1207 (2004).

30. Lee, K. J. *et al.* Requirement for Plk2 in orchestrated ras and rap signaling, homeostatic structural plasticity, and memory. *Neuron* **69,** 957–973 (2011).

31. Zimmerman, W. C. & Erikson, R. L. Polo-like kinase 3 is required for entry into S phase. *Proc. Natl. Acad. Sci. U. S. A.* **104,** 1847–1852 (2007).

32. Helmke, C., Becker, S. & Strebhardt, K. The role of Plk3 in oncogenesis. *Oncogene* (2015). doi:10.1038/onc.2015.105

33. de Cárcer, G. *et al.* Plk5, a polo box domain-only protein with specific roles in neuron differentiation and glioblastoma suppression. *Mol. Cell. Biol.* **31,** 1225–1239 (2011).

34. Lee, K. S., Yuan, Y. L., Kuriyama, R. & Erikson, R. L. Plk is an M-phase-specific protein kinase and interacts with a kinesin-like protein, CHO1/MKLP-1. *Mol Cell Biol* **15,** 7143–7151 (1995).

35. Archambault, V. & Glover, D. M. Polo-like kinases: conservation and divergence in their functions and regulation. *Nat Rev Mol Cell Biol* **10,** 265–275 (2009).

36. Ferris, D. K., Maloid, S. C. & Li, C. C. Ubiquitination and proteasome mediated degradation of polo-like kinase. *Biochem. Biophys. Res. Commun.* **252,** 340–344 (1998).

37. Lindon, C. & Pines, J. Ordered proteolysis in anaphase inactivates Plk1 to contribute to proper mitotic exit in human cells. *J Cell Biol* **164,** 233–241 (2004).

38. Jang, Y.-J., Lin, C.-Y., Ma, S. & Erikson, R. L. Functional studies on the role of the C-terminal domain of mammalian polo-like kinase. *Proc. Natl. Acad. Sci. U. S. A.* **99,** 1984–1989 (2002).

39. Elia, A. E. H. *et al.* The molecular basis for phosphodependent substrate targeting and regulation of Plks by the Polo-box domain. *Cell* **115,** 83–95 (2003).

40. Xu, J., Shen, C., Wang, T. & Quan, J. Structural basis for the inhibition of Polo-like kinase 1. *Nat Struct Mol Biol* **20,** 1047–53 (2013).

41. Seki, A., Coppinger, J. A., Jang, C.-Y., Yates, J. R. & Fang, G. Bora and the kinase Aurora a cooperatively activate the kinase Plk1 and control mitotic entry. *Science* **320,** 1655–1658 (2008).

42. Lee, K. S. & Erikson, R. L. Plk is a functional homolog of Saccharomyces cerevisiae Cdc5, and elevated Plk activity induces multiple septation structures. *Mol Cell Biol* **17,** 3408–3417 (1997).

43. Carmena, M. *et al.* The chromosomal passenger complex activates Polo kinase at centromeres. *PLoS Biol.* **10,** (2012).

44. Bruinsma, W., Macurek, L., Freire, R., Lindqvist, A. & Medema, R. H. Bora and Aurora-A continue to activate Plk1 in mitosis. *J. Cell Sci.* **127,** 801–811 (2014).

45. Nakojima, H., Toyoshima-Morimoto, F., Taniguchi, E. & Nishida, E. Identification

of a consensus motif for PlK (Polo-like kinase) phosphorylation reveals Myt1 as a Plk1 substrate. *J. Biol. Chem.* **278,** 25277–25280 (2003).

46. Santamaria, A. *et al.* The Plk1-dependent phosphoproteome of the early mitotic spindle. *Mol. Cell. Proteomics* **10,** (2010).

47. Kettenbach, A. N. *et al.* Quantitative phosphoproteomics identifies substrates and functional modules of Aurora and Polo-like kinase activities in mitotic cells. *Sci. Signal.* **4,** (2011).

48. Cheng, K.-Y., Lowe, E. D., Sinclair, J., Nigg, E. A. & Johnson, L. N. The crystal structure of the human polo-like kinase-1 polo box domain and its phospho-peptide complex. *EMBO J* **22,** 5757–5768 (2003).

49. Elia, A. E. H., Cantley, L. C. & Yaffe, M. B. Proteomic screen finds pSer/pThr-binding domain localizing Plk1 to mitotic substrates. *Science* **299,** 1228–1231 (2003).

50. Lee, K. S., Grenfell, T. Z., Yarm, F. R. & Erikson, R. L. Mutation of the polo-box disrupts localization and mitotic functions of the mammalian polo kinase Plk. *Proc. Natl. Acad. Sci. U. S. A.* **95,** 9301–9306 (1998).

51. Hanisch, A., Wehner, A., Nigg, E. A. & Silljé, H. H. W. Different Plk1 functions show distinct dependencies on Polo-Box domain-mediated targeting. *Mol Biol Cell* **17,** 448–459 (2006).

52. Reindl, W., Yuan, J., Krämer, A., Strebhardt, K. & Berg, T. Inhibition of polo-like kinase 1 by blocking polo-box domain-dependent protein-protein interactions. *Chem Biol* **15,** 459–466 (2008).

53. Burkard, M. E. *et al.* Plk1 self-organization and priming phosphorylation of HsCYK-4 at the spindle midzone regulate the onset of division in human cells. *PLoS Biol.* **7,** (2009).

54. Lee, K. S., Park, J.-E., Kang, Y. H., Kim, T.-S. & Bang, J. K. Mechanisms Underlying Plk1 Polo-Box Domain-Mediated Biological Processes and Their Physiological Significance. *Mol Cells* **37,** 286-94 (2014).

55. Lee, K. S. *et al.* Mechanisms of mammalian polo-like kinase 1 (Plk1) localization:

self- versus non-self-priming. *Cell Cycle* **7,** 141–145 (2008).

56. Kang, Y. H. *et al.* Self-Regulated Plk1 Recruitment to Kinetochores by the Plk1-PBIP1 Interaction Is Critical for Proper Chromosome Segregation. *Mol. Cell* **24,** 409–422 (2006).

57. Qi, W., Tang, Z. & Yu, H. Phosphorylation- and polo-box-dependent binding of Plk1 to Bub1 is required for the kinetochore localization of Plk1. *Mol Biol Cell* **17,** 3705–3716 (2006).

58. Elowe, S., Hümmer, S., Uldschmid, A., Li, X. & Nigg, E. A. Tension-sensitive Plk1 phosphorylation on BubR1 regulates the stability of kinetochore-microtubule interactions. *Genes Dev.* **21,** 2205–2219 (2007).

59. Sumara, I. *et al.* Roles of polo-like kinase 1 in the assembly of functional mitotic spindles. *Curr Biol* **14,** 1712–1722 (2004).

60. van Vugt, M. A. T. M. *et al.* Polo-like kinase-1 is required for bipolar spindle formation but is dispensable for anaphase promoting complex/Cdc20 activation and initiation of cytokinesis. *J. Biol. Chem.* **279,** 36841–36854 (2004).

61. Lane, H. A. & Nigg, E. A. Antibody microinjection reveals an essential role for human polo-like kinase 1 (Plk1) in the functional maturation of mitotic centrosomes. *J Cell Biol* **135,** 1701–1713 (1996).

62. Casenghi, M. *et al.* Polo-like kinase 1 regulates Nlp, a centrosome protein involved in microtubule nucleation. *Dev Cell* **5,** 113–125 (2003).

63. Oshimori, N., Ohsugi, M. & Yamamoto, T. The Plk1 target Kizuna stabilizes mitotic centrosomes to ensure spindle bipolarity. *Nat. Cell Biol.* **8,** 1095–1101 (2006).

64. Peters, U., Cherian, J., Kim, J. H., Kwok, B. H. & Kapoor, T. M. Probing cell-division phenotype space and Polo-like kinase function using small molecules. *Nat Chem Biol* **2,** 618–626 (2006).

65. McInnes, C. *et al.* Inhibitors of Polo-like kinase reveal roles in spindle-pole maintenance. *Nat Chem Biol* **2,** 608–617 (2006).

66. Lénárt, P. *et al.* The small-molecule inhibitor BI 2536 reveals novel insights into mitotic roles of polo-like kinase 1. *Curr Biol* **17,** 304–315 (2007).

67. Haren, L., Stearns, T. & Lüders, J. Plk1-dependent recruitment of gamma-tubulin complexes to mitotic centrosomes involves multiple PCM components. *PLoS One* **4,** (2009).

68. Smith, E. *et al.* Differential control of Eg5-dependent centrosome separation by Plk1 and Cdk1. *EMBO J* **30,** 2233–2245 (2011).

69. Lee, K. & Rhee, K. PLK1 phosphorylation of pericentrin initiates centrosome maturation at the onset of mitosis. *J Cell Biol* **195,** 1093–1101 (2011).

70. Conduit, P. T. *et al.* The centrosome-specific phosphorylation of cnn by polo/plk1 drives cnn scaffold assembly and centrosome maturation. *Dev. Cell* **28,** 659–669 (2014).

71. Hauf, S. *et al.* Dissociation of cohesin from chromosome arms and loss of arm cohesion during early mitosis depends on phosphorylation of SA2. *PLoS Biol.* **3,** 0419–0432 (2005).

72. Zhang, L. *et al.* PLK1 phosphorylates mitotic centromere-associated kinesin and promotes its depolymerase activity. *J. Biol. Chem.* **286,** 3033–3046 (2011).

73. Nishino, M. *et al.* NudC Is Required for Plk1 Targeting to the Kinetochore and Chromosome Congression. *Curr. Biol.* **16,** 1414–1421 (2006).

74. Matsumura, S., Toyoshima, F. & Nishida, E. Polo-like kinase 1 facilitates chromosome alignment during prometaphase through BubR1. *J. Biol. Chem.* **282,** 15217–15227 (2007).

75. Watanabe, N. *et al.* Deficiency in chromosome congression by the inhibition of Plk1 polo box domain-dependent recognition. *J. Biol. Chem.* **284,** 2344–2353 (2009).

76. Colnaghi, R. & Wheatley, S. P. Liaisons between survivin and Plk1 during cell division and cell death. *J. Biol. Chem.* **285,** 22592–22604 (2010).

77. Maia, A. R. R. *et al.* Cdk1 and Plk1 mediate a CLASP2 phospho-switch that

stabilizes kinetochore-microtubule attachments. *J. Cell Biol.* **199,** 285–301 (2012).

78. Suijkerbuijk, S. J. E., Vleugel, M., Teixeira, A. & Kops, G. J. P. L. Integration of Kinase and Phosphatase Activities by BUBR1 Ensures Formation of Stable Kinetochore-Microtubule Attachments. *Dev. Cell* **23,** 745–755 (2012).

79. Liu, X. S. *et al.* Plk1 Phosphorylates Sgt1 at the Kinetochores To Promote Timely Kinetochore-Microtubule Attachment. *Mol. Cell. Biol.* **32,** 4053–4067 (2012).

80. Kakeno, M., Matsuzawa, K., Matsui, T., Akita, H. & Sugiyama, I. Plk1 Phosphorylates CLIP-170 and Regulates Its Binding to Microtubules for Chromosome Alignment. *Cell Struct Funct* **59,** 45–59 (2014).

81. Li, H., Wang, Y. & Liu, X. Plk1-dependent phosphorylation regulates functions of DNA topoisomerase IIalpha in cell cycle progression. *J Biol Chem* **283,** 6209–6221 (2008).

82. Hood, E. A., Kettenbach, A. N., Gerber, S. A. & Compton, D. A. Plk1 regulates the kinesin-13 protein Kif2b to promote faithful chromosome segregation. *Mol. Biol. Cell* **23,** 2264–2274 (2012).

83. Park, C. H. *et al.* Mammalian Polo-like Kinase 1 (Plk1) Promotes Proper Chromosome Segregation by Phosphorylating and Delocalizing the PBIP1·CENP-Q Complex from Kinetochores. *J. Biol. Chem.* **290,** 8569–8581 (2015).

84. Brennan, I. M., Peters, U., Kapoor, T. M. & Straight, A. F. Polo-like kinase controls vertebrate spindle elongation and cytokinesis. *PLoS One* **2,** 1–8 (2007).

85. Neef, R. *et al.* Phosphorylation of mitotic kinesin-like protein 2 by polo-like kinase 1 is required for cytokinesis. *J Cell Biol* **162,** 863–875 (2003).

86. Burkard, M. E. *et al.* Chemical genetics reveals the requirement for Polo-like kinase 1 activity in positioning RhoA and triggering cytokinesis in human cells. *Proc. Natl. Acad. Sci. U. S. A.* **104,** 4383–4388 (2007).

87. Petronczki, M., Glotzer, M., Kraut, N. & Peters, J.-M. Polo-like kinase 1 triggers the initiation of cytokinesis in human cells by promoting recruitment of the RhoGEF Ect2 to the central spindle. *Dev Cell* **12,** 713–725 (2007).

88. Santamaria, A. *et al.* Use of the Novel Plk1 Inhibitor ZK-Thiazolidinone to Elucidate Functions of Plk1 in Early and Late Stages of Mitosis. *Mol. Biol. Cell* **18,** 4024–4036 (2007).

89. Hasegawa, H. *et al.* The role of PLK1-phosphorylated SVIL in myosin II activation and cytokinetic furrowing. *J. Cell Sci.* **126,** 3627–3637 (2013).

90. Oppermann, F. S. *et al.* Combination of Chemical Genetics and Phosphoproteomics for Kinase Signaling Analysis Enables Confident Identification of Cellular Downstream Targets. *Mol. Cell. Proteomics* **11,** (2012).

91. Grosstessner-Hain, K. *et al.* Quantitative phospho-proteomics to investigate the Polo-like kinase 1-dependent phospho-proteome. *Mol. Cell. Proteomics* **10,** (2011).

92. Binder, J. X. *et al.* COMPARTMENTS: unification and visualization of protein subcellular localization evidence. *Database* **2014,** bau012 (2014).

93. Horiuchi, D. *et al.* Chemical-genetic analysis of cyclin dependent kinase 2 function reveals an important role in cellular transformation by multiple oncogenic pathways. *Proc. Natl. Acad. Sci. U. S. A.* **109,** E1019–27 (2012).

94. Merrick, K. A. *et al.* Switching Cdk2 on or off with small molecules to reveal requirements in human cell proliferation. *Mol Cell* **42,** 624–636 (2011).

95. Karaman, M. W. *et al.* A quantitative analysis of kinase inhibitor selectivity. *Nat Biotechnol* **26,** 127–132 (2008).

96. Bain, J. *et al.* The selectivity of protein kinase inhibitors: a further update. *Biochem J* **408,** 297–315 (2007).

97. Echalier, A. *et al.* An integrated chemical biology approach provides insight into cdk2 functional redundancy and inhibitor sensitivity. *Chem Biol* **19,** 1028–1040 (2012).

98. Bishop, A. C. *et al.* A chemical switch for inhibitor-sensitive alleles of any protein kinase. *Nature* **407,** 395–401 (2000).

99. Bishop, A. C. *et al.* Design of allele-specific inhibitors to probe protein kinase

signaling. *Curr. Biol.* **8,** 257–266 (1998).

100. Cipak, L. *et al.* Generation of a set of conditional analog-sensitive alleles of essential protein kinases in the fission yeast Schizosaccharomyces pombe. *Cell Cycle* **10,** 3527–3532 (2011).

101. Hochegger, H. *et al.* An essential role for Cdk1 in S phase control is revealed via chemical genetics in vertebrate cells. *J Cell Biol* **178,** 257–268 (2007).

102. Frank, C. J., Hyde, M. & Greider, C. W. Regulation of telomere elongation by the cyclin-dependent kinase CDK1. *Mol Cell* **24,** 423–432 (2006).

103. Larochelle, S. *et al.* Requirements for Cdk7 in the assembly of Cdk1/cyclin B and activation of Cdk2 revealed by chemical genetics in human cells. *Mol Cell* **25,** 839–850 (2007).

104. Hengeveld, R. C. C. *et al.* Development of a chemical genetic approach for human aurora B kinase identifies novel substrates of the chromosomal passenger complex. *Mol Cell Proteomics* **11,** 47–59 (2012).

105. Koch, A., Krug, K., Pengelley, S., Macek, B. & Hauf, S. Mitotic substrates of the kinase aurora with roles in chromatin regulation identified through quantitative phosphoproteomics of fission yeast. *Sci. Signal.* **4,** (2011).

106. Sliedrecht, T., Zhang, C., Shokat, K. M. & Kops, G. J. P. L. Chemical genetic inhibition of Mps1 in stable human cell lines reveals novel aspects of Mps1 function in mitosis. *PLoS One* **5,** (2010).

107. Maciejowski, J. *et al.* Mps1 directs the assembly of Cdc20 inhibitory complexes during interphase and mitosis to control M phase timing and spindle checkpoint signaling. *J Cell Biol* **190,** 89–100 (2010).

108. Jones, M. H. *et al.* Chemical genetics reveals a role for Mps1 kinase in kinetochore attachment during mitosis. *Curr. Biol.* **15,** 160–165 (2005).

109. Snead, J. L. *et al.* A coupled chemical-genetic and bioinformatic approach to Polo-like kinase pathway exploration. *Chem Biol* **14,** 1261–1272 (2007).

110. Burkard, M. E., Santamaria, A. & Jallepalli, P. V. Enabling and disabling polo-like

kinase 1 inhibition through chemical genetics. *ACS Chem. Biol.* **7,** 978–981 (2012).

111. Donaldson, M. M., Tavares, A. A., Ohkura, H., Deak, P. & Glover, D. M. Metaphase arrest with centromere separation in polo mutants of Drosophila. *J Cell Biol* **153,** 663–676 (2001).

112. Barr, F. A., Silljé, H. H. W. & Nigg, E. A. Polo-like kinases and the orchestration of cell division. *Nat. Rev. Mol. Cell Biol.* **5,** 429–440 (2004).

113. Liu, F. *et al.* Identification of high affinity polo-like kinase 1 (Plk1) polo-box domain binding peptides using oxime-based diversification. *ACS Chem. Biol.* **7,** 805–810 (2012).

114. Lowery, D. M. *et al.* Proteomic screen defines the Polo-box domain interactome and identifies Rock2 as a Plk1 substrate. *EMBO J.* **26,** 2262–2273 (2007).

115. Randall, C. L., Burkard, M. E. & Jallepalli, P. V. Polo kinase and cytokinesis initiation in mammalian cells: harnessing the awesome power of chemical genetics. *Cell Cycle* **6,** 1713–1717 (2007).

116. Wolfe, B. A., Takaki, T., Petronczki, M. & Glotzer, M. Polo-like kinase 1 directs assembly of the HsCyk-4 RhoGAP/Ect2 RhoGEF complex to initiate cleavage furrow formation. *PLoS Biol* **7,** (2009).

117. Gilmartin, A. G. *et al.* Distinct concentration-dependent effects of the polo-like kinase 1-specific inhibitor GSK461364A, including differential effect on apoptosis. *Cancer Res.* **69,** 6969–6977 (2009).

118. Maresca, T. J. & Salmon, E. D. Welcome to a new kind of tension: translating kinetochore mechanics into a wait-anaphase signal. *J. Cell Sci.* **123,** 825–835 (2010).

119. Clarke, D. J., Johnson, R. T. & Downes, C. S. Topoisomerase II inhibition prevents anaphase chromatid segregation in mammalian cells independently of the generation of DNA strand breaks. *J. Cell Sci.* **105,** 563–569 (1993).

120. Baumann, C., Körner, R., Hofmann, K. & Nigg, E. A. PICH, a Centromere-Associated SNF2 Family ATPase, Is Regulated by Plk1 and Required for the

Spindle Checkpoint. *Cell* **128,** 101–114 (2007).

121. Chan, K.-L., North, P. S. & Hickson, I. D. BLM is required for faithful chromosome segregation and its localization defines a class of ultrafine anaphase bridges. *EMBO J* **26,** 3397–3409 (2007).

122. Alexandru, G., Uhlmann, F., Mechtler, K., Poupart, M. A. & Nasmyth, K. Phosphorylation of the cohesin subunit Scc1 by Polo/Cdc5 kinase regulates sister chromatid separation in yeast. *Cell* **105,** 459–472 (2001).

123. Cimini, D. *et al.* Merotelic kinetochore orientation is a major mechanism of aneuploidy in mitotic mammalian tissue cells. *J Cell Biol* **153,** 517–527 (2001).

124. Cimini, D., Moree, B., Canman, J. C. & Salmon, E. D. Merotelic kinetochore orientation occurs frequently during early mitosis in mammalian tissue cells and error correction is achieved by two different mechanisms. *J. Cell Sci.* **116,** 4213–4225 (2003).

125. Medema, R. H., Lin, C.-C. & Yang, J. C.-H. Polo-like kinase 1 inhibitors and their potential role in anticancer therapy, with a focus on NSCLC. *Clin Cancer Res* **17,** 6459–6466 (2011).

126. Schöffski, P. *et al.* A phase I, dose-escalation study of the novel Polo-like kinase inhibitor volasertib (BI 6727) in patients with advanced solid tumours. *Eur J Cancer* **48,** 179–186 (2012).

127. Gascoigne, K. E. & Taylor, S. S. How do anti-mitotic drugs kill cancer cells? *J. Cell Sci.* **122,** 2579–2585 (2009).

128. Neef, R. *et al.* Choice of Plk1 docking partners during mitosis and cytokinesis is controlled by the activation state of Cdk1. *Nat. Cell Biol.* **9,** 436–444 (2007).

129. Yun, S.-M. *et al.* Structural and functional analyses of minimal phosphopeptides targeting the polo-box domain of polo-like kinase 1. *Nat Struct Mol Biol* **16,** 876–882 (2009).

130. Kishi, K., van Vugt, M. A. T. M., Okamoto, K., Hayashi, Y. & Yaffe, M. B. Functional dynamics of Polo-like kinase 1 at the centrosome. *Mol. Cell. Biol.* **29,** 3134–3150 (2009).

131. Cimini, D., Fioravanti, D., Salmon, E. D. & Degrassi, F. Merotelic kinetochore orientation versus chromosome mono-orientation in the origin of lagging chromosomes in human primary cells. *J. Cell Sci.* **115,** 507–515 (2002).

132. Moutinho-Santos, T., Conde, C. & Sunkel, C. E. POLO ensures chromosome bi-orientation by preventing and correcting erroneous chromosome-spindle attachments. *J. Cell Sci.* **125,** 576–583 (2012).

133. Paschal, C. R., Maciejowski, J. & Jallepalli, P. V. A stringent requirement for Plk1 T210 phosphorylation during K-fiber assembly and chromosome congression. *Chromosoma* **121,** 565–572 (2012).

134. Crasta, K. *et al.* DNA breaks and chromosome pulverization from errors in mitosis. *Nature* **482,** 53–58 (2012).

135. Debnath, J., Muthuswamy, S. K. & Brugge, J. S. Morphogenesis and oncogenesis of MCF-10A mammary epithelial acini grown in three-dimensional basement membrane cultures. *Methods* **30,** 256–268 (2003).

136. Schneider, C. A., Rasband, W. S. & Eliceiri, K. W. NIH Image to ImageJ: 25 years of image analysis. *Nat Methods* **9,** 671–675 (2012).

137. Lampson, M. A. & Kapoor, T. M. The human mitotic checkpoint protein BubR1 regulates chromosome-spindle attachments. *Nat Cell Biol* **7,** 93–98 (2005).

138. Godek, K. M., Kabeche, L. & Compton, D. A. Regulation of kinetochore-microtubule attachments through homeostatic control during mitosis. *Nat Rev Mol Cell Biol* **16,** 57–64 (2015).

139. London, N. & Biggins, S. Signalling dynamics in the spindle checkpoint response. *Nat. Rev. Mol. Cell Biol.* **15,** 736–748 (2014).

140. Foley, E. A. & Kapoor, T. M. Microtubule attachment and spindle assembly checkpoint signalling at the kinetochore. *Nat. Rev. Mol. Cell Biol.* **14,** 25–37 (2013).

141. Liu, D., Vader, G., Vromans, M. J. M., Lampson, M. A. & Lens, S. M. A. Sensing chromosome bi-orientation by spatial separation of aurora B kinase from

kinetochore substrates. *Science* **323,** 1350–1353 (2009).

142. Welburn, J. P. I. *et al.* Aurora B Phosphorylates Spatially Distinct Targets to Differentially Regulate the Kinetochore-Microtubule Interface. *Mol. Cell* **38,** 383–392 (2010).

143. Arnaud, L., Pines, J. & Nigg, E. A. GFP tagging reveals human Polo-like kinase 1 at the kinetochore/centromere region of mitotic chromosomes. *Chromosoma* **107,** 424–429 (1998).

144. Liu, D., Davydenko, O. & Lampson, M. A. Polo-like kinase-1 regulates kinetochore-microtubule dynamics and spindle checkpoint silencing. *J Cell Biol* **198,** 491–499 (2012).

145. Lera, R. F. & Burkard, M. E. High mitotic activity of polo-like kinase 1 is required for chromosome segregation and genomic integrity in human epithelial cells. *J. Biol. Chem.* **287,** 42812–42825 (2012).

146. Park, J.-E., Erikson, R. L. & Lee, K. S. Feed-forward mechanism of converting biochemical cooperativity to mitotic processes at the kinetochore plate. *Proc. Natl. Acad. Sci. U. S. A.* **108,** 8200–8205 (2011).

147. Goto, H. *et al.* Complex formation of Plk1 and INCENP required for metaphase-anaphase transition. *Nat. Cell Biol.* **8,** 180–187 (2006).

148. Chu, Y. *et al.* Aurora B kinase activation requires survivin priming phosphorylation by PLK1. *J. Mol. Cell Biol.* **3,** 260-267 (2010).

149. Kothe, M. *et al.* Selectivity-determining residues in Plk1. *Chem. Biol. Drug Des.* **70,** 540–546 (2007).

150. Cheerambathur, D. K. & Desai, A. Linked in: Formation and regulation of microtubule attachments during chromosome segregation. *Current Opinion in Cell Biology* **26,** 113–122 (2014).

151. Liu, D., Davydenko, O. & Lampson, M. A. Polo-like kinase-1 regulates kinetochore-microtubule dynamics and spindle checkpoint silencing. *J. Cell Biol.* **198,** 491–499 (2012).

152. Suzuki, A., Badger, B. L., Wan, X., DeLuca, J. G. & Salmon, E. D. The Architecture of CCAN Proteins Creates a Structural Integrity to Resist Spindle Forces and Achieve Proper Intrakinetochore Stretch. *Dev. Cell* **30,** 717–730 (2014).

153. Wan, X. *et al.* Protein Architecture of the Human Kinetochore Microtubule Attachment Site. *Cell* **137,** 672–684 (2009).

154. Domnitz, S. B., Wagenbach, M., Decarreau, J. & Wordeman, L. MCAK activity at microtubule tips regulates spindle microtubule length to promote robust kinetochore attachment. *J. Cell Biol.* **197,** 231–237 (2012).

155. Honnappa, S. *et al.* An EB1-Binding Motif Acts as a Microtubule Tip Localization Signal. *Cell* **138,** 366–376 (2009).

156. Phanstiel, D., Unwin, R., McAlister, G. C. & Coon, J. J. Peptide quantification using 8-plex isobaric tags and electron transfer dissociation tandem mass spectrometry. *Anal. Chem.* **81,** 1693–1698 (2009).

157. Maney, T., Hunter, A. W., Wagenbach, M. & Wordeman, L. Mitotic centromere-associated kinesin is important for anaphase chromosome segregation. *J. Cell Biol.* **142,** 787–801 (1998).

158. Kang, Y. H. *et al.* Mammalian polo-like kinase 1-dependent regulation of the PBIP1-CENP-Q complex at kinetochores. *J. Biol. Chem.* **286,** 19744–19757 (2011).

159. Meppelink, A., Kabeche, L., Vromans, M. J. M., Compton, D. A. & Lens, S. M. A. Shugoshin-1 Balances Aurora B Kinase Activity via PP2A to Promote Chromosome Bi-orientation. *Cell Rep.* **11,** 508–515 (2015).

160. Foley, E. A., Maldonado, M. & Kapoor, T. M. Formation of stable attachments between kinetochores and microtubules depends on the B56-PP2A phosphatase. *Nature Cell Biology* **13,** 1265–1271 (2011).

161. Liu, D. *et al.* Regulated targeting of protein phosphatase 1 to the outer kinetochore by KNL1 opposes Aurora B kinase. *J. Cell Biol.* **188,** 809–820 (2010).

162. Beck, J. *et al.* Ubiquitylation-dependent localization of PLK1 in mitosis. *Nat. Cell*

Biol. **15,** 430–439 (2013).

163. Hornbeck, P. V *et al.* PhosphoSitePlus, 2014: mutations, PTMs and recalibrations. *Nucleic Acids Res.* **43,** D512–20 (2015).

164. Wenger, C. D., Phanstiel, D. H., Lee, M. V., Bailey, D. J. & Coon, J. J. COMPASS: A suite of pre- and post-search proteomics software tools for OMSSA. *Proteomics* **11,** 1064–1074 (2011).

165. Taus, T. *et al.* Universal and confident phosphorylation site localization using phosphoRS. *J. Proteome Res.* **10,** 5354–5362 (2011).

166. Kraft, C. *et al.* Mitotic regulation of the human anaphase-promoting complex by phosphorylation. *EMBO J.* **22,** 6598–6609 (2003).

167. Bader, J. R. *et al.* Polo-like kinase1 is required for recruitment of dynein to kinetochores during mitosis. *J. Biol. Chem.* **286,** 20769–20777 (2011).

168. Chi, Y. H. *et al.* Requirements for protein phosphorylation and the kinase activity of polo-like kinase 1 (Plk1) for the kinetochore function of mitotic arrest deficiency protein 1 (Mad1). *J. Biol. Chem.* **283,** 35834–35844 (2008).

169. Mondal, G., Ohashi, A., Yang, L., Rowley, M. & Couch, F. J. Tex14, a Plk1-Regulated Protein, Is Required for Kinetochore-Microtubule Attachment and Regulation of the Spindle Assembly Checkpoint. *Mol. Cell* **45,** 680–695 (2012).

170. Benada, J., Burdová, K., Lidak, T., von Morgen, P. & Macurek, L. Polo-like kinase 1 inhibits DNA damage response during mitosis. *Cell Cycle* **14,** 219–231 (2015).

171. Kim, J. H. *et al.* The condensin component NCAPG2 regulates microtubule-kinetochore attachment through recruitment of Polo-like kinase 1 to kinetochores. *Nat. Commun.* **5,** 4588 (2014).

172. Li, H. *et al.* Phosphorylation of CLIP-170 by Plk1 and CK2 promotes timely formation of kinetochore-microtubule attachments. *EMBO J.* **29,** 2953–2965 (2010).

173. Taylor, S. S., Hussein, D., Wang, Y., Elderkin, S. & Morrow, C. J. Kinetochore localisation and phosphorylation of the mitotic checkpoint components Bub1 and

BubR1 are differentially regulated by spindle events in human cells. *J. Cell Sci.* **114,** 4385–4395 (2001).

174. Liu, S.-T. *et al.* Human CENP-I specifies localization of CENP-F, MAD1 and MAD2 to kinetochores and is essential for mitosis. *Nat. Cell Biol.* **5,** 341–345 (2003).

175. Gascoigne, K. E. *et al.* Induced ectopic kinetochore assembly bypasses the requirement for CENP-A nucleosomes. *Cell* **145,** 410–422 (2011).

176. Mazumdar, M., Sundareshan, S. & Misteli, T. Human chromokinesin KIF4A functions in chromosome condensation and segregation. *J Cell Biol* **166,** 613–620 (2004).

177. Kurasawa, Y., Earnshaw, W. C., Mochizuki, Y., Dohmae, N. & Todokoro, K. Essential roles of KIF4 and its binding partner PRC1 in organized central spindle midzone formation. *EMBO J* **23,** 3237–3248 (2004).

178. Hu, C.-K., Coughlin, M., Field, C. M. & Mitchison, T. J. KIF4 regulates midzone length during cytokinesis. *Curr. Biol.* **21,** 815–824 (2011).

179. Zhuo, X. *et al.* Usp16 regulates kinetochore localization of Plk1 to promote proper chromosome alignment in mitosis. *J Cell Biol* **210,** 727–735 (2015).

180. Hooser, A. A. Van *et al.* Specification of kinetochore-forming chromatin by the histone H3 variant CENP-A. *J. Cell Sci.* **114,** 3529–3542 (2001).

181. Liu, S.-T., Rattner, J. B., Jablonski, S. A. & Yen, T. J. Mapping the assembly pathways that specify formation of the trilaminar kinetochore plates in human cells. *J Cell Biol* **175,** 41–53 (2006).

182. McKinley, K. L. & Cheeseman, I. M. Polo-like kinase 1 licenses CENP-A deposition at centromeres. *Cell* **158,** 397–411 (2014).

183. Bodor, D. L., Valente, L. P., Mata, J. F., Black, B. E. & Jansen, L. E. T. Assembly in G1 phase and long-term stability are unique intrinsic features of CENP-A nucleosomes. *Mol. Biol. Cell* **24,** 923–932 (2013).

184. Hemmerich, P. *et al.* Dynamics of inner kinetochore assembly and maintenance in

living cells. *J Cell Biol* **180,** 1101–1114 (2008).

185. Jansen, L. E. T., Black, B. E., Foltz, D. R. & Cleveland, D. W. Propagation of centromeric chromatin requires exit from mitosis. *J Cell Biol* **176,** 795–805 (2007).

186. Fachinetti, D. *et al.* A two-step mechanism for epigenetic specification of centromere identity and function. *Nat. Cell Biol.* **15,** 1056–66 (2013).